

The hominoid-specific gene TBC1D3 promotes generation of basal neural progenitors and induces cortical folding in mice

Xiang-Chun Ju^{1,3,9}, Qiong-Qiong Hou^{1,3,9}, Ai-Li Sheng¹, Kong-Yan Wu¹, Yang Zhou⁸, Ying Jin⁸, Tieqiao Wen⁷, Zhengang Yang⁶, Xiaoqun Wang^{2,5}, Zhen-Ge Luo^{1,2,3,4}

¹Institute of Neuroscience, State Key Laboratory of Neuroscience, Shanghai Institutes for Biological Sciences, Chinese Academy of Sciences, Shanghai, China.

²CAS Center for Excellence in Brain Science and Intelligence Technology, Shanghai, China.

³Chinese Academy of Sciences University, Beijing, China.

⁴ShanghaiTech University, Shanghai, China

⁵Institute of Biophysics, Chinese Academy of Sciences, Beijing, China.

⁶Institutes of Brain Science, State Key Laboratory of Medical Neurobiology, Fudan University, Shanghai, China.

⁷School of Life Sciences, Shanghai University, Shanghai, China.

⁸The Institute of Health Sciences, Shanghai Institutes for Biological Sciences, Chinese Academy of Sciences, Shanghai, China.

⁹Co-first author

Correspondence should be addressed to Z.G.L (zgluo@ion.ac.cn)

Author contributions

X.-C.J and Q.-Q. H performed most experiments, analyzed data and wrote the paper. A.-L.S helped with in situ hybridization. K.-Y.W assisted with imaging analysis. T.W helped with the construction of *nestin* promoter construct. Y. Z and Y. J helped with ReNeuron cell culture and analysis. Z.Y provided human fetal samples and assisted with

immunohistochemistry analysis. X.W provided help with live-imaging analysis. Z.-G.L supervised the whole study, designed the research, analyzed data and wrote the paper.

Abstract

Cortical expansion and folding are often linked to the evolution of higher intelligence, but molecular and cellular mechanisms underlying cortical folding remain poorly understood. The hominoid-specific gene *TBC1D3* undergoes segmental duplications during hominoid evolution, but its role in brain development has not been explored. Here, we found that expression of *TBC1D3* in ventricular cortical progenitors of mice via *in utero* electroporation caused delamination of ventricular radial glia cells (vRGs) and promotes generation of self-renewing basal progenitors with typical morphology of outer radial glia (oRG), which are most abundant in primates. Furthermore, down-regulation of *TBC1D3* in cultured human brain slices decreased generation of oRGs. Interestingly, localized oRG proliferation resulting from either *in utero* electroporation or transgenic expression of *TBC1D3*, was often found to underlie cortical regions exhibiting folding. Thus, we have identified a hominoid gene that is required for oRG generation in regulating the cortical expansion and folding.

Introduction

It is generally assumed that the expansion of the mammalian neocortex during evolution correlates with the increase in intelligence, and this process involves increased production of cortical neurons, resulting from an extended neurogenic period as well as increased proliferative ability of neural stem cells and progenitors (Geschwind and Rakic, 2013; Lui et al., 2011; Sun and Hevner, 2014; Zilles et al., 2013). To fit into a limited cranium, expanded cortical surfaces are folded to form gyri and sulci. Recent cross-species studies have shown the emergence of an outer subventricular zone (OSVZ) in the primate cortex, consisting of a massive pool of proliferating basal progenitors (BPs) and post-mitotic neurons (Betizeau et al., 2013; Fietz et al., 2010; Hansen et al., 2010; Reillo et al., 2011; Smart et al., 2002). Unlike the neuroepithelia-derived ventricular radial glial cells, which undergo repeated and typically asymmetric cell division at the apical surface of the ventricular zone, the BPs, after delamination from the apical surface, translocate to the SVZ, where they exhibit symmetric or asymmetric divisions. In primates, the recently identified outer (basal) radial glia (referred to as oRG or bRG) and the intermediate progenitors (IPs) in the OSVZ, which can undergo multiple rounds of symmetric or asymmetric divisions (Betizeau et al., 2013; Hansen et al., 2010), are two major forms of BPs. By contrast, the IPs and minimal oRG cells in the mouse SVZ usually exhibit final division to generate a pair of post-mitotic neurons (Shitamukai et al., 2011; Wang et al., 2011). The radial and lateral expansion of BPs is thought to be a main cause of cortical folding of gyrencephalic species (Fietz and Huttner, 2011; Fietz et al., 2010; Hansen et al., 2010; Lewitus et al., 2014; Lui et al., 2011; Reillo et al., 2011). In support of this hypothesis, forced expansion of BPs by down-regulating the DNA-associated protein Trnp1 or overexpressing cell cycle regulatory proteins Cdk4/Cyclin D1 resulted in gyrification of the cerebral cortex in naturally lissencephalic mouse or gyrencephalic ferret (Nonaka-Kinoshita et al., 2013; Stahl et al., 2013).

71 Given that genetic differences between humans and other species are likely to be the
72 causes of human-specific traits, including complexity of cortical morphology, extensive
73 studies have been performed in comparing genes and genetic elements of different
74 species of primates and mammals (Arcila et al., 2014; Fietz et al., 2012; Florio et al.,
75 2015; Johnson et al., 2009; Johnson et al., 2015; Kang et al., 2011; Konopka et al., 2012;
76 Lui et al., 2014; Miller et al., 2014; O'Bleness et al., 2012). In particular, several recent
77 studies have aimed to uncover the distinctive transcriptional signature of the expanded
78 human OSVZ or BPs that reside there, leading to the identification of a group of genes
79 highly expressed in the human OSVZ (Miller et al., 2014), and human-specific orthologs
80 preferentially expressed in human RGs (Florio et al., 2015; Lui et al., 2014; Miller et al.,
81 2014; Pollen et al., 2015; Thomsen et al., 2016). For examples, platelet-derived growth
82 factor D is expressed specifically and functionally important in human but not mouse
83 RGs (Lui et al., 2014). A human lineage-specific Rho GTPase-activating protein could
84 enhance the generation of IPs and cause neocortex expansion when expressed in the
85 mouse brain (Florio et al., 2015). Since cortical folding emerges progressively during
86 primate evolution, multiple primate- and hominid-specific genes are likely to be involved
87 in the emergence of cortical folding.

88
89 Gene duplication may play critical roles in brain evolution (Geschwind and Rakic,
90 2013). In particular, duplication of specific genes in humans may be responsible for the
91 marked increase in cortical folding. The *TBC1D3* gene is derived from a segmental
92 duplication, with multiple copies present in the human chromosome 17 and present in the
93 chimpanzee genome as a single copy gene (but absent in other species) (Hodzic et al.,
94 2006; Pei et al., 2002; Perry et al., 2008; Zody et al., 2006). Indeed, *TBC1D3* corresponds
95 to one of the core duplicons that have been implicated in the expansion of
96 intrachromosomal segmental duplications during hominoid evolution (Jiang et al., 2007).
97 Because the timing of origination and amplification of the *TBC1D3* gene is consistent

with the evolutionary divergence of primates (Perry et al., 2008; Stahl and Wainszelbaum, 2009), we decided to explore its role in brain development by expressing this gene in mice.

We found *TBC1D3* expression markedly elevated the generation and proliferation of BPs and resulted in extensive cortex folding in the mouse brain, and further delineated the molecular and cellular mechanisms underlying its action. Furthermore, *TBC1D3* is essential for the generation of BPs in cultured developing human brain slices. The transgenic mice generated in this study may provide a feasible model to link cortical folding to higher brain functions.

Results

***TBC1D3* expression in mice delaminates ventricular neuroprogenitors**

A previous study showed that *TBC1D3* paralogues are expressed in most human tissues, including the brain (Hodzic et al., 2006). By using reverse transcription PCR, we found that the expression of *TBC1D3* in the fetal human brain (gestational week, GW 26 to 40) was higher than that in the adult (Figure 1A). Immunofluorescence staining of cortical sections obtained from GW18 human specimens during the peak period of neurogenesis revealed high *TBC1D3* expression near the ventricular surface and in the subventricular zone (SVZ) (Figure 1B), suggesting a role of *TBC1D3* in cortex development.

To investigate the potential role of *TBC1D3* in neural development, we introduced human *TBC1D3* expression construct pE/nestin-*TBC1D3* together with pCAG-YFP into neural precursors in the ventricular zone (VZ) of fetal mice at embryonic day 13.5 (E13.5), using *in utero* electroporation. At E15.5, *in situ* hybridization with an antisense *TBC1D3* probe showed that the transcript was expressed in *TBC1D3*-electroporated mice but not in control mice injected with the vehicle construct (Figure 1C), consistent with

the absence of *TBC1D3* in the murine genome (Hodzic et al., 2006). Interestingly, expression of *TBC1D3* caused delamination of ventricular radial glia (vRG), and a decreased level of N-cadherin at adherens junctions (AJs) (Figure 1D) at the ventricular surface. The reduction in N-cadherin was probably due to either the transcriptional inhibition or destabilization of transcripts, because *in situ* hybridization and real-time PCR showed marked reduction of *N-cadherin* (*Cdh2*) transcript in VZ cells (Figure 1-figure supplement 1A) and flow cytometry-sorted YFP⁺ cells expressing *TBC1D3* (Figure 1-figure supplement 1B-D), respectively. Further analyses showed that expression of *TBC1D3* indeed caused destabilization of *Cdh2* mRNA in ReNeuron human neural progenitor cell line (Figure 1-figure supplement 1E, F). Since N-cadherin is known to be important for maintaining the alignment of radial glial cells at VZ (Kadowaki et al., 2007), reduction of N-cadherin due to *TBC1D3* expression may be causally related to the delamination of ventricular neuroprogenitors. Indeed, we found that expression of *TBC1D3* caused dislocalization of Numb and integrin beta 1 (ITGB1) which were originally polarized distributed in endfeet of vRGs (Campos et al., 2004; Katayama et al., 2011; Rasin et al., 2007), without disrupting the junction integrity of the VZ as revealed by actin filaments (F-actin) (Figure 1-figure supplement 2).

Observation in the SVZ and intermediate zone (IZ) of E16.5 mice (electroporated at E13.5) showed that delaminated *TBC1D3*-expressing cells often exhibited clustered distribution by forming vertical column-like structures (Figure 1E), reminiscent of ontogenic radial units (Rakic, 1988), expansion of which has been proposed to underlie cortical folding (Borrell and Gotz, 2014; Florio and Huttner, 2014; Lui et al., 2011; Rakic, 1988). This column-like aggregation of basal cells induced by *TBC1D3* expression may result from increased number of proliferating cells originated from VZ (see below), and leads to lateral heterogeneity in the rate of neuronal production that may contribute to cortical folding.

TBC1D3 expression increases expansion of basal progenitors

Previous studies have shown that disruption of AJs due to the loss of RhoA in neural progenitors is accompanied by an elevated proliferation of neuroprogenitors (Katayama et al., 2011). We thus examine the effect of TBC1D3 expression via *in utero* electroporation on neuroprogenitor proliferation by calculating the proportion of cells in S phase, as assayed by the incorporation of pyrimidine analog bromodeoxyuridine (BrdU) for 2 hr before sacrificing the electroporated mice (Figure 2A, B). We found that TBC1D3 expression caused an increase in BrdU-positive (BrdU^+) proliferating cells, as compared to that of control mice electroporated with vehicle construct (Figure 2C, E). In an additional control experiment, we found that expressing a mutated form of TBC1D3, with the deletion of amino acids 286 to 353 ($\Delta 286-353$) essential for its cytoplasmic retention (He et al., 2014), in neural progenitors had no effect on BrdU incorporation (Figure 2C, E). These results suggest that cytoplasmic presence of TBC1D3 promotes the proliferation of early neural precursors. Interestingly, the TBC1D3-induced population of BrdU^+ cells scattered widely across the cortex, from VZ to CP, with the highest concentration in SVZ (Figure 2B, C, F), indicating increased generation of BPs. The identity of these basal localized cells as BPs was further revealed by positive labeling by Ki67, a marker for cells in cell cycle, and negative labeling by NeuN, a marker for post-mitotic neurons (Figure 2-figure supplement 1). This effect of TBC1D3 expression was also confirmed by the increase in the proportion of cells stained with the mitotic marker phosphorylated Histone (PH3^+) in basal regions and a decrease in cells attached to the ventricular surface (Figure 2D, G). The seemingly non-cell autonomous effect of TBC1D3 expression on proliferation of BPs was most likely caused by different dosages of pE/nestin-TBC1D3 and pCAG-YFP (3:1) used in electroporation, because electroporation with pCAGGS-TBC1D3-IRES-EGFP, a vector co-expressing both TBC1D3 and EGFP, caused increase in numbers of basal BrdU^+ or PH3^+ cells in EGFP^+

179 but not in EGFP⁻ cells (Figure 2-figure supplement 2). The notable slight decrease of
180 EGFP⁻ apical neural progenitors might be due to the disruption of proliferation niche in
181 VZ regions (Figure 2-figure supplement 2B, D, left).

182
183 This increased number of proliferating BPs in basal regions could be caused by
184 increased number of delaminated cells as well as by elevated proliferative capacity of
185 BPs upon TBC1D3 expression. We found that the increase in PH3⁺ BPs was largely
186 abolished when TBC1D3 and N-cadherin were co-expressed in neuroprogenitors via *in*
187 *utero* electroporation (Figure 2D, G), consistent with the contribution of delamination to
188 the increased number of proliferating BPs. To determine whether delamination itself is
189 sufficient to transform vRG to BPs, we over-expressed in vRG the extracellular domain
190 (EC1) of N-cadherin, which has been shown to be capable of disrupting the homophilic
191 intercellular N-cadherin interaction (Tan et al., 2010), and found that EC1 expression
192 caused detachment of vRG cells (Figure 2-figure supplement 3A, B) but had no effect on
193 the proliferation of either apical or basal cells (Figure 2-figure supplement 3C-F). Thus,
194 detachment of vRG cells is a necessary but not a sufficient step for the generation of
195 proliferative BPs.

196
197 How does TBC1D3 expression maintain the high proliferative capacity of detached
198 RG cells? TBC1D3 has been shown to promote cell proliferation (Pei et al., 2002),
199 activate Ras and enhance EGF/EGFR and insulin signaling in non-neuronal cells
200 (Wainszelbaum et al., 2008; Wainszelbaum et al., 2012). In line with this notion, we
201 found that the effect of TBC1D3 on the proliferation of BPs was markedly abrogated by
202 co-expression with Ras^{S17N} (Ras-DN), a dominant-negative form of Ras (Figure 2-figure
203 supplement 4). This result suggests the involvement of Ras signaling in the proliferation
204 of TBC1D3-induced BPs, indicating multiple actions of TBC1D3 in causing increased
205 expansion of BPs.

Expansion of BPs is caused by elevated oRG proliferation

In mice, intermediate progenitors (IPs) that express the transcription factor Tbr2 in the SVZ are the major type of BPs, which undergo terminal division (Lui et al., 2011; Noctor et al., 2004). In primates, however, a recently identified subtype of BPs, namely outer radial glia (oRG) or basal radial glia (bRG), represents the predominant BPs in the expanded OSVZ (Smart et al., 2002). These oRG cells express RG marker Pax6 and/or Sox2 and can divide multiple times to generate many daughter oRG or IPs (Fietz et al., 2010; Hansen et al., 2010). By contrast, the lissencephalic mouse embryonic cortex contains very few oRG cells, which divide only once to generate two neurons (Wang et al., 2011). Highly proliferative oRG cells are thought to be critical for the expansion of primate brain cerebral cortex (Hansen et al., 2010; Sun and Hevner, 2014).

Remarkably, we found that TBC1D3 expression caused an increase in Pax6⁺ cells in the mouse cortex, especially in the basal regions (Figure 3A-C). The RG identity of these cells was further corroborated by the oRG-like morphology and the mode of division. In TBC1D3-expressing mouse cortical slices, we observed that many Sox2⁺ or Pax6⁺ BPs exhibited a single process pointing to the pial surface with intense signals of mitosis-specific phospho-Vimentin (p-Vim) (Figure 3-figure supplement 1A-D), similar to unipolar oRGs identified in the human fetal brain (Fietz et al., 2010; Hansen et al., 2010). However, in control mice, the percentage of Sox2⁺/p-Vim⁺ or Pax6⁺/p-Vim⁺ cells with a basal process was much lower (Figure 3-figure supplement 1A-D). This pial surface contact by oRG process was further examined by application of fluorescent membrane probe DiI to the isolated brain prior to sectioning. In TBC1D3-expressing cortices, we observed many oRG-like cells with a basal process attaching the pial surface and without the apical process attached to the VZ surface (Figure 3D, F). In the control cortices, however, most RGs had both apical and basal processes attaching the pial and

VZ surfaces respectively (Figure 3D, F). Thus, TBC1D3 expression promoted production of oRG cells, which are normally rather rare in mice. In addition, we observed an increase in Tbr2⁺ BPs at 96 hr after electroporation with TBC1D3 construct at E13.5 (Figure 3-figure supplement 1E, F), in accordance with the lineage relationship between oRG cells and IPs (Hansen et al., 2010).

To further identify oRG cells among proliferating BPs, we performed time-lapse imaging of ‘mitotic somal translocation’ (MST) before cytokinesis, a typical oRG behavior during cell division (Hansen et al., 2010). We labeled individual progenitors with H2B-GFP to trace nuclear motion and tdTomato to reveal cell morphology without or with co-electroporation with TBC1D3 expression vector pCS2-Myc-TBC1D3, and brains were sliced 24 hr later for time-lapse imaging. In agreement with the above finding of increased oRG population, the number of cells with MST was markedly higher in TBC1D3-expressing slices, as compared to controls (Figure 3E, G). To visualize and identify the types of oRGs and their daughter cells generated by TBC1D3 expression, we electroporated E13.5 mice with pCAGGS-TBC1D3-IRES-EGFP plasmids (or pCAGGS-IRES-EGFP as the control), followed with time-lapse imaging (Videos 1, 2) and immunostaining (Figure 3H-L) of E14.5 brain slices. More than half (74/120) of proliferating cells labeled by pCAGGS-TBC1D3-IRES-EGFP were typical oRG with a single basal process and an upward MST (Figure 3H, I). In agreement with that observed in the primate OSVZ (Betizeau et al., 2013), we also observed other types of oRGs, including bipolar cells with both apical and basal processes (42/120) and a few cells with a single apical process and a downward MST (4/120) (Figure 3H, I). Post-imaging immunostaining of cell markers showed that, in TBC1D3-electroporated samples, a large fraction of either apical or basal daughter cells derived from oRG cells exhibiting MST continued to express Sox2 but not Tbr2 (Figure 3J-L), consistent with oRG cells with the capacity for multiple rounds of cell division. In line with this notion, birth dating analysis

using sequential labeling with BrdU and EdU showed that the fraction of BrdU⁺EdU⁺ cells was higher in basal regions of TBC1D3-expressing cortices, as compared to that of controls (Figure 3-figure supplement 2). Thus, TBC1D3 expression in mice had endowed the primate-like proliferative potency of oRG cells. Taken together, these results show that the primary action of TBC1D3 expression is to promote the generation of oRG cells with high proliferative capacity, leading to expansion of BPs.

TBC1D3 is essential for the generation of oRGs in cultured human brain slices

To further determine whether TBC1D3 is really essential for the generation of oRG cells in the developing human brain, we took advantage of small interference RNA (siRNA) and investigated the effect of TBC1D3 down-regulation on basal cortical neural progenitors of human brain slices (Figure 4A-F). As shown in Figure 4A, the constructs encoding TBC1D3 siRNAs (1033, 3B, or 440) down-regulated the expression of TBC1D3 in cultured Hela cells in various degrees with siTBC1D3-440 exhibiting most effective effect. Next, vRG cells in cultured fetal human brain slices were transfected with TBC1D3 or control siRNA using electroporation (Figure 4B). After culture for 72 hr, we found that electroporated cells in control samples exhibited normal delamination and a large fraction of them translocated to SVZ regions with typical morphology of oRG cells, whereas majority of siTBC1D3-electroporated cells remained in VZ regions (Figure 4C, D). These results suggest that TBC1D3 is critical for the generation of oRG cells. In line with this notion, basal cells positive for Sox2, which largely represents oRG cells (Pollen et al., 2015; Thomsen et al., 2016), were also markedly decreased in siTBC1D3-expressing samples (Figure 4E, F). This effect was unlikely caused by off-target effect of siTBC1D3, because co-expression with TBC1D3 largely rescued the defect caused by TBC1D3 down-regulation (Figure 4E, F). In agreement with the result that TBC1D3 destabilized N-cadherin transcript, we found that transfection with TBC1D3 siRNA markedly increased stability of N-cadherin mRNA in human neural

progenitor ReNeuron cells (Figure 4G). Taken together, TBC1D3 plays a critical role in the generation of BPs during human brain development.

TBC1D3 expression induces gyrus-like cortical folding in mice

Although the cortex of small rodents is lissencephalic, it has the potential of forming fissures and folds, as shown in recent studies using regional down-regulation of a DNA-associated protein *Trnp1* (Stahl et al., 2013) or exogenous application of FGF2 protein in early mouse embryos (Rash et al., 2013). We found that about one third of mice electroporated with the TBC1D3 construct in neuroprogenitors at E13.5 showed apparent folding of the cortex at regions containing electroporated cells when observed three days postnatal (P3) (Figure 5A). At P7, the cortical folding was more pronounced (Figure 5A), suggesting a cumulative effect of TBC1D3 on the formation of gyrus-like cortical folding in mice. The cortical surface 48 hr after electroporation showed continuous signals of laminin in both control and TBC1D3-electroporated samples (Figure 5-figure supplement 1), largely excluding the possibility that the later observed cortical folding might be attributed to the disruption of pial basement membrane.

To further determine the effect of TBC1D3 expression on cortical cytoarchitecture, we generated transgenic (TG) mice that expressed TBC1D3 under the control of the *nestin* promoter (Figure 5-figure supplement 2A). Three independent founder lines were generated with line 10 exhibiting highest copy number and expression level (Figure 5-figure supplement 2B, C), and thus line 10 was used for further breeding and analyses. Immunostaining indicated that TBC1D3 is mainly distributed in the cytoplasm of Pax6⁺ RG cells (Figure 5-figure supplement 2D). Notably, the expression level of TBC1D3 was progressively increased from early to later embryonic stages (Figure 5-figure supplement 2E). Beginning from E14.5, we observed apparent protrusion of layer 2/3 cells towards the pial surface in the cortex of all TG mice examined (Figure 5B, C; arrows), clear

314 folding of cortical surface could be discerned on cortical surfaces or slices with Nissl
315 staining in P3.5 and in adult mice (Figure 5D-F; asterisks and arrows). Immunostaining
316 of Cux1 and Ctip2, markers for layer 2/3 and layer 5 cortical neurons, respectively,
317 showed clear lamination in the cortex of both control and TG mice, but the TG cortex
318 showed gyrus-like folding (Figure 5C, G). Staining of pan-neuronal marker NeuN and
319 astrocyte marker GFAP also showed folding of the cortical surface in adult TG mice
320 (Figure. 5G, H). We did not observe apparent difference in vertical distribution of new
321 born cortical neurons in TG mice (Figure 5- figure supplement 3), suggesting that cortical
322 folding was unlikely due to neuronal migration defects.

323
324 Gross observation showed that all P3.5 TG mice examined exhibited gyrus-like
325 phenotypes in various degrees (Figure 5-figure supplement 4A). Analysis for whole-brain
326 serial sections showed that these gyrus-like structures were mainly distributed in the
327 primary (M1) and secondary (M2) motor cortex (Figure 5-figure supplement 4B-E). This
328 localized effect may be attributed to temporal restriction of TBC1D3 expression in RG
329 cells of TG mice and the rostral-to-caudal temporal progression of neurogenesis observed
330 in several mammalian species (Caviness et al., 1995; McSherry and Smart, 1986; Rakic,
331 1974).

332
333 Furthermore, we have determined the pattern of neurogenesis in TG mice. At E12.5,
334 the TG mice exhibited an increase in proliferating PH3⁺ BPs, with a wide distribution
335 across basal regions of the cortex, whereas only a single distinct layer contained PH3⁺
336 cells in control mice (Figure 6-figure supplement 1A-D). More strikingly, we observed a
337 marked increase in the population of Sox2⁺Pax6⁺Tbr2⁻ cells in basal regions (Figure 6A,
338 B) and more than half of them exhibited typical morphology of oRG cells (Figure 6C).
339 The presence of elevated oRG cells in the basal regions was also determined by DiI
340 back-labeling on embryos of TG mice (Figure 6D, E). Similar to that observed in

electroporation experiment (see Figure 1E), some of the basal Sox2⁺Tbr2⁻ cells exhibited clustered distribution (Figure 6F, G). Notably, clustered columns of Sox2⁺Pax6⁺Tbr2⁻ cells were observed beneath regions of protrusion (as defined by DAPI staining of cells) at E14.5 (Figure 6H), supporting the ontogeny unit hypothesis for cortex expansion (Rakic, 1988). Unlike basal Pax6⁺ cells, relative density of total Pax6⁺ only slightly increased (Figure 6-figure supplement 1E, F). Sequential labeling with BrdU and EdU for mice at E13.5 and E16.5 also showed an increase in the number of EdU⁺BrdU⁺ basal progenitors in TG mice (Figure 6-figure supplement 2). These results further support the conclusion based on *in utero* electroporation studies that TBC1D3 expression promotes the generation of highly proliferative BPs in mice. Besides morphological features and mode of division, several molecular markers have been identified for oRG cells, including HOPX (Pollen et al., 2015; Thomsen et al., 2016). Interestingly, many HOPX⁺ cells were observed in basal extra-VZ regions of TG mice, whereas these cells were barely detectable in WT control mice (Figure 6I, J). Thus, we conclude that TBC1D3 expression promotes generation of oRG cells in mice.

We next examined whether neuronal density in the cortex is affected in TG mice expressing TBC1D3. Brain sections were immunostained with Cux1/Ctip2 or NeuN/GFAP. At both P3.5 and P28, TG mice exhibited increased neuronal density in the motor cortex showing surface folding, particularly in the layer 2/3 (Cux1⁺), as compared to corresponding regions in WT littermates (Figure 6-figure supplement 3A-E). In adult mice (P28), we did not observe apparent changes in the density of GFAP⁺ astrocytes (Figure 6-figure supplement 3C, F). These results suggest that TBC1D3-induced cortical expansion is mainly due to increased number of neurons rather than astrocytes. Although cortical folding was enriched in motor cortex, we also observed a mild increase in the density of Cux1⁺ in sensory cortex, which formed much less folds (Figure 5-figure supplement 4 and Figure 6-figure supplement 3G, H).

TBC1D3 expression down-regulates *Trnp1* transcription and up-regulates ERK signaling

Because delamination and elevation of the proliferative capacity of BPs are both required to account for the observed TBC1D3-induced oRG generation and cortical folding, we further examined the effect of TBC1D3 expression on the intrinsic stemness signaling pathways in BPs. Interestingly, we found that TBC1D3 expression in neuroprogenitors by *in utero* electroporation at E13.5 caused a reduced expression of *Trnp1* in flow cytometry-sorted cells at E15.5, as compared to that found in control cells sorted from vehicle-electroporated mice (Figure 7A), consistent with the finding that regional down-regulation of *Trnp1* expression causes cortical folding in mice (Stahl et al., 2013). Unlike the role in destabilizing N-cadherin transcript, TBC1D3 expression had no effect on the stability of *Trnp1* mRNA (Figure 7E). This result indicates a linkage between TBC1D3 and known factors that modulate fate transition from RGs to BPs. In addition to *Trnp1*, Notch signaling has been proposed to play a role in maintaining the progenitor status of human oRG cells (Hansen et al., 2010). However, we found that TBC1D3 expression had no effect on the transcriptional level of *Hes1* and *Hes5*, effectors of Notch signaling, as well as *Numb*, which encodes an endocytic adaptor protein that acts as a Notch pathway inhibitor localized to the apical membrane (Figure 7B-D). The Ras-Raf-ERK signaling cascade mediates the mitotic role of EGF/EGFR signaling pathway in promoting cell proliferation (Citri and Yarden, 2006). We found that the signals for activated phospho-ERK1/2 (pERK1/2) was elevated in TBC1D3 TG mice, mostly in VZ/SVZ regions (Figure 7F, G), in line with the previous observation that TBC1D3 enhanced the ERK signaling (Wainszelbaum et al., 2008; Wainszelbaum et al., 2012). Notably, almost all (99.1%) of Pax6⁺Tbr2⁻ oRG cells in developing human cortex were positively stained by pERK1/2 (Figure 7H, I), further supporting the role of ERK signaling in oRG proliferation. The combined actions of TBC1D3 on parallel or separate

cell proliferation pathways may account for the observed role of TBC1D3 in maintaining cell stemness potency.

Discussion

In this study, we found a remarkable effect of the hominoid-specific gene TBC1D3 in promoting the generation of oRG cells in mice with a high proliferative ability previously observed in primates. Importantly, this oRG generation is accompanied by the appearance of cortical folding. Furthermore, we elucidated the cellular mechanisms underlying the generation of proliferative oRG cells by showing that TBC1D3 expression caused increased delamination of VZ neuroprogenitors via down-regulation of N-cadherin, and elevated proliferative ability of BPs is accompanied by a reduced expression of *Trnp1* and likely involves Ras-ERK signaling cascade. These effects together resulted in the expansion and dispersion of BPs, giving rise to increased number of newborn neurons and leading to cortical folding (for model see Figure 7J).

In small rodents, RGs in the VZ and IPs in the SVZ are two major cell types responsible for cortex development. However, amplification of VZ progenitors via overexpression of β -catenin in the mouse brain led to the folding of the ventricular rather than cortical surface (Chenn and Walsh, 2002), and amplification of IPs only increased the brain size without inducing cortical folding in mice (Nonaka-Kinoshita et al., 2013). Recent studies have established the association between the relative abundance of oRG and the degree of cortical folding in various species (Betizeau et al., 2013; Hansen et al., 2010; Reillo et al., 2011; Shitamukai et al., 2011; Wang et al., 2011). In the present study, we showed that increased population of oRG in mice is accompanied with cortical fold formation, supporting the critical role of highly proliferative oRG in cortical expansion and gyrification in primates.

It is postulated that oRG cells are derived from the ventricular RGs, presumably requiring delamination from apical anchoring (Borrell and Gotz, 2014). However, loss of adherens junction proteins or breaking their linkage to the cytoskeletal belts by down-regulating the small GTPase RhoA (Cappello et al., 2012; Lien et al., 2006) had little effect on oRG generation or cortical folding, although apically anchored progenitor cells became delaminated. Thus, delamination of VZ progenitors is not sufficient for generating highly proliferative BPs, and changes in cell cycle regulatory factors are also be required. In the present study, we showed that expression of TBC1D3 led to not only down-regulation of N-cadherin, leading to VZ progenitor delamination, but also reduced Trnp1 expression and enhanced ERK signaling that could be involved in elevated proliferation of delaminated cells. Furthermore, other functions of TBC1D3 may also contribute to the cortical folding phenotype we observed. For examples, cell culture studies of TBC1D3 have suggested its potential role in membrane endocytosis, as well as Ras activation and epidermal growth factor receptor (EGFR) signaling (Wainszelbaum et al., 2008), processes that may be involved in various aspects of neural development leading to cortical folding and gyrification. Indeed, we found that Ras activity was involved in TBC1D3-induced proliferation of BPs. Recent single-cell transcriptome analyses of human oRG cells have identified multiple preferentially expressed genes related to extracellular matrix formation, cell migration, and stemness, including the most specific oRG marker HOPX (Pollen et al., 2015; Thomsen et al., 2016). Strikingly, many HOPX positive cells were observed in TBC1D3 TG mice. The relationship between TBC1D3 expression and these oRG markers remains to be clarified. Simple ectopic localization of RG cells outside of the ventricular zone may not be sufficient to cause cortical expansion or folding as shown in a previous study (Yoon et al., 2014). Appearance of oRG-like features, including the contact with pia surface by the basal process, multiple rounds of cell division, expression of specific markers, as well as clustered regional distribution of BPs observed in this study, may play prominent roles in

cortical folding.

Cortical expansion is assumed to be associated with the emergence of uniquely cognitive skills in primates (Luders et al., 2008; Zilles et al., 2013). However, this hypothesis has been mainly based on across species comparative studies. Global or regional-specific changes in gyrification index (GI) have been observed in brains of subjects following various types of extensive training (Amunts et al., 1997; Luders et al., 2012; Luders et al., 2008). For example, in keyboard players, the local GI increases in response to early onset of professional training and duration of practice, and correlates with motor performance (Amunts et al., 1997). Conversely, a significant decline in the cortical GI was observed in patients with mental disorders (Bonnici et al., 2007; Wolosin et al., 2009). Understanding of the precise contribution of cortical expansion and gyrification to cognition functions has been challenging due to the lack of appropriate animal model systems. The deliberate behavior analyses for TG mice generated in this work may provide a link between cortex expansion and higher brain functions.

Recently, a human-specific gene *ARHGAP11B* has been shown to promote production of basal IPs and cause cortical folding in the electroporated mouse brain (Florio et al., 2015). We propose that *TBC1D3*, which appeared earlier than *ARHGAP11B* during human evolution (Florio et al., 2015; Hodzic et al., 2006; Perry et al., 2008), acts as a candidate gene that controls many other genes involved in cortex expansion and folding. Multiple genes underlying different or shared cellular processes associated with neurogenesis may all contribute in part to the formation of cortical folding and gyrification found in primates. Thus, it would be of great interest to elucidate gene expression networks related with *TBC1D3* expression. Identification of the ‘hub’ genes of such networks may further clarify the role of *TBC1D3* in the cytoarchitectural

development on the cortex. This study provides proof-of-concept that the brain development can be regulated by duplicated genes during hominoid evolution.

Materials and methods

Human fetal brain collection

Human fetal brain tissue samples were collected at autopsy within 3 hr of spontaneous abortion with the informed consent of the patients following protocols and institutional ethic guidelines stated in our previous study (Ma et al., 2013). Brain tissues were stored in ice-cold Leibowitz-15 medium and transported to the laboratory for further examination and processing (Lui et al., 2014).

Animals

ICR mice were used for all *in utero* electroporation experiments, and the TBC1D3-transgenic mouse was constructed and kept in the C57BL/6 background. All the mice were housed in the institutional animal care facility with a 12 hr light-dark schedule. The use of all mice in this study was in compliance with the guidelines of the Institutional Animal Care and Use Committee.

Analysis for TBC1D3 mRNA levels in human samples

Fetal (GW 26 to 40) or adult (21 to 29 years) human brain RNA samples (Clontech) were reverse transcribed into cDNA with QuantScript RT kit using oligo (dT)₁₅ primers (Tiangen) followed by PCR using TBC1D3 primers: 5'-ATCGAGCGTACAAGGGAATG-3' (forward), 5'-CCGTATCGATCCCTGAAGAA-3' (reverse). GAPDH was used as the control.

Plasmids and *in utero* electroporation

Fetal human brain RNA (Clontech) was reverse transcribed with QuantScript RT kit using oligo (dT)₁₅ primers (Tiangen). TBC1D3 cDNA was acquired by PCR and cloned into pE/nestin-EGFP vectors (a kind gift from Dr. H. Okano) (Kawaguchi et al., 2001), to generate the pE/nestin-TBC1D3 plasmid after replacing the EGFP sequence. To construct the pCAGGS-TBC1D3-IRES-EGFP plasmid, TBC1D3 cDNA was amplified by PCR from pE/nestin-TBC1D3 and subcloned into the AscI-XhoI site of pCAGGS-IRES-EGFP. The pE/nestin-TBC1D3^{Δ286-353} (Δ286-353) plasmid was produced by site-directed PCR mutagenesis method. The pCS2-Myc-TBC1D3 construct was generated by inserting TBC1D3 cDNA fragment into the EcoRI-XhoI site of pCS2-MT vector. The pKH3-N-cadherin and pCS2-EC1 (Tan et al., 2010) plasmids were kind gifts from Dr. X. Yu. Following oligonucleotides were synthesized (Invitrogen) for the generation of vectors encoding small interference RNA targeting TBC1D3:

siTBC1D3-1033 (forward, 5'-
GATCCCCGCCTCTATGAAGAACTAATTCAAGAGATTAGTTTCTTCATAGAGG
CTTTTTGGAAA -3', reverse, 5'-
AGCTTTTCCAAAAAGCCTCTATGAAGAACTAATCTCTTGAATTAGTTTCTTC
ATAGAGGCGGG -3'), siTBC1D3-440 (forward, 5'-
GATCCCCGGGACGTAAGCGGGACATTAATTCAAGAGATTAATGTCCCGCTTA
CGTCCCTTTTTGGAAA -3', reverse, 5'-
AGCTTTTCCAAAAAGGGACGTAAGCGGGACATTAATCTCTTGAATTAATGTC
CCGCTTACGTCCCGGG -3'); siTBC1D3-3B forward, 5'-
GATCCCCGGATATTGATTGACGGGATTCTCAAGAGAATCCCGTCAATCAATAT
CCTTTTTGGAAA -3', reverse, 5'-
AGCTTTTCCAAAAAGGATATTGATTGACGGGATTCTCTTGAATCCCGTCAAT
CAATATCCGGG -3') (Frittoli et al., 2008). After annealing, the oligos were inserted into BglIII/HindIII digested pSuper plasmid. *In utero* electroporation was performed according to the previously reported protocol (Saito, 2006). In brief, a timed pregnant

mouse at E13.5 was anesthetized with pentobarbital sodium, the uterine horns were exposed, and ~1 µl of plasmids mixed with 0.1 mg/ml fast green (Sigma) were manually microinjected into the lateral ventricle with a beveled sharp glass micropipette (VWR International). For electroporation, five 50-ms pulses of 35 mV with a 950-ms interval were applied across the uterus with two 3-mm, in radius, disc electrodes (BEX, LF650P3) located on either side of the head (BTX, ECM830) and the pre-warmed (37°C) 0.9% NaCl was used to keep the uterus wet. After electroporation, the uterus was put back into the abdominal cavity, filled with warmed 0.9% NaCl, and the wound was surgically sutured. The mouse was then placed on a warmed blanket before recovery and resuming normal activity.

mRNA stability assay

The human neural progenitor cell line ReNeuron was cultured on 0.5% (v/v) of 1 mg/ml laminin-coated dishes in DMEM/F12 full media containing 2% B27 (Gibco), 10 units/ml heparin (Sigma), 20 ng/ml EGF (Millipore), and 10 ng/ml bFGF (Millipore). For plasmid transfection, the cultured ReNeuron cells were dissociated into single cells with accutase (Sigma) and electroporated in the program X-001 by using the NucleofectorTM 2b device (Lonza), with plasmids encoding TBC1D3, siRNA against TBC1D3, or corresponding vehicle plasmids. At the second (for TBC1D3 over-expression) or third day (for TBC1D3 knockdown) post transfection, cells were treated with 1 µg/ml actinomycin D (Sigma) for 0, 2 or 4 hr to inhibit gene transcription. Total RNA was extracted with Trizol (Ambion) and analyzed by RT-qPCR to detect the respective mRNA levels with following primers:

human *Cdh2* (forward, 5' -ATGAAAGACCCATCCACG- 3', reverse, 5'-TCCTGCTCACCACCACTA-3'); human *Fos* (forward, 5'-TCCGAAGGGAAAGGAATAA-3', reverse, 5'-TGAGCTGCCAGGATGAACT-3'); human *Hprt* (forward, 5'-TGACCTGCTGGATTACAT-3', reverse, 5'-TTGGATTATACTGCCTGA-3'); human *TBC1D3* (forward,

5'-AGGTTTCAGCAGAAGCGCCTCA-3', reverse
5'-GCCTGGATGCCGACGACCCTT-3'); human *Trnp1* (forward,
5'-GGAGGGGACGGCAGAGCAGA-3', reverse
5'-GGGTCGGGGTAGGAGTCAAGGT-3'). The vitality and transfection efficiency of
ReNeuron cells were monitored under fluorescence microscopy during actinomycin D
treatment and before RNA extraction.

Histology, immunohistochemistry and confocal imaging

Postnatal mouse was perfused with phosphate buffered saline (PBS) followed with cold
4% paraformaldehyde (PFA) and prenatal mouse was perfused with cold 4% PFA
directly, and then the brain was dissected out and post-fixed into cold 4% PFA in PBS at
4°C overnight. The fixed brain was dehydrated in 20% sucrose in PBS at 4°C and
ultimately sectioned into 30 µm cryosections collected on glass slides, or 50 µm
cryosections floating in PBS. The fetal human brain tissues were fixed in 4% PFA in PBS
at 4°C for 3 days and dehydrated in 30% sucrose in PBS. After embedded and frozen at
-80°C in O.C.T. compound (Tissue-Tek), the tissues were sectioned into 40 µm
cryosections and stored at -80°C. For histological analysis, frozen sections were stained
with 1% cresyl violet (Sigma) for *Nissl* staining. For immunohistochemistry, mouse brain
slices were washed in PBS for 3 times and permeated in 0.3% (v/v) Triton X-100 in PBS
for 30 min at room temperature (RT). After above treatments, brain sections were
incubated directly in a blocking solution (10% (v/v) donkey serum in PBS) for 1 hr,
followed by the incubation with the primary antibodies at 4 °C overnight. Sections were
then washed with PBS for 3 times followed by incubation with the appropriate secondary
antibodies for 1-2 hr at room temperature (RT). For the labeling of actin filaments, mouse
brain slices were incubated with phalloidin-Alexa 647 (1:40, Invitrogen) in blocking
solution with 0.1% Triton X-100 for 1-2 hr at RT. Fetal human brain cryosections were
subjected to heat-induced antigen retrieval in 10 mM sodium citrate (pH = 6.0) for 10

min, then followed by above procedures. All labeled sections were mounted with fluorescent mounting medium (Dako) and stored at 4°C. The primary antibodies used were: mouse anti-TBC1D3 (Santa Cruz sc-376073, 1:100), mouse anti-NeuN (Millipore MAB377, 1:500), rat anti-Ctip2 (Abcam ab18465, 1:1,000), rabbit anti-Cux1 (Santa Cruz sc-13024, 1:200), rabbit anti-GFP (Invitrogen A11122, 1:1,000), chicken anti-GFP (Aves Lab #GFP-1020, 1:500), goat anti-Sox2 (Santa Cruz sc-17320, 1:200), rabbit anti-Sox2 (Millipore ab5603, 1:500), rabbit anti-Pax6 (Covance PRB-278P, 1:1,000), rabbit anti-Tbr2 (Abcam ab23345, 1:500), chicken anti-Tbr2 (Millipore AB15894, 1:200), mouse anti-phospho-Vimentin (MBL International D076-3s, 1:500), rat anti-BrdU (Abcam ab6326, 1:1,000), rabbit anti-phospho-histone H3 (ser10) (Santa Cruz sc-8656-R, 1:400), rabbit anti-N-cadherin (Abcam ab12221, 1:500), rabbit anti-GFAP (Dako z0334, 1:1,000), goat anti-Numb (Abcam ab4147, 1:400), rat anti-ITGB1 (Millipore MAB1997, 1:500), rabbit anti-pERK1/2 (Cell Signaling Technology #4370, 1:500), rabbit anti-laminin (Sigma L9393, 1:400), rabbit anti-HOPX (Sigma HPA030180, 1:1000). Secondary antibodies were: AlexaFluor 488 (1: 1,000), 546 (1: 1,000), 594 (1: 500), or 647 (1: 1,000) -conjugated donkey anti-goat, -rabbit, -rat, -mouse IgG (Invitrogen), or -chicken (Sigma). All images were acquired on a Nikon A1R laser confocal microscope except that the labeled brain slices from time-lapse imaging were imaged on the Olympus FV10i-O with a 10x (zoom x2) air objective lens.

***In situ* hybridization**

Fresh mice brains were mounted in O.C.T. compound (Tissue-Tek) and frozen at -80°C to be sectioned coronally (30 µm) with a cryostat (Leica CM1950). Cryosections were collected on superfrost plus microscope slides (Fisher Scientific). To generate template cDNA for RNA probe synthesis, mouse total RNA was extracted from cortical samples of E15.5 fetus by standard Trizol (Life Technologies) method and reverse transcribed with QuantScript RT kit using oligo (dT)₁₅ primers (Tiangen). *N-cadherin* gene was

amplified using primers: 5'-CTGCCATGACTTTCTACGG-3' (forward),
5'-GGTTGATGGTCCAGTTTC-3' (reverse). *TBC1D3* was amplified using primers:
5'-ATGGACGTGGTAGAGGTCGC-3' (forward),
5'-CTAGAAGCCTGGAGGGAACTG-3' (reverse). PCR products of predicted band size
were gel extracted and ligated into the pGEM®T Vector System (Promega). Ligation
products were transfected into DH5α competent E.coli (Tiangen) and confirmed by
sequencing. Digoxigenin labeled RNA probes for in situ hybridization were generated by
amplifying target DNA fragments from pGEM®T vector using T7 or SP6 RNA
Polymerase (Promega) in the presence of DIG RNA Labeling Mix (Roche). Synthesized
anti-sense or sense RNA probes (1 ng/μl) were applied in hybridization. The detailed
procedure for *in situ* hybridization was performed as described previously (Wallace and
Raff, 1999). Images were collected with Nikon microscope ECLIPSE E600FN with an
Optonics MicroFire digital camera.

Mouse brain slice culture and time-lapse imaging

The detailed procedure for brain slice culture and time-lapse imaging was performed
mainly as reported previously (Wang et al., 2011) with some modifications. E13.5 fetal
mice brain cortices were electroporated with 0.6 μg/μl pCAGGS-TBC1D3-IRES-EGFP
plasmids, or 1 μg/μl pCS2-Myc-TBC1D3 plus 0.5 μg/μl pCAG-H2BGFP-2A-tdTomato,
with pCAGGS-IRES-EGFP or pCS2-MT as respective control. And at 24 hr
post-electroporation, brain tissues were dissected out into ice-cold artificial cerebrospinal
fluid (ACSF) containing 125 mM NaCl, 5 mM KCl, 1.25 mM NaH₂PO₄, 1 mM MgSO₄,
2 mM CaCl₂, 25 mM NaHCO₃ and 20 mM D-(+)-glucose (all from Sigma); pH 7.4, 310
mOsm l⁻¹. Brains were embedded into 3% low melting temperature agarose in ACSF and
sectioned at 300 μm thickness using a Leica VT1200S vibratome. Then brain slices were
transferred and collected temporarily in ice-cold ACSF pre-oxygenated with 95% O₂, 5%
CO₂. Rostral brain slices containing EGFP-positive cells were selected and transferred

onto a slice culture insert (Millicell, Millipore) in a glass-bottom Petri dish (Eppendorf) with pre-warmed (37°C) culture medium containing (v/v) 66% Eagle's basal medium, 25% Hanks balanced salt solution (without calcium and magnesium), 5% FBS, 1% N₂ supplement, 1% penicillin/streptomycin, 2 mM L-glutamine (all from Gibco) and 0.66% (w/v) D-(+)-glucose (Sigma). Brain slices were maintained in a humidified incubator at 37°C with constant 5% CO₂ supply for 2-3 hr before time-lapse imaging. All the time-lapse images in this study were collected in 20 min intervals and 14-hr duration by using Olympus laser confocal microscope FV10i-W with a Built-in incubator (37°C) streamed with 5% CO₂, 95% O₂ and an 10x (zoom x2) air objective lens. For identifying the types of daughter cells divided from oRG-like cells, brain slices, after time-lapse imaging, were fixed immediately in cold 4% PFA overnight and then stained using the method mentioned above.

Culture and electroporation of embryonic human brain slices

Fresh embryonic brain samples obtained from voluntary abortions were treated mainly following the procedures described in a previous study (Pollen et al., 2015). Briefly, samples were transferred and dissected in filtered ACSF containing antibiotic antimycotic (Gibco) equilibrated with 5% CO₂, 95% O₂, embedded in 4% low melting point agarose (Invitrogen) and 300 µm coronal sections were prepared in the presence of ACSF using vibrating microtome. Brain slices were transferred into slice culture inserts (Millicell, Millipore) in 6-well culture plates (Corning) with culture media containing 66% Eagle's basal medium, 25% Hanks balanced salt solution, 5% fetal bovine serum, 1% N-2 supplement, 1% antimycotic, and 1% glutaMAX supplement (all from Gibco), and equilibrated at 37 °C in 95% O₂, 5% CO₂ for 2-3 hr. Then the brain slices were subjected to electroporation with 1-3 µg indicated plasmids using a pair of home-made electrode (five 50-ms 40 mV pulses with a 950-ms interval). After electroporation, slices were cultured in fresh medium in a 37 °C incubator at 5% CO₂, 95% O₂ for three days,

followed by fixation in 4% PFA overnight, three washes with PBS, antigen retrieval (Beyotime) for 4 hr at RT, permeabilization with 2% Triton-X 100 in PBS at 4°C overnight, and finally immunostaining with indicated antibodies, which were diluted in blocking buffer containing 10% donkey serum, 0.5% Triton-X 100 and 0.2% gelatin in PBS.

Fluorescence-activated cell sorting and quantitative real-time PCR

Mice brains (E15.5) were dissected out at 48 hr post-electroporation with pE/nestin-TBC1D3 or vehicle control, mixed with pCAG-YFP in a ratio of 3:1, and placed in cold ACSF pre-oxygenated with 95% O₂, 5% CO₂. The YFP-positive cortical region was removed using an inverted fluorescence microscope (Olympus CKX41) and digested in 0.025% trypsin (Sigma) in ACSF for 20 min at 37°C and then centrifuged for 5 min at 1200 rpm. After removing the trypsin supernatant, tissue was re-suspended in 1 ml of ACSF containing 3% FBS (Hyclone) and manually triturated by pipetting up and down approximately nine times. The suspension was passed through a 40-µm nylon cell strainer (BD Falcon) to obtain single-cell suspension and stored on ice before sorting. The YFP-positive cells were sorted into RNase-free tubers (Axygen) on ice by using a MoFlo XDP flow cytometry (Beckman Counter). The sorted cells (5×10^4 - 2×10^5) were centrifuged for 10 min at 300 g and the supernatant was removed. Total RNA from sorted YFP-positive cells (5×10^4 - 2×10^5) was extracted immediately by using an RNeasy Micro Kit (Qiagen) and reverse transcribed with QuantScript RT kit using oligo(dT)₁₅ primers (Tiangen). Real-time PCR was performed by using the Agilent Mx3000P qPCR system with the SYBR[®] Premix Ex Taq[™] II (Takara). Quantification was performed by the delta cycle time method, with mouse GAPDH used for normalization. The specific primers are:

GAPDH, 5'-AGAGTGTTCCTCGTCCCG-3' (forward),
5'-CCGTTGAATTTGCCGTGA-3' (reverse); *N-cadherin*,
5'-CCCCAAGTCCAACATTTC-3' (forward), 5'-CGCCGTTTCATCCATACC-3'

690 (reverse); *Numb*, 5'-TAGAGCGTAAACAGAAGCG-3' (forward),
 691 5'-CACTGATGGACCAACAAC-3' (reverse); *Hes1*,
 692 5'-TGACGGCCAATTTGCCTTTC-3' (forward), 5'-TTCCGCCACGGTCTCCACA-3'
 693 (reverse); *Hes5*, 5'-GCACCAGCCCAACTCCAA-3' (forward),
 694 5'-TCAGGAACTGTACCGCCTCC-3' (reverse); *Trnp1*,
 695 5'-CCCAGGAAGGGACGGCAGAA-3' (forward),
 696 5'-CCTCGGGTAAGGGCGGTGA-3' (reverse).

697

698 **BrdU/EdU double labeling**

699 Sequential 5-bromo-2'-deoxyuridine/5-ethynyl-2'-deoxyuridine (BrdU/EdU) double
 700 labeling was performed mainly as previously described with some modifications
 701 (Insolera et al., 2014). *In utero* electroporation was conducted at E13.5 according to the
 702 method described above. The pregnant female mouse was injected intraperitoneally (i.p.)
 703 with 50 mg/kg BrdU (Sigma) at E14.5 and 100 µg EdU (Life Technologies) at E15.5.
 704 After 2 hr, fetal mice brains were dissected and fixed immediately in cold 4% PFA in
 705 PBS at 4°C overnight, followed by dehydration in 20% sucrose in PBS at 4°C. For
 706 transgenic mice, BrdU and EdU were sequentially injected at E13.5 and E16.5,
 707 respectively. Frozen sections (50 µm) were collected in PBS as described above. BrdU
 708 staining was performed using the manufacturer's protocol (Abcam). In brief, brain
 709 sections were successively treated with 1 M HCl for 10 min on ice, 2 M HCl for 10 min
 710 at RT and another 20 min at 37°C to denature the DNA. Immediately after the acid
 711 incubations, sections were transferred into 0.1 M borate buffer, pH 9.0, for 10 min of
 712 neutralization at RT. After washes with PBS, brain sections were treated with 0.3%
 713 Triton X-100 in PBS for 30 min followed by incubation in 10% donkey serum in PBS for
 714 1 hr at RT, followed by incubation with primary antibodies (mouse anti-BrdU, Life
 715 Technologies B35128, 1:200; chicken anti-GFP, Aves Lab #GFP-1020, 1:500) at 4°C
 716 overnight, washes and incubation with the appropriate secondary antibodies for 1-2 hr at

RT. EdU staining was performed using a Click-iT[®] Plus EdU Imaging Kit (Life Technologies C10640) immediately after the incubation of secondary antibodies.

Transgenic mice

The detailed procedure for producing TBC1D3-transgenic mice was performed mainly as described previously (Behringer et al., 2013). Briefly, to obtain *nestin*-TBC1D3 fragments, pE/*nestin*-TBC1D3 plasmids were digested with *Dra*III and *Mfe*I (New England BioLabs). The target fragments were purified directly from the gel using a Whatman S&S ELUTRAP Electro-Separation System and diluted into 3 ng/ul in injection buffer for microinjection. Then the *nestin*-TBC1D3 fragments were injected into the pronucleus of C57BL/6 mouse zygotes and the injected embryos were implanted into the oviducts of day 1 pseudopregnant foster females (ICR). The TBC1D3-transgenic mice were identified by PCR using tail genomic DNA with specific primers: 5'-CCCACAACCTCCGATTACTCAA -3' (forward, P1), 5' -CGCCTGTTCGCCTTCTAC -3' (reverse, P2). The analysis and maintenance for TBC1D3-transgenic mouse was performed in the background of C57BL/6.

DiI labeling

Mouse brains were dissected out in cold PBS and fixed in cold 4% PFA in PBS at 4°C overnight, followed by removal of the meninges that covers the cortical surface. The DiI crystals (Life Technologies) were dissolved in 100% ethanol to a final concentration of 1 mg/ml in 1 ml final volume. Then each brain sample was transferred to 1 ml fresh 4% PFA in PBS added with 30 µl of 1 mg/ml DiI solution and incubated at 37°C for another 24 hr. After DiI labeling, brains were washed with PBS, sectioned on the vibratome (Leica VT1200S) into 100 µm slices, and stained with DAPI before mounting.

Image processing, quantitative analysis, and presentation

All images were processed by ImageJ or Fiji software. For each experiment with mice or cells, at least 3 biological replicates were performed. Biological replicates are defined as independent experiments in cells or the same experiment with different mouse embryos. For all experiments, statistical tests were performed using SigmaStat software: one way ANOVA followed by *Student-Newman-Keuls* test for multiple comparisons, or one way ANOVA on Ranks followed with Dunn's test for multiple comparisons for raw data without passing normality test or equal variance test, except for Figure 2-figure supplement 2B and 2D where two-way ANOVA followed with *Student-Newman-Keuls* test for multiple comparisons was used. Results presented as dot plots were accompanied by the mean value (red line) and a box plot in the background depicting confident interval. The sample size (n), the mean, the standard error of the mean (SEM), and the p-value are presented in the figure legends. The statistical significance was indicated by: *, $P < 0.05$; **, $P < 0.01$; ***, $P < 0.001$; ns, no significant difference.

Acknowledgements

This study was partially supported by grants from the National Key Basic Research Program of China (2014CB910203), National Natural Science Foundation of China (31330032, 31490591, 31321091, and 61327902), and the Strategic Priority Research Program of the Chinese Academy of Sciences (XDB02040003). We are grateful to Dr. M.M. Poo for critical reading of the manuscript. We thank L. Li for the assistance in the generation of transgenic mice, Dr. Q. Hu of ION Imaging Facility with microscope analysis, Dr. X. Zhang for expert assistance with in situ hybridization, Dr. X. Yu for providing the N-cadherin constructs, and Dr. H. Okano for providing the pE/nestin-EGFP construct.

References

Amunts K, Schlaug G, Jancke L, Steinmetz H, Schleicher A, Dabringhaus A, Zilles K. 1997. Motor cortex and hand motor skills: structural compliance in the human brain. *Hum Brain Mapp* **5**: 206-15. doi: 10.1002/(SICI)1097-0193(1997)

Arcila ML, Betizeau M, Cambronner XA, Guzman E, Doerflinger N, Bouhallier F, Zhou H, Wu B, Rani N, Bassett DS, Borello U, Huissoud C, Goodman RH, Dehay C, Kosik KS. 2014. Novel primate miRNAs coevolved with ancient target genes in germinal zone-specific expression patterns. *Neuron* **81**: 1255-62. doi: 10.1016/j.neuron.2014.01.017

Behringer R, Gertsenstein M, Nagy K, Nagy A. 2013. *Manipulating the Mouse Embryo: A Laboratory Manual*. New York: Cold Spring Harbor Laboratory Press

Betizeau M, Cortay V, Patti D, Pfister S, Gautier E, Bellemin-Menard A, Afanassieff M, Huissoud C, Douglas RJ, Kennedy H, Dehay C. 2013. Precursor diversity and complexity of lineage relationships in the outer subventricular zone of the primate. *Neuron* **80**: 442-57. doi: 10.1016/j.neuron.2013.09.032

Bonnici HM, William T, Moorhead J, Stanfield AC, Harris JM, Owens DG, Johnstone EC, Lawrie SM. 2007. Pre-frontal lobe gyrification index in schizophrenia, mental retardation and comorbid groups: an automated study. *NeuroImage* **35**: 648-54. doi: 10.1016/j.neuroimage.2006.11.031

Borrell V, Gotz M. 2014. Role of radial glial cells in cerebral cortex folding. *Curr Opin Neurobiol* **27**: 39-46. doi: 10.1016/j.conb.2014.02.007

Campos LS, Leone DP, Relvas JB, Brakebusch C, Fassler R, Suter U, French-Constant C. 2004. Beta1 integrins activate a MAPK signalling pathway in neural stem cells that contributes to their maintenance. *Development* **131**: 3433-44. doi: 10.1242/dev.01199

Cappello S, Bohringer CR, Bergami M, Conzelmann KK, Ghanem A, Tomassy GS, Arlotta P, Mainardi M, Allegra M, Caleo M, van Hengel J, Brakebusch C, Gotz M. 2012. A radial glia-specific role of RhoA in double cortex formation. *Neuron* **73**: 911-24. doi: 10.1016/j.neuron.2011.12.030

Caviness VS, Jr., Takahashi T, Nowakowski RS. 1995. Numbers, time and neocortical neurogenesis: a general developmental and evolutionary model. *Trends Neurosci* **18**: 379-83. doi: 10.1016/0166-2236(95)93933-O

Chenn A, Walsh CA. 2002. Regulation of cerebral cortical size by control of cell cycle exit in neural precursors. *Science* **297**: 365-9. doi: 10.1126/science.1074192

Citri A, Yarden Y. 2006. EGF-ERBB signalling: towards the systems level. *Nat Rev Mol Cell Biol* **7**: 505-16. doi: 10.1038/nrm1962

Fietz SA, Huttner WB. 2011. Cortical progenitor expansion, self-renewal and neurogenesis-a polarized perspective. *Curr Opin Neurobiol* **21**: 23-35. doi: 10.1016/j.conb.2010.10.002

Fietz SA, Kelava I, Vogt J, Wilsch-Brauninger M, Stenzel D, Fish JL, Corbeil D, Riehn A, Distler W, Nitsch R, Huttner WB. 2010. OSVZ progenitors of human and ferret neocortex are epithelial-like and expand by integrin signaling. *Nat Neurosci* **13**: 690-9. doi: 10.1038/nn.2553

Fietz SA, Lachmann R, Brandl H, Kircher M, Samusik N, Schroder R, Lakshmanaperumal N, Henry I, Vogt J, Riehn A, Distler W, Nitsch R, Enard W, Paabo S, Huttner WB. 2012. Transcriptomes of germinal zones of human and mouse fetal neocortex suggest a role of extracellular matrix in progenitor self-renewal. *Proc Natl Acad Sci U S A* **109**: 11836-41. doi: 10.1073/pnas.1209647109

Florio M, Albert M, Taverna E, Namba T, Brandl H, Lewitus E, *et al.* 2015. Human-specific gene ARHGAP11B promotes basal progenitor amplification and neocortex expansion. *Science* **347**: 1465-70. doi: 10.1126/science.aaa1975

Florio M, Huttner WB. 2014. Neural progenitors, neurogenesis and the evolution of the neocortex. *Development* **141**: 2182-94. doi: 10.1242/dev.090571

Frittoli E, Palamidessi A, Pizzigoni A, Lanzetti L, Garre M, Troglio F, Troilo A, Fukuda M, Di Fiore PP, Scita G, Confalonieri S. 2008. The primate-specific protein TBC1D3 is required for optimal macropinocytosis in a novel ARF6-dependent pathway. *Mol Biol Cell* **19**: 1304-16. doi: 10.1091/mbc.E07-06-0594

Geschwind DH, Rakic P. 2013. Cortical evolution: judge the brain by its cover. *Neuron* **80**: 633-47. doi: 10.1016/j.neuron.2013.10.045

Hansen DV, Lui JH, Parker PR, Kriegstein AR. 2010. Neurogenic radial glia in the outer subventricular zone of human neocortex. *Nature* **464**: 554-61. doi: 10.1038/nature08845

He Z, Tian T, Guo D, Wu H, Chen Y, Zhang Y, Wan Q, Zhao H, Wang C, Shen H, Zhao L, Bu X, Wan M, Shen C. 2014. Cytoplasmic retention of a nucleocytoplasmic protein TBC1D3 by microtubule network is required for enhanced EGFR signaling. *PLoS One* **9**: e94134. doi: 10.1371/journal.pone.0094134

Hodzie D, Kong C, Wainszelbaum MJ, Charron AJ, Su X, Stahl PD. 2006. TBC1D3, a hominoid oncoprotein, is encoded by a cluster of paralogues located on chromosome 17q12. *Genomics* **88**: 731-6. doi: 10.1016/j.ygeno.2006.05.009

Insolera R, Bazzi H, Shao W, Anderson KV, Shi SH. 2014. Cortical neurogenesis in the absence of centrioles. *Nat Neurosci* **17**: 1528-35. doi: 10.1038/nn.3831

Jiang Z, Tang H, Ventura M, Cardone MF, Marques-Bonet T, She X, Pevzner PA, Eichler EE. 2007. Ancestral reconstruction of segmental duplications reveals punctuated cores of human genome evolution. *Nat Genet* **39**: 1361-8. doi: 10.1038/ng.2007.9

Johnson MB, Kawasawa YI, Mason CE, Krsnik Z, Coppola G, Bogdanovic D, Geschwind DH, Mane SM, State MW, Sestan N. 2009. Functional and evolutionary insights into human brain development through global transcriptome analysis. *Neuron* **62**: 494-509. doi: 10.1016/j.neuron.2009.03.027

Johnson MB, Wang PP, Atabay KD, Murphy EA, Doan RN, Hecht JL, Walsh CA. 2015. Single-cell analysis reveals transcriptional heterogeneity of neural progenitors in human cortex. *Nat Neurosci* **18**: 637-46. doi: 10.1038/nn.3980

Kadowaki M, Nakamura S, Machon O, Krauss S, Radice GL, Takeichi M. 2007. N-cadherin mediates cortical organization in the mouse brain. *Dev Biol* **304**: 22-33. doi: 10.1016/j.ydbio.2006.12.014

Kang HJ, Kawasawa YI, Cheng F, Zhu Y, Xu X, Li M, *et al.* 2011. Spatio-temporal transcriptome of the human brain. *Nature* **478**: 483-9. doi: 10.1038/nature10523

Katayama K, Melendez J, Baumann JM, Leslie JR, Chauhan BK, Nemkul N, Lang RA, Kuan CY, Zheng Y, Yoshida Y. 2011. Loss of RhoA in neural progenitor cells causes the disruption of adherens junctions and hyperproliferation. *Proc Natl Acad Sci U S A* **108**: 7607-12. doi: 10.1073/pnas.1101347108

Kawaguchi A, Miyata T, Sawamoto K, Takashita N, Murayama A, Akamatsu W, Ogawa M, Okabe M, Tano Y, Goldman SA, Okano H. 2001. Nestin-EGFP transgenic mice: visualization of the self-renewal and multipotency of CNS stem cells. *Mol Cell Neurosci* **17**: 259-73. doi: 10.1006/mcne.2000.0925

849 Konopka G, Friedrich T, Davis-Turak J, Winden K, Oldham MC, Gao F, Chen L, Wang GZ, Luo R, Preuss
 850 TM, Geschwind DH. 2012. Human-specific transcriptional networks in the brain. *Neuron* **75**: 601-17. doi:
 851 10.1016/j.neuron.2012.05.034
 852 Lewitus E, Kelava I, Kalinka AT, Tomancak P, Huttner WB. 2014. An adaptive threshold in mammalian
 853 neocortical evolution. *PLoS Biol* **12**: e1002000. doi: 10.1371/journal.pbio.1002000
 854 Lien WH, Klezovitch O, Fernandez TE, Delrow J, Vasioukhin V. 2006. alphaE-catenin controls cerebral
 855 cortical size by regulating the hedgehog signaling pathway. *Science* **311**: 1609-12. doi:
 856 10.1126/science.1121449
 857 Luders E, Kurth F, Mayer EA, Toga AW, Narr KL, Gaser C. 2012. The unique brain anatomy of
 858 meditation practitioners: alterations in cortical gyrification. *Front Hum Neurosci* **6**: 34. doi:
 859 10.3389/fnhum.2012.00034
 860 Luders E, Narr KL, Bilder RM, Szeszkó PR, Gurbani MN, Hamilton L, Toga AW, Gaser C. 2008.
 861 Mapping the relationship between cortical convolution and intelligence: effects of gender. *Cereb Cortex*
 862 **18**: 2019-26. doi: 10.1093/cercor/bhm227
 863 Lui JH, Hansen DV, Kriegstein AR. 2011. Development and evolution of the human neocortex. *Cell* **146**:
 864 18-36. doi: 10.1016/j.cell.2011.06.030
 865 Lui JH, Nowakowski TJ, Pollen AA, Javaherian A, Kriegstein AR, Oldham MC. 2014. Radial glia require
 866 PDGFR- β signalling in human but not mouse neocortex. *Nature* **515**: 264-8. doi:
 867 10.1038/nature13973
 868 Ma T, Wang C, Wang L, Zhou X, Tian M, Zhang Q, *et al.* 2013. Subcortical origins of human and monkey
 869 neocortical interneurons. *Nat Neurosci* **16**: 1588-97. doi: 10.1038/nn.3536
 870 McSherry GM, Smart IH. 1986. Cell production gradients in the developing ferret isocortex. *J Anat* **144**:
 871 1-14.
 872 Miller JA, Ding SL, Sunkin SM, Smith KA, Ng L, Szafer A, *et al.* 2014. Transcriptional landscape of the
 873 prenatal human brain. *Nature* **508**: 199-206. doi: 10.1038/nature13185
 874 Noctor SC, Martinez-Cerdeno V, Ivic L, Kriegstein AR. 2004. Cortical neurons arise in symmetric and
 875 asymmetric division zones and migrate through specific phases. *Nat Neurosci* **7**: 136-44. doi:
 876 10.1038/nn1172
 877 Nonaka-Kinoshita M, Reillo I, Artigiani B, Martinez-Martinez MA, Nelson M, Borrell V, Calegari F.
 878 2013. Regulation of cerebral cortex size and folding by expansion of basal progenitors. *EMBO J* **32**:
 879 1817-28. doi: 10.1038/emboj.2013.96
 880 O'Bleness M, Searles VB, Varki A, Gagneux P, Sikela JM. 2012. Evolution of genetic and genomic
 881 features unique to the human lineage. *Nat Rev Genet* **13**: 853-66. doi: 10.1038/nrg3336
 882 Pei L, Peng Y, Yang Y, Ling XB, Van Eyndhoven WG, Nguyen KC, Rubin M, Hoey T, Powers S, Li J.
 883 2002. PRC17, a novel oncogene encoding a Rab GTPase-activating protein, is amplified in prostate cancer.
 884 *Cancer Res* **62**: 5420-4.
 885 Perry GH, Yang F, Marques-Bonet T, Murphy C, Fitzgerald T, Lee AS, Hyland C, Stone AC, Hurles ME,
 886 Tyler-Smith C, Eichler EE, Carter NP, Lee C, Redon R. 2008. Copy number variation and evolution in
 887 humans and chimpanzees. *Genome Res* **18**: 1698-710. doi: 10.1101/gr.082016.108

888 Pollen AA, Nowakowski TJ, Chen J, Retallack H, Sandoval-Espinosa C, Nicholas CR, Shuga J, Liu SJ,
 889 Oldham MC, Diaz A, Lim DA, Leyrat AA, West JA, Kriegstein AR. 2015. Molecular Identity of Human
 890 Outer Radial Glia during Cortical Development. *Cell* **163**: 55-67. doi: 10.1016/j.cell.2015.09.004
 891 Rakic P. 1974. Neurons in rhesus monkey visual cortex: systematic relation between time of origin and
 892 eventual disposition. *Science* **183**: 425-7.
 893 Rakic P. 1988. Specification of cerebral cortical areas. *Science* **241**: 170-6.
 894 Rash BG, Tomasi S, Lim HD, Suh CY, Vaccarino FM. 2013. Cortical gyrification induced by fibroblast
 895 growth factor 2 in the mouse brain. *J Neurosci* **33**: 10802-14. doi: 10.1523/JNEUROSCI.3621-12.2013
 896 Rasin MR, Gazula VR, Breunig JJ, Kwan KY, Johnson MB, Liu-Chen S, Li HS, Jan LY, Jan YN, Rakic P,
 897 Sestan N. 2007. Numb and Numbl are required for maintenance of cadherin-based adhesion and polarity of
 898 neural progenitors. *Nat Neurosci* **10**: 819-27. doi: 10.1038/nn1924
 899 Reillo I, de Juan Romero C, Garcia-Cabezas MA, Borrell V. 2011. A role for intermediate radial glia in the
 900 tangential expansion of the mammalian cerebral cortex. *Cereb Cortex* **21**: 1674-94. doi:
 901 10.1093/cercor/bhq238
 902 Saito T. 2006. In vivo electroporation in the embryonic mouse central nervous system. *Nat Protoc* **1**:
 903 1552-8. doi: 10.1038/nprot.2006.276
 904 Shitamukai A, Konno D, Matsuzaki F. 2011. Oblique radial glial divisions in the developing mouse
 905 neocortex induce self-renewing progenitors outside the germinal zone that resemble primate outer
 906 subventricular zone progenitors. *J Neurosci* **31**: 3683-95. doi: 10.1523/JNEUROSCI.4773-10.2011
 907 Smart IH, Dehay C, Giroud P, Berland M, Kennedy H. 2002. Unique morphological features of the
 908 proliferative zones and postmitotic compartments of the neural epithelium giving rise to striate and
 909 extrastriate cortex in the monkey. *Cereb Cortex* **12**: 37-53. doi: 10.1093/cercor/12.1.37
 910 Stahl PD, Wainszelbaum MJ. 2009. Human-Specific Genes May Offer a Unique Window into Human Cell
 911 Signaling. *Science Signaling* **2**: pe59. doi: 10.1126/scisignal.289pe59
 912 Stahl R, Walcher T, De Juan Romero C, Pilz GA, Cappello S, Irmeler M, Sanz-Aquila JM, Beckers J, Blum
 913 R, Borrell V, Gotz M. 2013. Trnp1 regulates expansion and folding of the mammalian cerebral cortex by
 914 control of radial glial fate. *Cell* **153**: 535-49. doi: 10.1016/j.cell.2013.03.027
 915 Sun T, Hevner RF. 2014. Growth and folding of the mammalian cerebral cortex: from molecules to
 916 malformations. *Nat Rev Neurosci* **15**: 217-32. doi: 10.1038/nrn3707
 917 Tan ZJ, Peng Y, Song HL, Zheng JJ, Yu X. 2010. N-cadherin-dependent neuron-neuron interaction is
 918 required for the maintenance of activity-induced dendrite growth. *Proc Natl Acad Sci U S A* **107**: 9873-8.
 919 doi: 10.1073/pnas.1003480107
 920 Thomsen ER, Mich JK, Yao Z, Hodge RD, Doyle AM, Jang S, Shehata SI, Nelson AM, Shapovalova NV,
 921 Levi BP, Ramanathan S. 2016. Fixed single-cell transcriptomic characterization of human radial glial
 922 diversity. *Nat Methods* **13**: 87-93. 10.1038/nmeth.3629
 923 Wainszelbaum MJ, Charron AJ, Kong C, Kirkpatrick DS, Srikanth P, Barbieri MA, Gygi SP, Stahl PD.
 924 2008. The hominoid-specific oncogene TBC1D3 activates Ras and modulates epidermal growth factor
 925 receptor signaling and trafficking. *J Biol Chem* **283**: 13233-42. doi: 10.1074/jbc.M800234200
 926 Wainszelbaum MJ, Liu J, Kong C, Srikanth P, Samovski D, Su X, Stahl PD. 2012. TBC1D3, a
 927 hominoid-specific gene, delays IRS-1 degradation and promotes insulin signaling by modulating p70 S6
 928 kinase activity. *PLoS One* **7**: e31225. doi: 10.1371/journal.pone.0031225

Wallace VA, Raff MC. 1999. A role for Sonic hedgehog in axon-to-astrocyte signalling in the rodent optic nerve. *Development* **126**: 2901-9.

Wang X, Tsai JW, LaMonica B, Kriegstein AR. 2011. A new subtype of progenitor cell in the mouse embryonic neocortex. *Nat Neurosci* **14**: 555-61. doi: 10.1038/nn.2807

Wolosin SM, Richardson ME, Hennessey JG, Denckla MB, Mostofsky SH. 2009. Abnormal cerebral cortex structure in children with ADHD. *Hum Brain Mapp* **30**: 175-84. doi: 10.1002/hbm.20496

Yoon KJ, Nguyen HN, Ursini G, Zhang F, Kim NS, Wen Z, *et al.* 2014. Modeling a genetic risk for schizophrenia in iPSCs and mice reveals neural stem cell deficits associated with adherens junctions and polarity. *Cell Stem Cell* **15**: 79-91. 10.1016/j.stem.2014.05.003

Zilles K, Palomero-Gallagher N, Amunts K. 2013. Development of cortical folding during evolution and ontogeny. *Trends Neurosci* **36**: 275-84. doi: 10.1016/j.tins.2013.01.006

Zody MC, Garber M, Adams DJ, Sharpe T, Harrow J, Lupski JR, *et al.* 2006. DNA sequence of human chromosome 17 and analysis of rearrangement in the human lineage. *Nature* **440**: 1045-9. doi: 10.1038/nature04689

Figures and legends

Figure 1. TBC1D3 expression in developing mice cortex disrupts adherens junctions and induces formation of column-like structures. (A) RT-PCR analysis for the expression of *TBC1D3* mRNA in developing (GW26 - 40) and adult (21 - 29 years) human whole brain with *GAPDH* as control. (B) The expression pattern of TBC1D3 in fetal human cortex at GW18. VZ, ventricular zone; ISVZ, inner subventricular zone; OSVZ, outer subventricular zone; IZ, intermediate zone; CP, cortical plate. Scale bars, 50 μ m. (C-E) *In utero* electroporation (IUE) of the mouse cerebral cortex was performed at E13.5 and analyzed at E15.5 (C and D) or E16.5 (E). TBC1D3 or control plasmid was mixed with YFP. (C) *In situ* hybridization analysis for the expression of *TBC1D3* in mouse brain sections. Scale bar, 500 μ m. (D) Adherens junctions in the ventricular surface were marked by N-cadherin staining. Scale bars, 50 μ m. (E) Distribution of GFP⁺ cells in E16.5 mice cortex. The right panels show magnified regions indicated by asterisks in left panels, with histograms outlining relative fluorescence intensity of tangentially distributed GFP⁺ cells. Scale bars, 50 μ m.

Figure 1-figure supplement 1. The mRNA level of *N-cadherin* gene is reduced by TBC1D3 expression in mouse cortex. (A) *In utero* electroporation (IUE) of TBC1D3 or control plasmid, together with YFP, in mouse at E13.5 and examined at E15.5. Adjacent sections were subjected to *in situ* hybridization (ISH) to determine the mRNA level of *N-cadherin* (*Cdh2*) (left panel) or *TBC1D3* (right panel). Asterisks indicate areas electroporated with TBC1D3. Scale bar, 50 μ m. (B) Schematic diagram of electroporation, FACS sorting and real-time PCR analysis. (C) FACS sorting of YFP⁺ cells. Cells satisfied to the level of YFP expression (boxed areas) were selected for further RNA extraction and analysis. Blank, cells from cortical tissues without IUE. (D) Relative expression levels of *Cdh2* relative to *GAPDH*, analyzed by real-time PCR, with control group normalized as 1 (n = 3 for each analysis; control: mean = 1.0, SEM = 0.1; TBC1D3: mean = 0.7, SEM = 0.013). p = 0.018. (E and F) Stability of *Cdh2* or *Fos* mRNA relative to that of *Hprt* in ReNeuron cells, which were transfected with TBC1D3 or vehicle plasmid and treated with actinomycin D for indicated time. Data are shown as mean \pm SEM of the percentage of remaining mRNA with the value from 0 hr treatment normalized as 100 (n = 3 experiments for each time point). Note the significant difference (p = 0.025) between *Cdh2* mRNA levels in control (mean = 74.22, SEM = 6.41) and TBC1D3 (mean = 35.51, SEM = 6.13) groups 4 h after actinomycin D treatment.

Figure 1-figure supplement 2. Dislocalization of adherens junctions proteins upon TBC1D3 expression in the VZ. E13.5 mouse brain was subject to IUE with pCAGGS-TBC1D3-IRES-EGFP or vehicle control plasmids, following by staining at E15.5 with antibodies of Numb or integrin beta 1 (ITGB1), or fluorescein-labeled phalloidin for F-actin. Scale bars, 20 μ m.

Figure 2. Expression of TBC1D3 induces an increase in cell proliferation in basal regions of developing mouse cortex. (A) Schematic of BrdU pulse labeling. (B) E15.5 whole brain section incorporated with BrdU after IUE at E13.5. Dashed rectangle indicates cortical area for quantification. Scale bar, 200 μ m. (C) BrdU incorporation in mice subjected to IUE with indicated plasmids. Scale bar, 50 μ m. (D) Staining for phosphorylated Histone H3 (PH3) in E15.5 mice subjected to IUE at E13.5. Scale bar, 50 μ m. (E) Quantification for the percentage of BrdU⁺ cells among electroporated YFP-labeled cells (control: n = 5 mice, mean = 19.18, SEM = 0.69; TBC1D3: n = 10 mice, mean = 31.91, SEM = 2.02; Δ 286-353: n = 9 mice, mean = 21.62, SEM = 1.36). Respective p-values are 0.0003 (control vs TBC1D3) and 0.0004 (TBC1D3 vs Δ 286-353). (F) Mean cortical distribution of BrdU⁺ cells among electroporated YFP-labeled cells (n = 5 mice). (G) Quantification for the percentage of PH3⁺ cells among electroporated YFP-labeled cells attached to ventricular surface (VZ surface) or out of ventricular zone (extra-VZ). Total number of PH3⁺ cells in VZ surface and extra-VZ were normalized to 100 for each group (n = 8 mice, mean = 28.10, SEM = 3.43 for extra-VZ of control; n = 10 mice, mean = 57.22, SEM = 2.24 for extra-VZ of TBC1D3; n = 8 mice, mean = 35.99, SEM = 3.26 for extra-VZ of TBC1D3 plus N-cadherin). ***p<0.001.

Figure 2-figure supplement 1. Colocalization between BrdU and Ki67 in TBC1D3-expressing BPs. E13.5 mouse brain was subjected to IUE with TBC1D3 and YFP, followed by BrdU injection for 2 hr at E15.5, and immunostaining with Ki67 or NeuN antibody. Yellow arrows show BrdU⁺YFP⁺ cells co-labeled with Ki67 (top row) but not NeuN (bottom row) in the cortical plate. Scale bars, 10 μ m.

Figure 2-figure supplement 2. Cell autonomous and non-cell autonomous effects of TBC1D3 on neural progenitors. E13.5 mice were subjected to IUE with

pCAGGS-TBC1D3-IRES-EGFP plasmid or pCAGGS-IRES-EGFP as the control, followed by 2 hr BrdU incorporation (A) or staining with PH3 antibody (C) at E15.5. Number of BrdU⁺ or PH3⁺ cells among EGFP⁺ or EGFP⁻ cells, in apical or basal regions, were analyzed to determine cell autonomous or non-cell autonomous effects (B and D). Data are presented as mean \pm SEM in each group (n = 7 brains for control, n = 10 brains for TBC1D3). **p<0.01, ***p<0.001. White arrows indicate EGFP⁺BrdU⁺ or EGFP⁺PH3⁺ cells. Scale bar, 20 μ m. Apical, ventricular zone; Basal, regions outside of ventricular zone.

Figure 2-figure supplement 3. Detachment of vRGs induced by blocking N-cadherin-mediated adhesion does not promote generation of BPs. (A) E13.5 mice were subjected to IUE with Myc-EC1 or vehicle plasmid, together with YFP plasmid to mark cell morphology. Dash lines indicate endfeet of vRG cells attached to the ventricular surface of E14.5 mouse cortex. Scale bar, 20 μ m. (B) Quantification for the percentage of YFP⁺ cells with endfeet attached to the ventricular surface (control: n = 9 slices, mean = 13.98, SEM = 1.61; EC1: n = 10 slices, mean = 5.21, SEM = 1.15). p = 0.0003. (C) E15.5 mouse brain subjected to IUE at E13.5 was labeled by BrdU for 2 hr and stained with indicated antibody. Scale bar, 20 μ m. (D-F) Quantification for the percentage of BrdU⁺YFP⁺ (control apical: mean = 39.51, SEM = 2.68; EC1 apical: mean = 44.26, SEM = 1.71; control basal: mean = 4.19, SEM = 0.73; EC1 basal: mean = 5.40, SEM = 0.91), or PH3⁺YFP⁺ (control apical: mean = 6.48, SEM = 0.80; EC1 apical: mean = 8.16, SEM = 0.69; control basal: mean = 0.29, SEM = 0.19; EC1 basal: mean = 0.47, SEM = 0.24) cells in apical or basal regions or total YFP⁺ cells in basal regions (control: mean = 57.53, SEM = 1.81; EC1: mean = 59.08, SEM = 2.28). No significant difference was observed between the EC1 and the control group (n = 7 slices for control, n = 9 slices for EC1).

Figure 2-figure supplement 4. Effect of dominant-negative form of Ras on proliferation of TBC1D3-induced BPs. (A) E13.5 mice were subjected to IUE with TBC1D3, Ras-DN (Ras^{S17N}), TBC1D3 plus Ras-DN, or control plasmids, mixed with EGFP, followed by BrdU incorporation for 2 hr at E15.5 and staining. Shown are representative images of TBC1D3 and TBC1D3 plus Ras-DN groups. Scale bar, 20 μ m. (B) Quantification for the percentage of BrdU⁺ among total EGFP⁺ cells in apical (control: n = 7 mice, mean = 15.30, SEM = 0.94; Ras-DN: n = 7 mice, mean = 12.07, SEM = 0.67; TBC1D3: n = 11 mice, mean = 16.59, SEM = 0.87; TBC1D3 plus Ras-DN : n = 6 mice, mean = 13.26, SEM = 0.41; p = 0.037, control vs Ras-DN; p = 0.023, TBC1D3 vs TBC1D3 plus Ras-DN.) or basal regions (n = 7 mice, mean = 1.40, SEM = 0.28 for control; n = 7 mice, mean = 1.39, SEM = 0.26 for Ras-DN; n = 11 mice, mean = 6.69, SEM = 1.52 for TBC1D3; n = 6 mice, mean = 3.40, SEM = 0.48 for TBC1D3 plus Ras-DN). p = 0.005, control vs TBC1D3; p = 0.049 TBC1D3 vs TBC1D3 plus Ras-DN.

Figure 3. TBC1D3 expression in the mouse cortex elevates proliferative oRG cells. (A) Staining for Pax6 in E15.5 mice after IUE at E13.5 with pE/nestin-TBC1D3 or pE/nestin (control), together with YFP to mark cell morphology. Scale bars, 50 μ m. (B) Quantification for the percentage of Pax6⁺YFP⁺ cells (control: n = 10 mice, mean = 36.40, SEM = 1.09; TBC1D3: n = 16 mice, mean = 56.68, SEM = 1.97). p<0.0001. (C) Mean distribution of Pax6⁺YFP⁺ cells. (D) Dil-labeling of bipolar ventricular RG cells (vRGs) and oRG-like cells with a basal process attaching the pial surface in E15.5 mouse cortex after IUE at E13.5. Scale bars, 20 μ m. (E) Time-lapse imaging of TBC1D3-expressing oRG cells (yellow arrows) undergoing division in cultured E14.5 mouse slices after IUE with pCS2-Myc-TBC1D3 and pCAG-H2BGFP-2A-tdTomato at E13.5. H2B-GFP represents cell nucleus. Scale bar, 10 μ m. (F) Quantification for the percentage of oRG-like cells with a basal process attached to the pial surface and soma located in SVZ or IZ regions, among total RGs including vRGs with soma located in the VZ (control: n =

5 mice, mean = 4.67, SEM = 1.60; TBC1D3: n = 10 mice, mean = 34.21, SEM = 7.56). $p = 0.018$. **(G)** Quantification for the relative number of basal progenitors with oRG-like divisions, identified by time-lapse imaging in **(E)**, per unit of tangential length of the VZ electroporated (control: n = 6 slices, mean = 1.00, SEM = 0.21; TBC1D3: n = 12 slices, mean = 2.14, SEM = 0.30). $p = 0.025$. **(H and I)** Types of TBC1D3-expressing oRG-like cells before division [n = 120 cells in **(I)**]. Scale bar, 10 μm . **(J)** Immunostaining for Tbr2 and Sox2 in the brain slices after time-lapse imaging. Note daughter cells toward basal (Db) or apical (Da) direction upon division. Scale bar, 20 μm . **(K and L)** Quantification for Sox2⁺Tbr2⁻ daughter cell pairs **(K)** and daughter cells with indicated marker combinations **(L)** (n = 18 cells for control, n = 31 cells for TBC1D3).

Figure 3-figure supplement 1. oRG-like cells and IPs increase in the basal region of TBC1D3-expressing mouse cortex. **(A and C)** Staining for phospho-Vimentin (p-Vim) and Sox2 **(A)** or p-Vim and Pax6 **(C)** in E15.5 mice subjected to IUE at E13.5. Dash lines indicate the boundary between basal (outer VZ) and apical (VZ) regions in mouse neocortex. Note the cells double positive for p-Vim and Sox2 or Pax6 (yellow arrows) with the basal process with coherent patterned intermittent p-Vim signals. Scale bars, 50 μm . **(B and D)** Quantification for the number of p-Vim⁺ Sox2⁺ (control: n = 6 mice, mean = 6.79, SEM = 1.02; TBC1D3: n = 9 mice, mean = 22.53, SEM = 2.91; $p = 0.0009$) or p-Vim⁺ Pax6⁺ (control: n = 15 mice, mean = 3.10, SEM = 1.16; TBC1D3: n = 19 mice, mean = 8.63, SEM = 1.39; $p = 0.009$) cells with basal processes in the basal region of electroporated cortex per unit length along the VZ surface. **(E)** Tbr2 staining for E17.5 mouse brains, which were subjected to IUE at E13.5 with TBC1D3 or vehicle control, together with YFP. Dash lines indicate boundaries between apical (VZ) and basal (outer VZ) regions. Scale bar, 50 μm . **(F)** Quantification for the percentage of Tbr2⁺ cells among electroporated YFP⁺ cells in apical (control: n = 4 mice, mean = 12.40, SEM =

0.79; TBC1D3: n = 7 mice, mean = 12.61, SEM = 2.01; p = 0.286) and basal regions (control: mean = 1.73, SEM = 0.49; TBC1D3: mean = 6.45, SEM = 0.72; p = 0.006).

Figure 3-figure supplement 2. Birth dating analysis for division patterns of neuroprogenitors after IUE. (A) Schematic of BrdU/EdU double labeling. (B) E13.5 mice were subjected to IUE with TBC1D3 or vehicle plasmid, together with YFP plasmid, and then injected with BrdU at E14.5 and EdU at E15.5, to label dividing cells sequentially. Boxed areas indicate apical [(A1) for control, (A2) for TBC1D3] or basal [(B1) for control, (B2) for TBC1D3] regions analyzed. Note the cells double labeled by BrdU and EdU in electroporated YFP-positive cells (yellow arrowheads). Scale bars, 50 μ m. (C) Quantification for the percentage of BrdU⁺EdU⁺ cells among YFP⁺BrdU⁺ cells in apical and basal regions. Apical: n = 10 mice, mean = 18.63, SEM = 3.41 for control, n = 14 mice, mean = 23.37, SEM = 2.0 for TBC1D3, p = 0.215; Basal: mean = 5.22, SEM = 1.48 for control, mean = 10.47, SEM = 1.79 for TBC1D3, p = 0.045.

Figure 4. Knockdown of TBC1D3 in human vRGs inhibits the generation of oRGs. (A) Detection of TBC1D3 protein levels in Hela cells transfected with pSuper-siTBC1D3 plasmids, with a scramble sequence as the control. (B) Paradigm of culture and electroporation of human brain slice. (C-E) The VZ of human brain slices at GW14.5 (C), GW17.1 (D), GW13.5 (E) were transfected with pSuper-siTBC1D3 plasmids or a plasmid encoding scrambled sequence as the control, without or with co-transfection with TBC1D3 expression plasmid (pCS2-Myc-TBC1D3) by electroporation method as described in (B), followed by staining with Sox2 antibody at 72 hr post electroporation. Scale bars, 50 μ m. (F) Quantification for the percentage of Sox2⁺ cells among total EGFP⁺ cells in basal regions (control: n = 4 slices, mean = 55.91, SEM = 5.76; siTBC1D3: n = 4 slices, mean = 13.32, SEM = 1.46; siTBC1D3 plus TBC1D3: n = 3 slices, mean = 37.47, SEM = 3.12). p = 0.0002, control vs siTBC1D3; p = 0.004,

siTBC1D3 vs siTBC1D3 plus TBC1D3. (G) Human ReNeuron cells were transfected with siTBC1D3 or control plasmid for 3 days followed by treatment with actinomycin D for 4 hr. The mRNA levels of *Cdh2* in ReNeuron cells after actinomycin D treatment were quantified (control: n = 6 experiments; mean = 66.99, SEM = 6.21; siTBC1D3: mean = 96.62, SEM = 7.62; p = 0.003), normalized to that in cells with 0 hr of actinomycin D treatment.

Figure 5. Cortical folding and gyrification induced by TBC1D3 expression in mice.

(A) E13.5 mice were subjected to IUE with pE/nestin-TBC1D3 or vehicle control plasmids, together with RFP to mark electroporated cells, and analyzed at the indicated time. White arrows indicate cortical folds. Scale bars, 200 μ m. (B and C) Slices from WT or TG mice at E14.5 (B) or E18.5 (C) were stained for Cux1 and Ctip2. Note the protrusions (white arrows) in TG mice (B2 and C2) compared to smooth surfaces in WT mice (B1 and C1). Scale bars, 50 μ m. (D) Images from whole mount P3.5 WT and TG brains. Note the convoluted cortical surfaces indicated by red asterisks in TG mice. Scale bar, 1 mm. (E and F) Nissl staining of sagittal sections of TG or WT mice at P3.5 (E) or adult stage (F, 3 months). Note the apparent gyrus-like structures (black arrows) in boxed areas. Scale bars, 1 mm (E and F) or 50 μ m (E1 and E2). (G and H) Immunostaining for Cux1 and Ctip2 (G) or NeuN and GFAP (H) in the adult WT and TG mouse brain sections. Note the folded cortical surfaces outlined by dash lines; Scale bars, 1 mm.

Figure 5-figure supplement 1. TBC1D3 electroporation has no effect on the pial basement membrane integrity. Shown are representative images of E15.5 brain slices (IUE with pCAGGS-TBC1D3-IRES-EGFP or control vehicle at E13.5) stained with laminin antibody. PS, pial surface; CP, cortical plate. Scale bar, 50 μ m.

Figure 5-figure supplement 2. Generation of TBC1D3 transgenic mouse. (A)

Schematic structure of the construct used for generating TBC1D3 transgenic mice. The expression of TBC1D3 was under the control of promoter composed of the second intron enhancer of rat *nestin* gene and the minimum promoter of heat shock protein 68 (hsp68) (Kawaguchi et al., 2001). P1 and P2, primers used for genotyping. (B) Relative copy numbers of *TBC1D3* genes inserted in the genome of transgenic mouse founders (10#, 14#, 51#) were determined by real-time PCR using the tail genomic DNA as template. The number of inserted *TBC1D3* gene was normalized to that of *glcoe4* (n = 8 mice, mean = 3.15, SEM = 0.47 for 10#; n = 2 mice, mean = 0.54, SEM = 0.03 for 14#; n = 4, mean = 0.46, SEM = 0.03 for 51#). (C) Protein levels of TBC1D3 in brains of E12.5 TG mouse lines (L10, L51), from founders 10# or 51#, were measured by immunoblot (left panel) and quantified (right panel). GAPDH was used as the internal control (L10: n = 4 mice, mean = 2.92, SEM = 0.72; L51: n = 5 mice, mean = 1.00, SEM = 0.08). (D) Immunostaining for the expression of TBC1D3 in E12.5 TG (L10) mouse brain. Note the magnified area (D1) showing cytosol distribution of TBC1D3. Scale bars, 200 μ m (D) and 20 μ m (D1). (E) TBC1D3 protein levels in TG mice (L10) at indicated developmental stages. Shown in the histogram is mean of 2 mice in each stage with GAPDH as control.

Figure 5-figure supplement 3. Normal neuronal migration in the cortical plate of

TG mice. (A) E13.5 WT or TG mice were subjected to IUE with EGFP expression plasmids, and the cortical plates of mice at E16.5 were examined for the distribution of EGFP⁺ cells. (B) Percentage of EGFP⁺ cells in different vertical layers of the cortical plate in WT or TG mice (n = 3 mice for WT, n = 4 mice for TG). Scale bar, 50 μ m.

Figure 5-figure supplement 4. Cortical folding mainly occurs in the motor cortex of

TBC1D3-transgenic mice. (A) Top view of a P3.5 TG mouse brain hemisphere shows

the position of a cortical fold (left panel) and a summary distribution of cortical folds (right panel) on the brain surfaces from 3 TG mice at P3.5. Red dots indicate the cortical folds. **(B)** Schematic locations of the primary (M1) and secondary (M2) cortex in mice. **(C)** Schematic of section positions (dash lines) in the whole brain visualized by *Nissl* staining in **(D)**. **(D)** *Nissl* staining in four consecutive brain sections, along the medial-lateral axis, of adult TG mice. S1, primary somatosensory cortex. V1, primary visual cortex. V2, secondary visual cortex. Scale bar, 1 mm. **(E)** Parallel sagittal section schematics corresponding to slices in **(D)** according to the Allen Brain Atlas. Dash lines indicate the boundary of brain regions.

Figure 6. Cortical basal progenitors are increased and display columnar distribution in the cortex of TBC1D3-transgenic mice. **(A)** Staining for Pax6, Sox2, and Tbr2 in E12.5 WT and TG mice. Dash lines indicate pial surfaces. Note the increase in Pax6⁺Sox2⁺Tbr2⁻ cells (white arrowheads) in the basal region of TG mice. Scale bar, 50 μ m. **(B)** Quantification for the density of Pax6⁺Sox2⁺Tbr2⁻ cells in extra-VZ regions (WT: n = 9 slices from 3 mice, mean = 0.26, SEM = 0.09; TG: n = 11 slices from 4 mice, mean = 4.01, SEM = 0.57). $p < 0.0001$. **(C)** E13.5 TG mice were subjected to IUE with EGFP-expressing plasmids to label cell morphology, and brain sections were stained for Pax6 at E16.5 (left panel). Scale bar, 5 μ m. Three types of oRG-like cells constitute more than half of Pax6⁺ BPs (right panel, 82 Pax6⁺EGFP⁺ cells from 5 brains were analyzed). **(D and E)** DiI labeling **(D)** and quantification **(E)** of RG cells in E14.5 WT and TG mice (WT: n = 9 slices, mean = 0.72, SEM = 0.37; TG: n = 13 slices, mean = 3.92, SEM = 0.88). $p = 0.009$. White arrows indicate typical oRG-like cells with soma located in the SVZ/IZ and a basal process attached to the pial surface. Scale bar, 50 μ m. **(F)** E12.5 TG mice were stained with Sox2, and Tbr2. Note the columnar distribution of Sox2⁺Tbr2⁻ cells in basal regions, as illustrated for the boxed area. Scale bar, 50 μ m. **(G)** Distribution profile of Sox2⁺Tbr2⁻ cells in the basal region of TG mice cortex ranging from dorsal to

lateral cortical regions. **(H)** Immunostaining for Sox2, Pax6, Tbr2 in E14.5 WT and TG mice cortex. Yellow dash lines indicate the brain surface. Note the apparent columnar distribution of Sox2⁺Pax⁺Tbr2⁻ cells (yellow dotted circles) in the boxed area below a cortical gyrus-like structure (white arrow). Scale bars, 50 μ m. **(I and J)** Immunostaining **(I)** and quantification **(J)** of HOPX cells in the extra-VZ (white arrowheads) of E14.5 WT and TG mice cortices (WT: n = 3 brains, mean = 0.03, SEM = 0.03; TG: n = 3 brains, mean = 2.66, SEM = 0.08). p < 0.0001. Scale bar, 20 μ m.

Figure 6-figure supplement 1. Cortical basal progenitors are increased in the cortex of TBC1D3-transgenic mice. **(A and B)** Immunostaining for PH3 in WT and TBC1D3 TG mice at E12.5. White dash lines in enlarged areas **(B)** indicate cortical surfaces, and yellow dash lines indicate the boundary between apical and basal regions. Scale bars, 50 μ m. **(C and D)** Quantification for the density of PH3⁺ cells distributed radially **(C)**, from ventricular to pial surface) or in apical/basal regions **(D)**, respectively. Apical: n = 3 mice, mean = 453.37, SEM = 24.89 for WT, n = 4 mice, mean = 432.36, SEM = 24.99 for TG; Basal: mean = 251.14, SEM = 13.09 for WT; mean = 378.62, SEM = 42.49 for TG. p-values are 0.570 (apical) and 0.017 (basal). **(E)** Staining for Pax6, Sox2, and Tbr2 in E12.5 WT and TG mice. Scale bar, 50 μ m. **(F)** The densitys of Pax6⁺ cells in the cortex of WT and TG mice were quantified (WT: n = 3 mice, mean = 55.5, SEM = 1.67; TG: n = 4 mice, mean = 61.59, SEM = 1.43). p = 0.014.

Figure 6-figure supplement 2. Increased proliferation potency of BPs in TBC1D3-transgenic Mice. **(A)** BrdU and EdU were sequentially administered into TG or WT mice, at E13.5 and E16.5, respectively. Double positive cells from cerebral cortex of mice 2 hr after EdU injection were analyzed. Note the cells indicated by white arrows in magnified areas **(A1 and A2)**. Dash lines indicate the boundary of apical and basal regions in cortex. Scale bars, 50 μ m. **(B)** Quantification for the density of BrdU/EdU

double positive (BrdU⁺EdU⁺) cells in the dorsal cerebral cortex of WT (apical: mean = 319.94, SEM = 52.36; basal: mean = 20.34, SEM = 5.09) and TG (apical: mean = 276.19, SEM = 43.31; basal: mean = 237.93, SEM = 81.52) mice. p-values WT vs TG are 0.544 (apical) and 0.029 (basal) (n = 4 mice in each group).

Figure 6-figure supplement 3. Increased neurons in the superficial layer of the cortex of TBC1D3-transgenic mice. (A) Schematic for the motor cortex (M1/M2) and sensory (S) cortex, and the brain regions (blue or red rectangle) for the staining analysis. (B) Staining for the superficial layer marker Cux1 and the deep layer marker Ctip2 in the motor cortex of P3.5 mice. Scale bar = 50 μ m. (C) Staining for NeuN and GFAP signals in the motor cortex of P28 mice. Scale bar = 50 μ m. (D) Quantification for the density of Cux1⁺ (WT: mean = 44.02, SEM = 5.91; TG: mean = 60.83, SEM = 0.92; p = 0.031) or Ctip2⁺ (WT: mean = 30.17, SEM = 2.43; TG: mean = 31.19, SEM = 2.64; p = 0.786) neurons in the motor cortex of P3.5 mice (n = 4 mice). (E and F) Quantification for the density of NeuN⁺ neurons (WT: n = 4 mice, mean = 14.70, SEM = 0.43; TG: n = 3 mice, mean = 16.79, SEM = 2.85; p = 0.014) and GFAP⁺ astrocytes (WT: n = 4 mice, mean = 1.19, SEM = 0.02; TG: n = 3 mice, mean = 1.25, SEM = 0.16; p = 0.645) in the motor cortex of P28 mice. (G and H) Immunostaining and quantification for the superficial layer marker Cux1 in the sensory cortex (red rectangle in A) of P3.5 mice. Scale bar, 50 μ m. n = 4 mice, mean = 69.33, SEM = 3.71 for WT; n = 5 mice, mean = 81.07, SEM = 1.59 for TG. p = 0.016.

Figure 7. Effect of TBC1D3 on intrinsic stemness signaling pathways and model for the TBC1D3 function in cortical folding. (A-D) E13.5 mice were subjected to IUE with TBC1D3 or vehicle control plasmid, together with YFP plasmid, and at E15.5, FACS-sorted transfected cells (see Figure 1-figure supplement 1B, C) were analyzed for mRNA levels of indicated genes relative to *GAPDH* with values from control groups

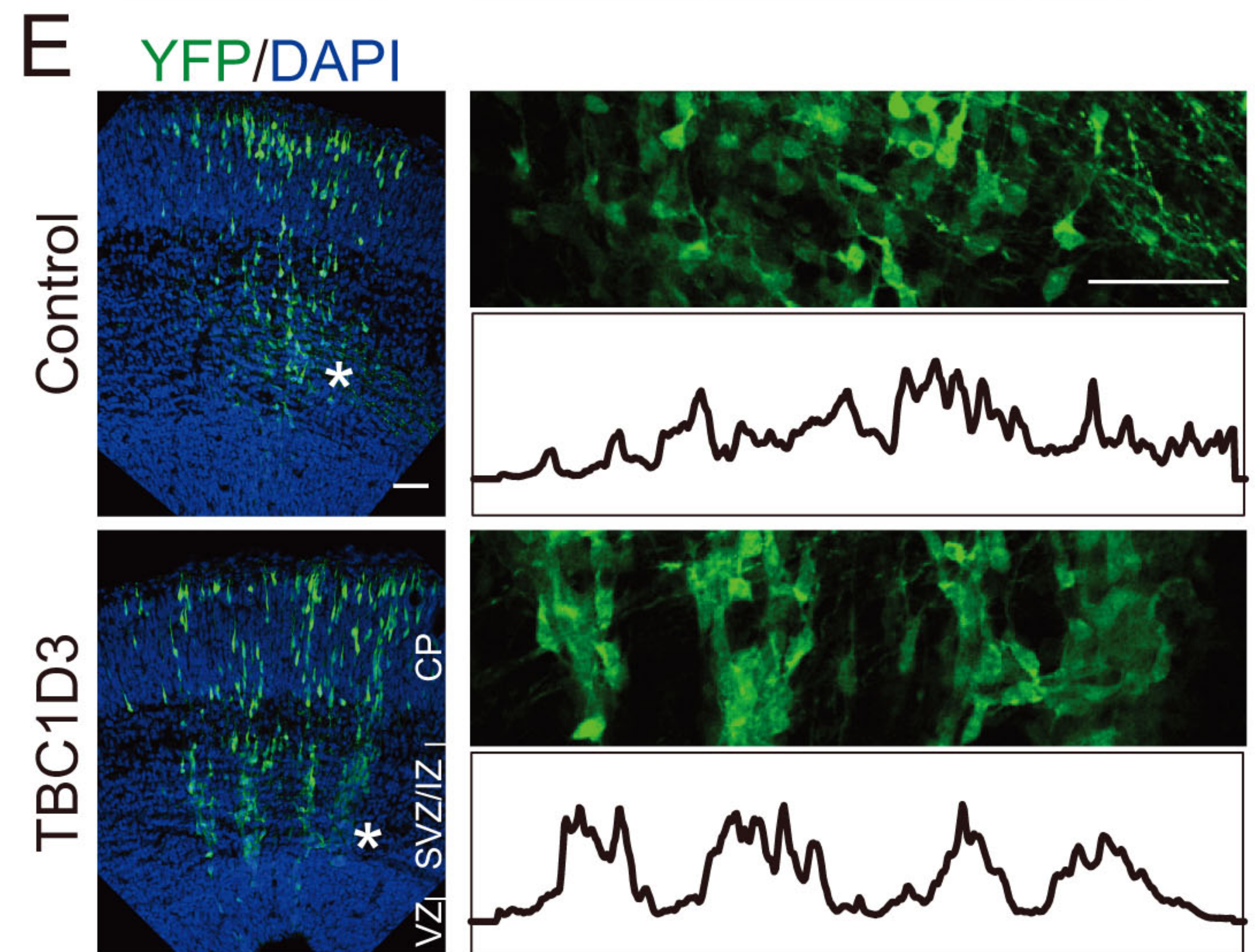
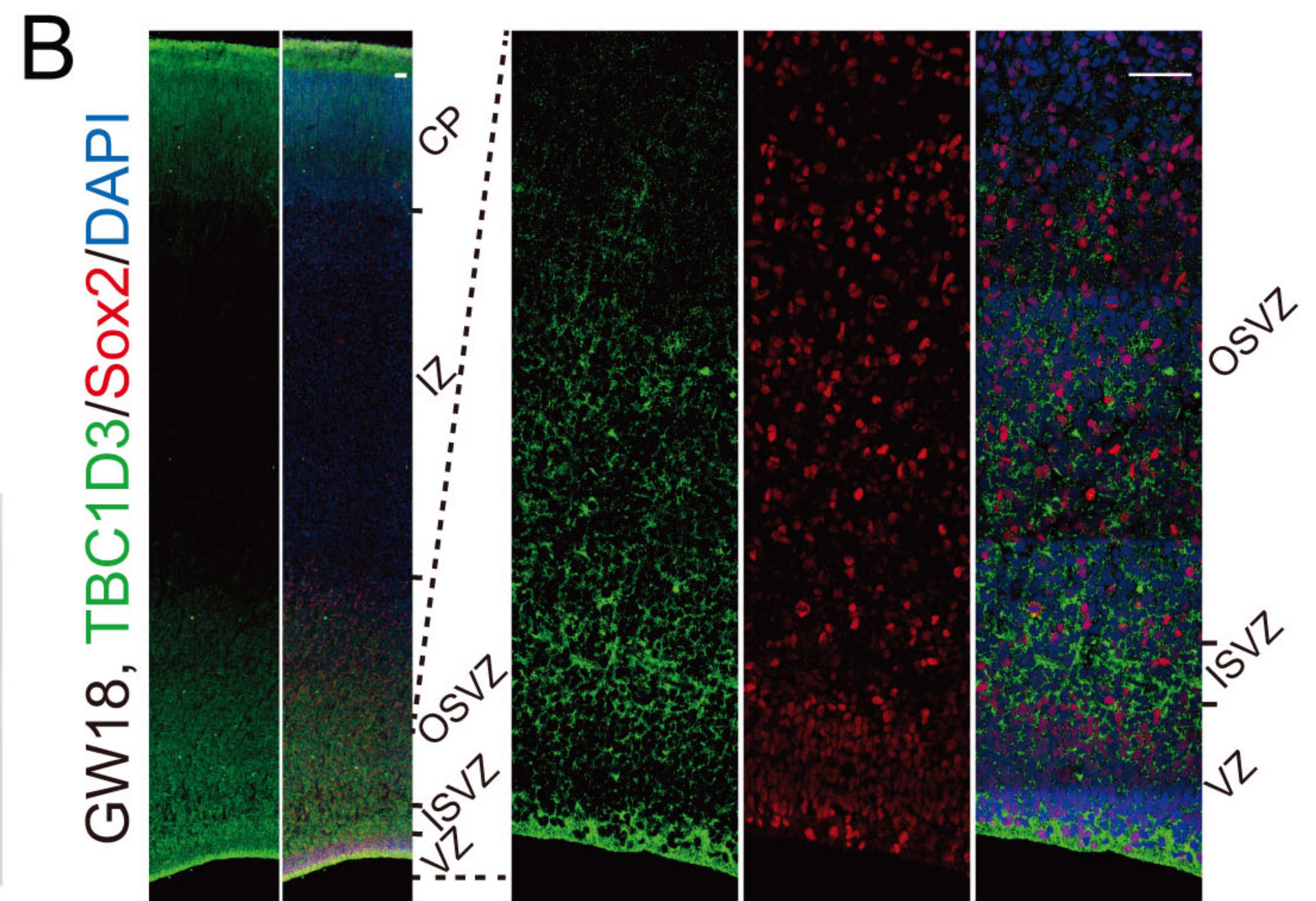
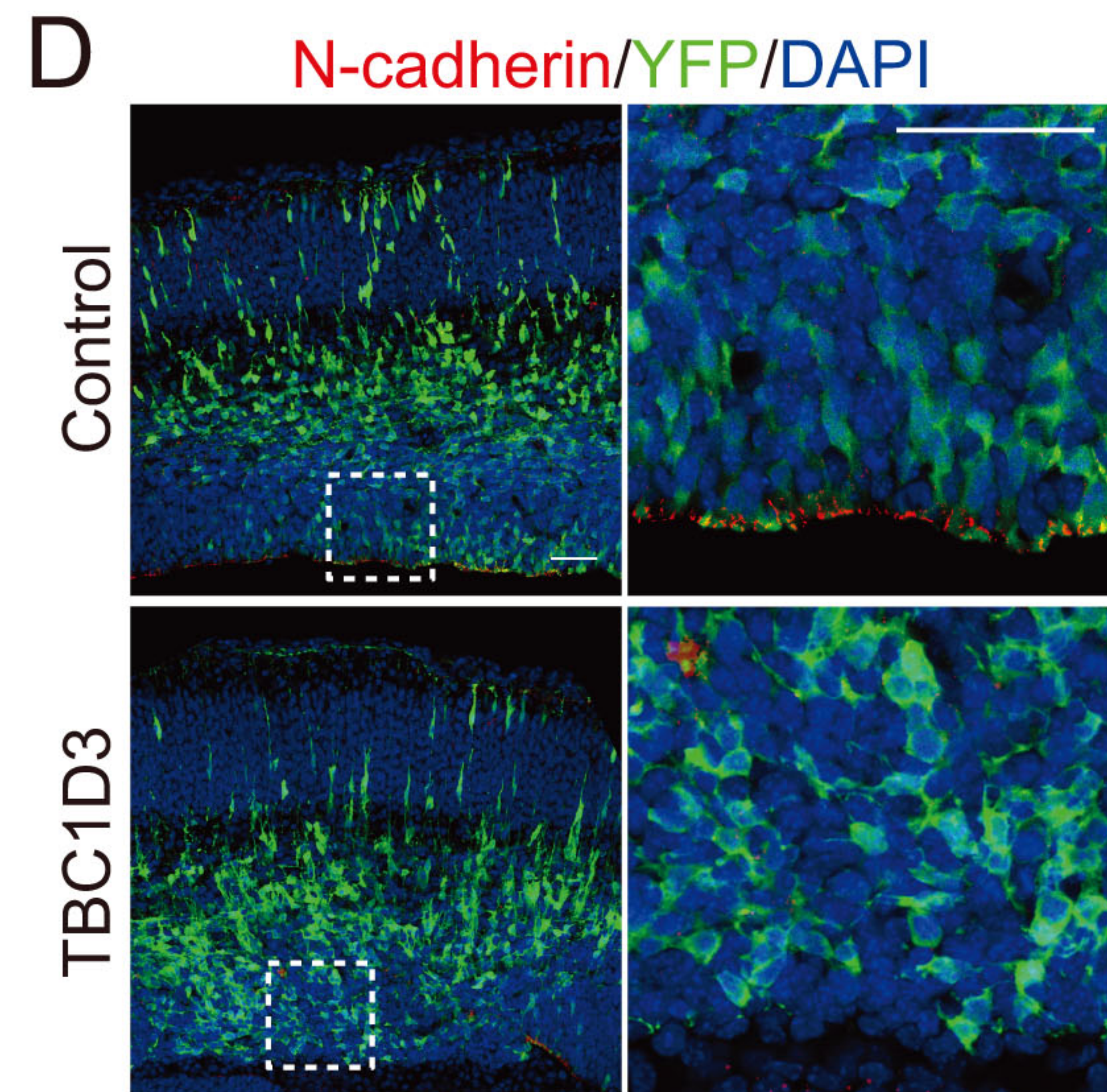
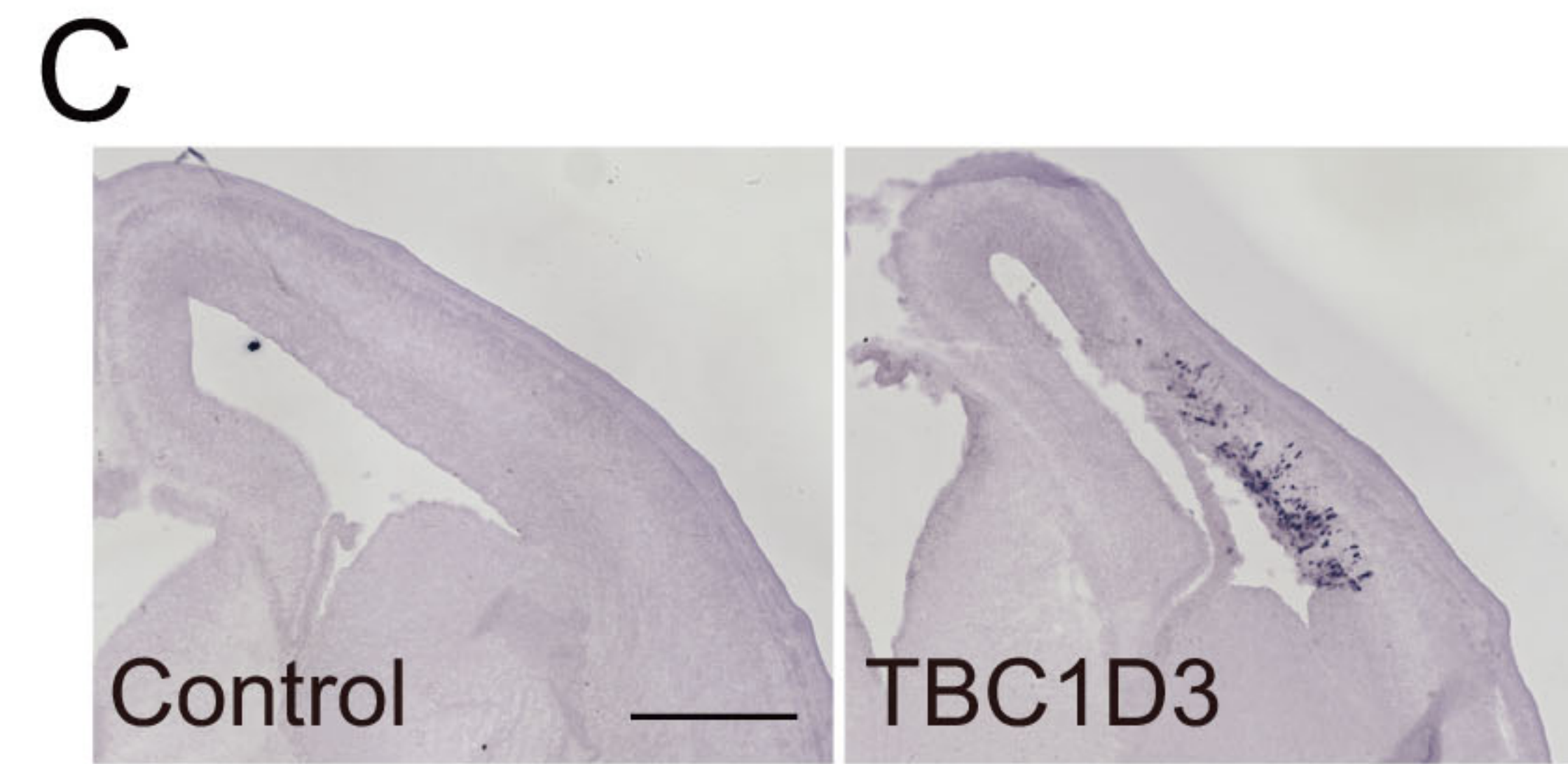
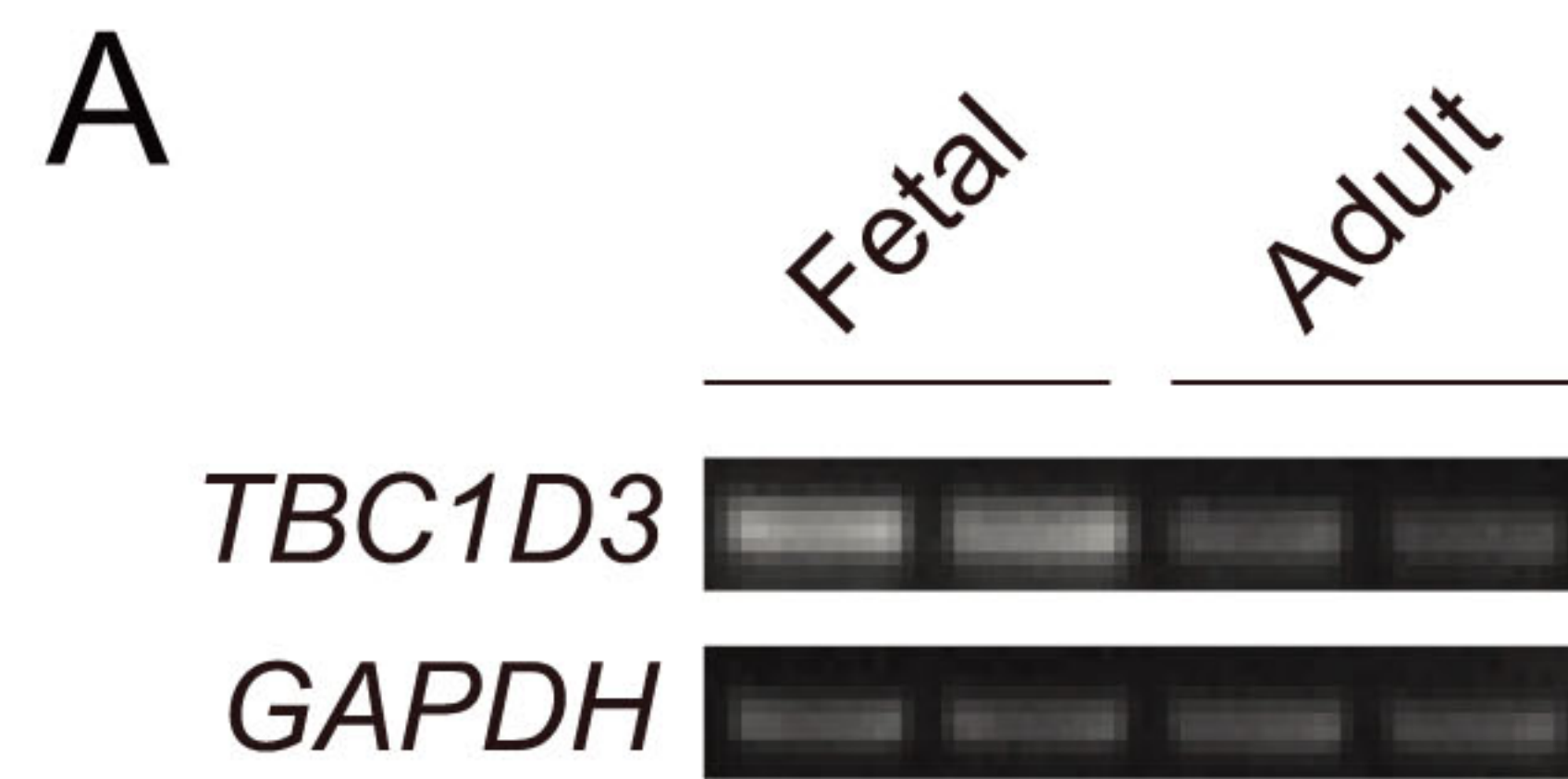
normalized as 1.0 (n = 3 experiments for each group). *Trnp1*: mean = 1.00, SEM = 0.03 for control; mean = 0.57, SEM = 0.07 for TBC1D3 (p = 0.0003). *Hes1*: mean = 1.00, SEM = 0.02 for control; mean = 0.96, SEM = 0.05 for TBC1D3 (p = 0.561). *Hes5*: mean = 1.00, SEM = 0.20 for control; mean = 0.85, SEM = 0.34 for TBC1D3 (p = 0.762). *Numb*: mean = 1.00, SEM = 0.17 for control; mean = 1.12, SEM = 0.14 for TBC1D3 (p = 0.612). (E) ReNeuron cells were transfected with constructs encoding siRNA targeting TBC1D3 or scrambled sequence. After 3 days, transfected cells were treated with actinomycin D for 4 hr and the mRNA level of *Trnp1* relative to *Hprt* was quantified (n = 4 experiments; mean = 94.40, SEM = 0.89 for control; mean = 94.67, SEM = 1.05 for siTBC1D3; p = 0.851). Data are presented as mean \pm SEM of percentage of *Trnp1* mRNA compared to the value prior to actinomycin D treatment. (F) Cortices of E14.5 WT and TG mice were stained for pERK1/2. and TBC1D3. Scale bars, 20 μ m (F), 10 μ m (F1). (G) Quantification for the ratio of pERK1/2 intensity in VZ/SVZ regions to that in CP (WT: n = 3 mice, mean = 1.17, SEM = 0.07; TG: n = 5 mice, mean = 1.50, SEM = 0.05). p = 0.006. (H) GW15.5 human brain slice was stained with pERK1/2, Pax6, and Tbr2 antibodies. Scale bars, 50 μ m (H) and 10 μ m (H1). (I) Quantification of pERK1/2 levels in different types of OSVZ progenitors (n = 2 slices). Note that almost all pERK1/2 signals are detected in Pax6⁺Tbr2⁻ cells. (J) Proposed model for the role of TBC1D3 in cortical folding. TBC1D3 expression causes delamination of vRG cells, through down-regulating the level of N-cadherin and *Trnp1*, and promotes proliferation of oRG-like cells by regulating cell stemness pathways, including Ras/ERK signaling. The increased generation of the oRG-like cells, the IP cells, and subsequently regional increase in the density of new born neurons, induces cortical folding in mice.

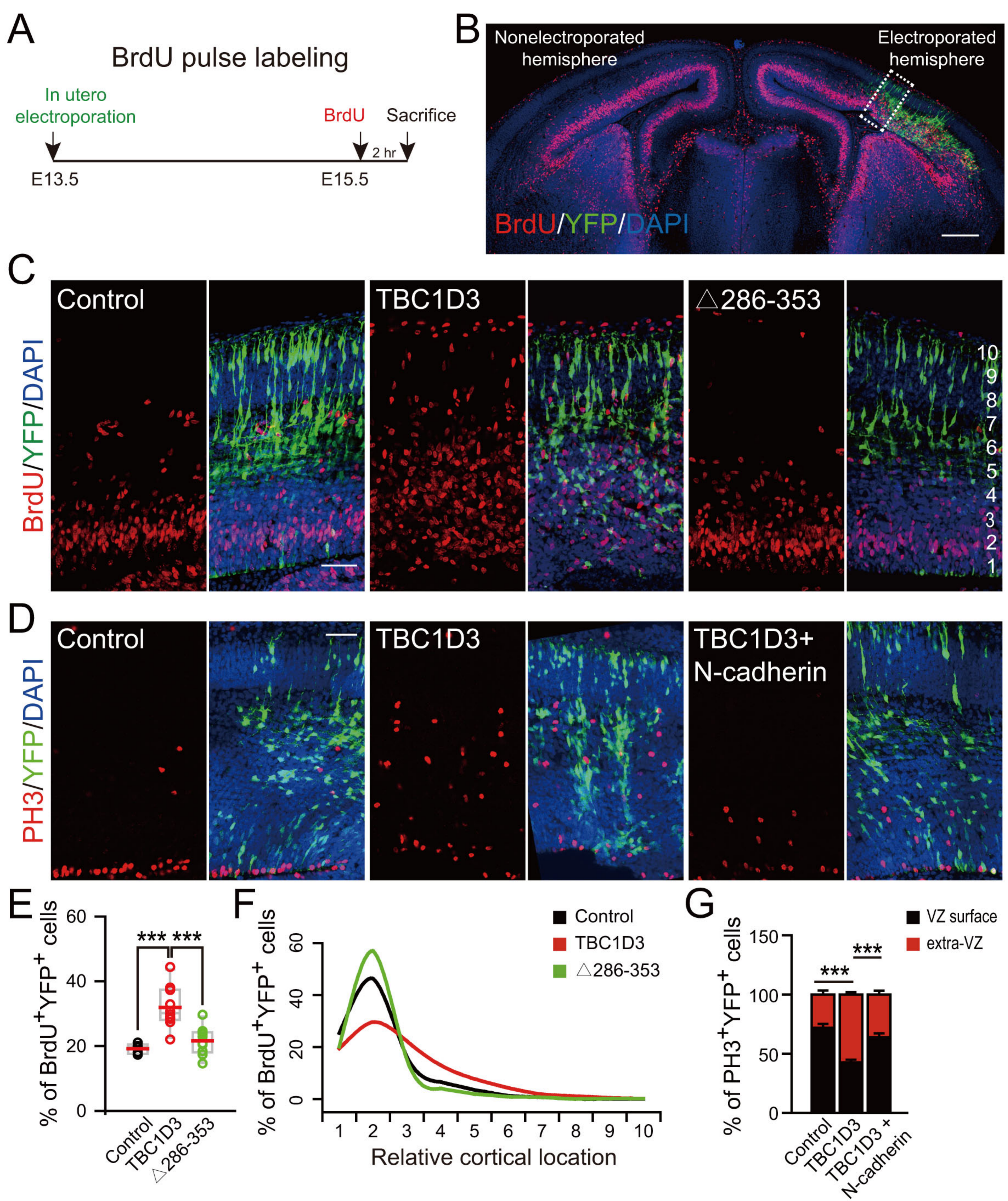
Video 1. oRGs in cultured organotypic slices from control mice. This movie illustrates the behavior of the sparse oRGs in organotypic slice cultures from control mice electroporated with vehicle plasmid. IUE was done at E13.5 and organotypic slice culture

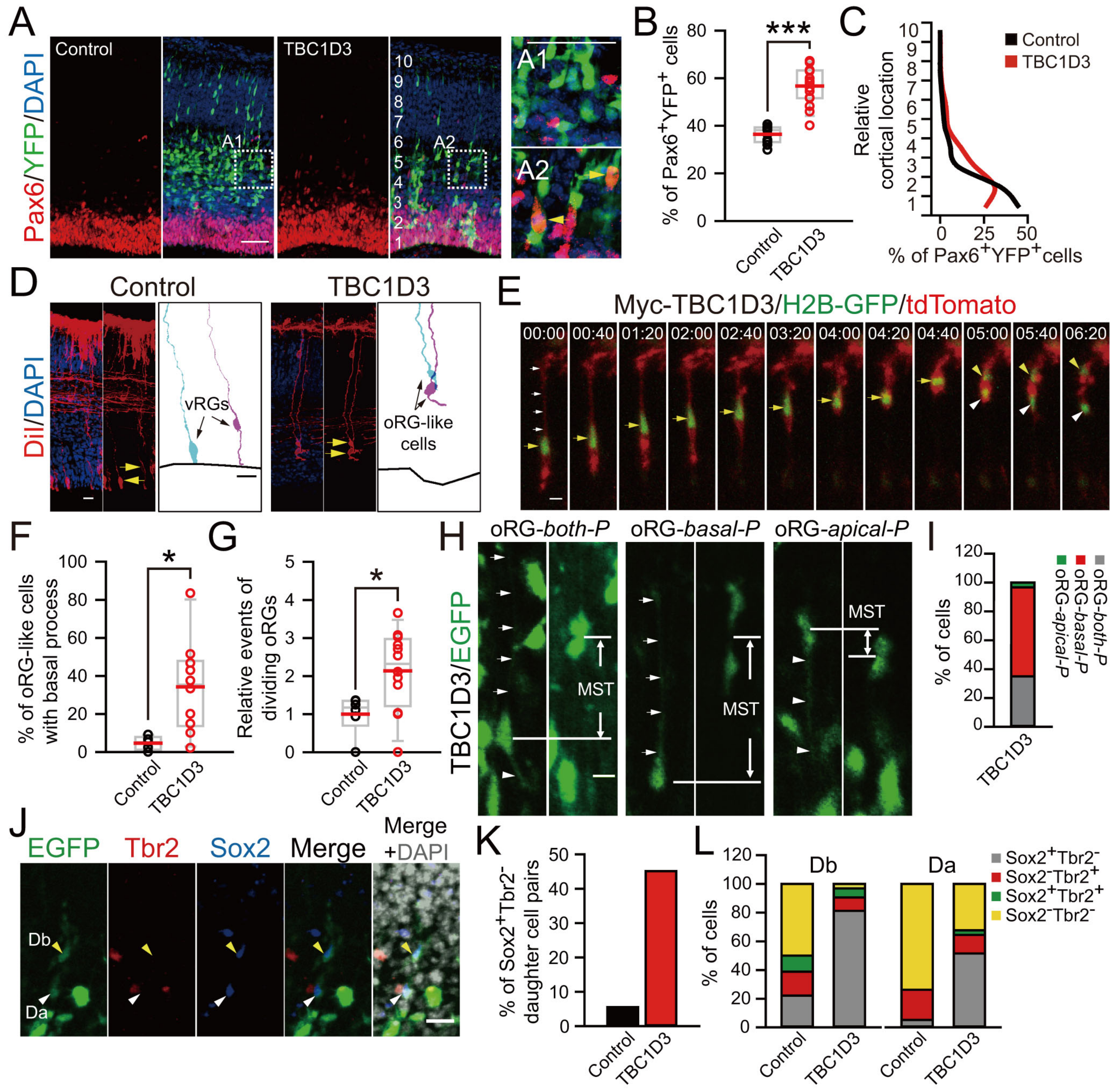
was prepared at E14.5 and observed 2-3 hr after culture preparation. White arrows indicate oRGs before division, and cyan and red arrowheads indicate daughter cells dividing towards the pial and ventricular surface, respectively. Scale bar, 50 μ m.

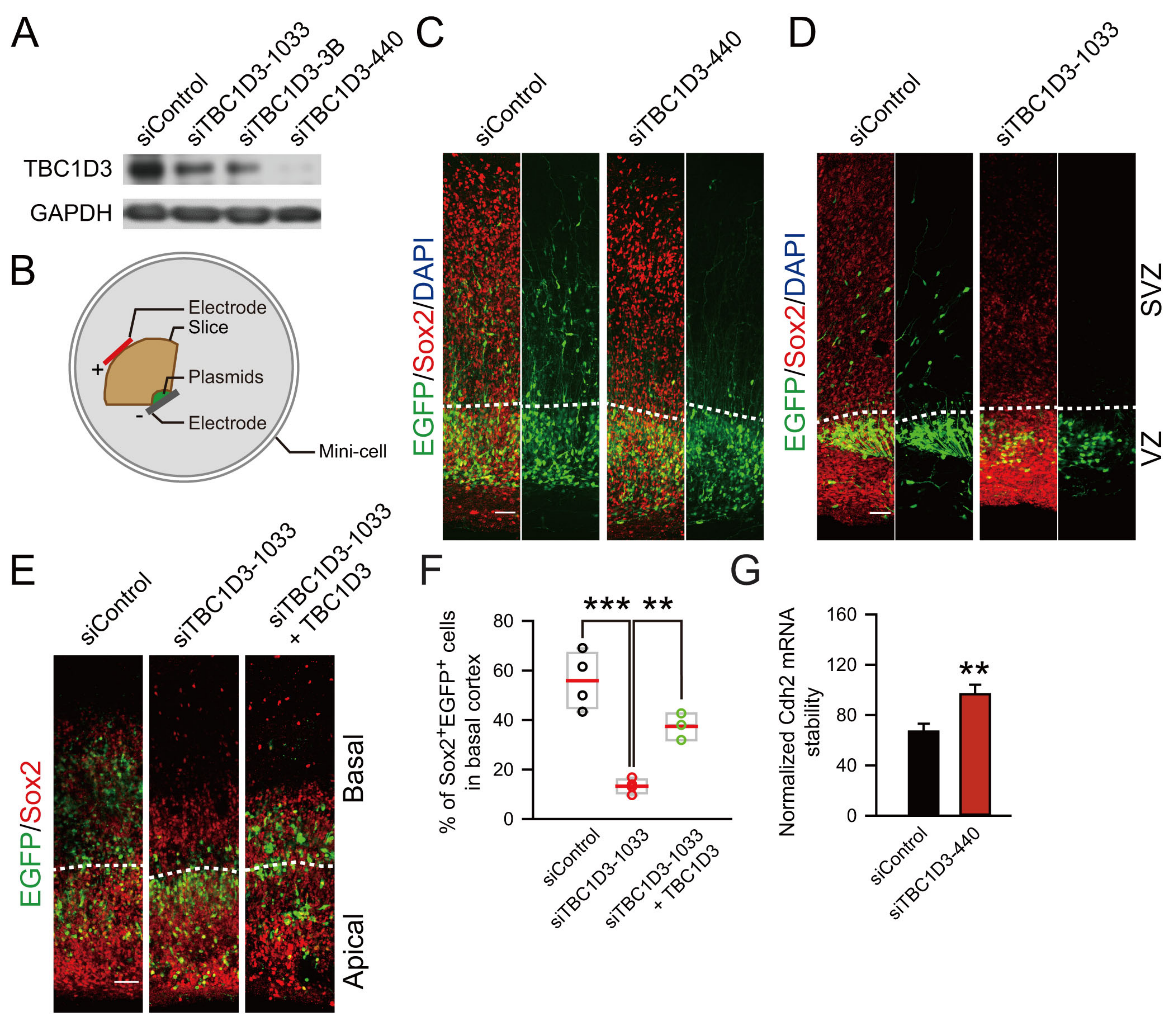
Video 2. oRGs in cultured organotypic slices from TBC1D3-electroporated mice.

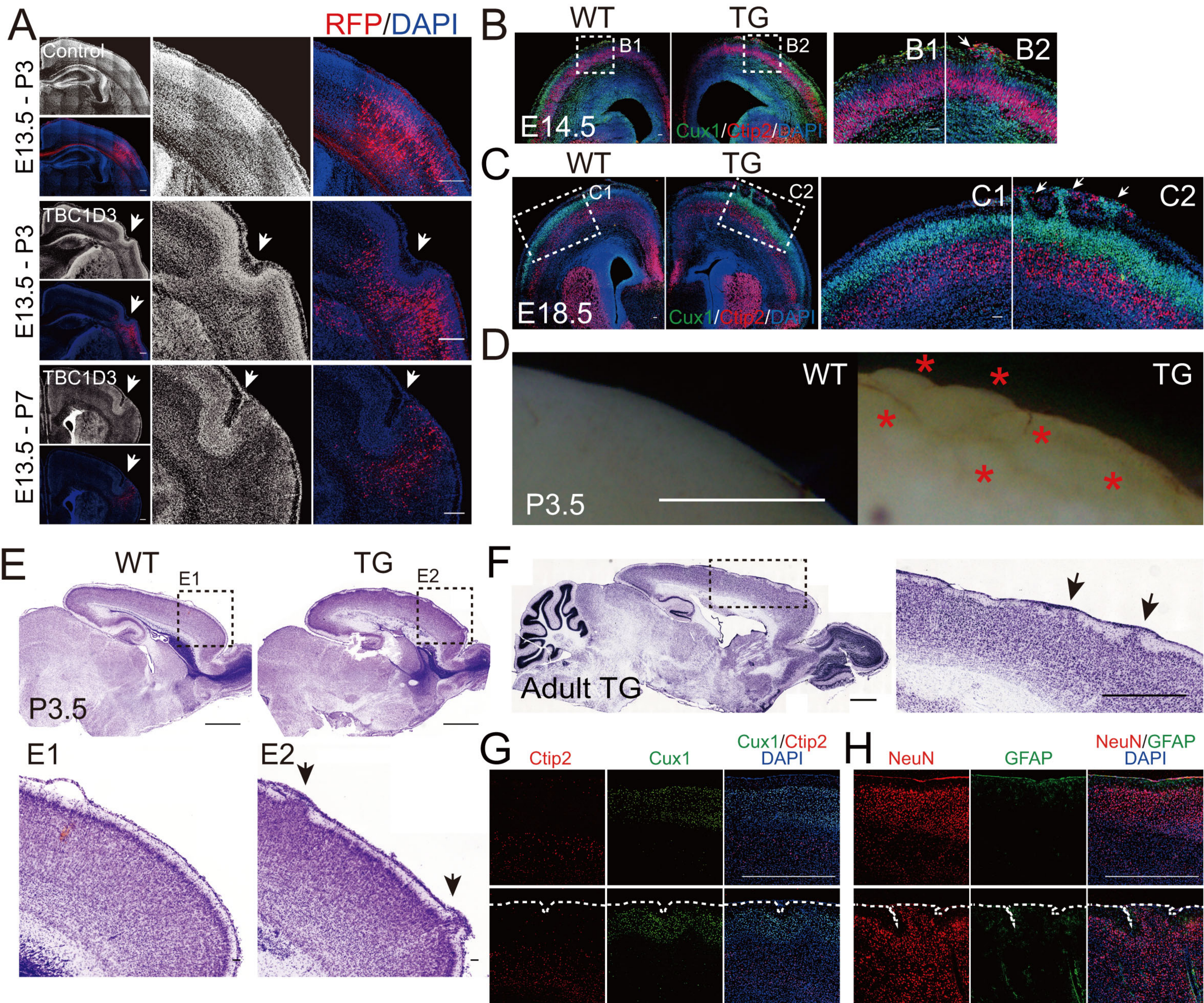
This movie illustrates the behavior of TBC1D3-expressing oRGs. IUE was done at E13.5 and organotypic slice culture prepared at E14.5 and observed 2-3 hr after culture preparation. White arrows indicate oRGs before division, and cyan and red arrowheads indicate daughter cells dividing towards the pial and ventricular surface, respectively. Scale bar, 50 μ m.

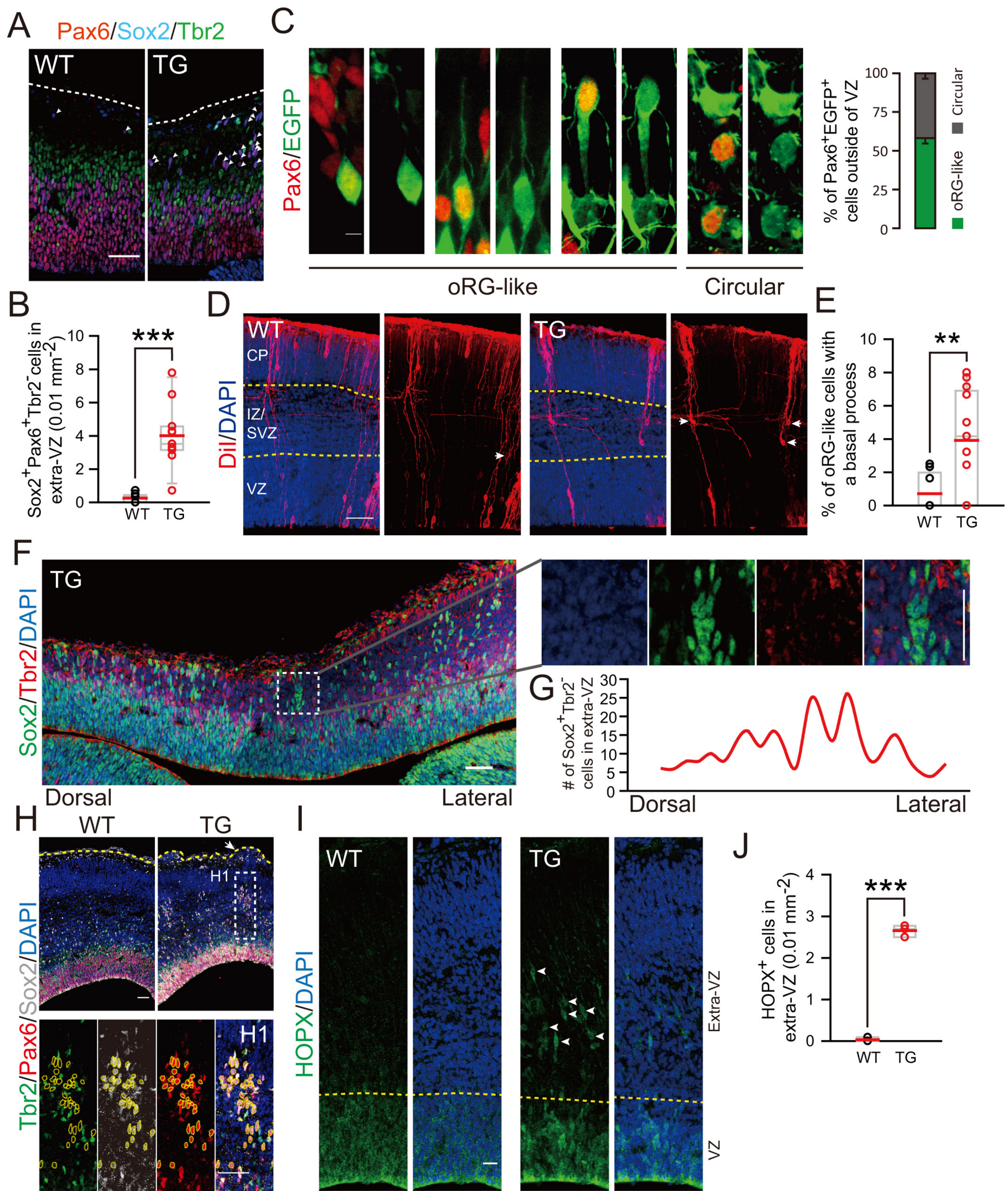


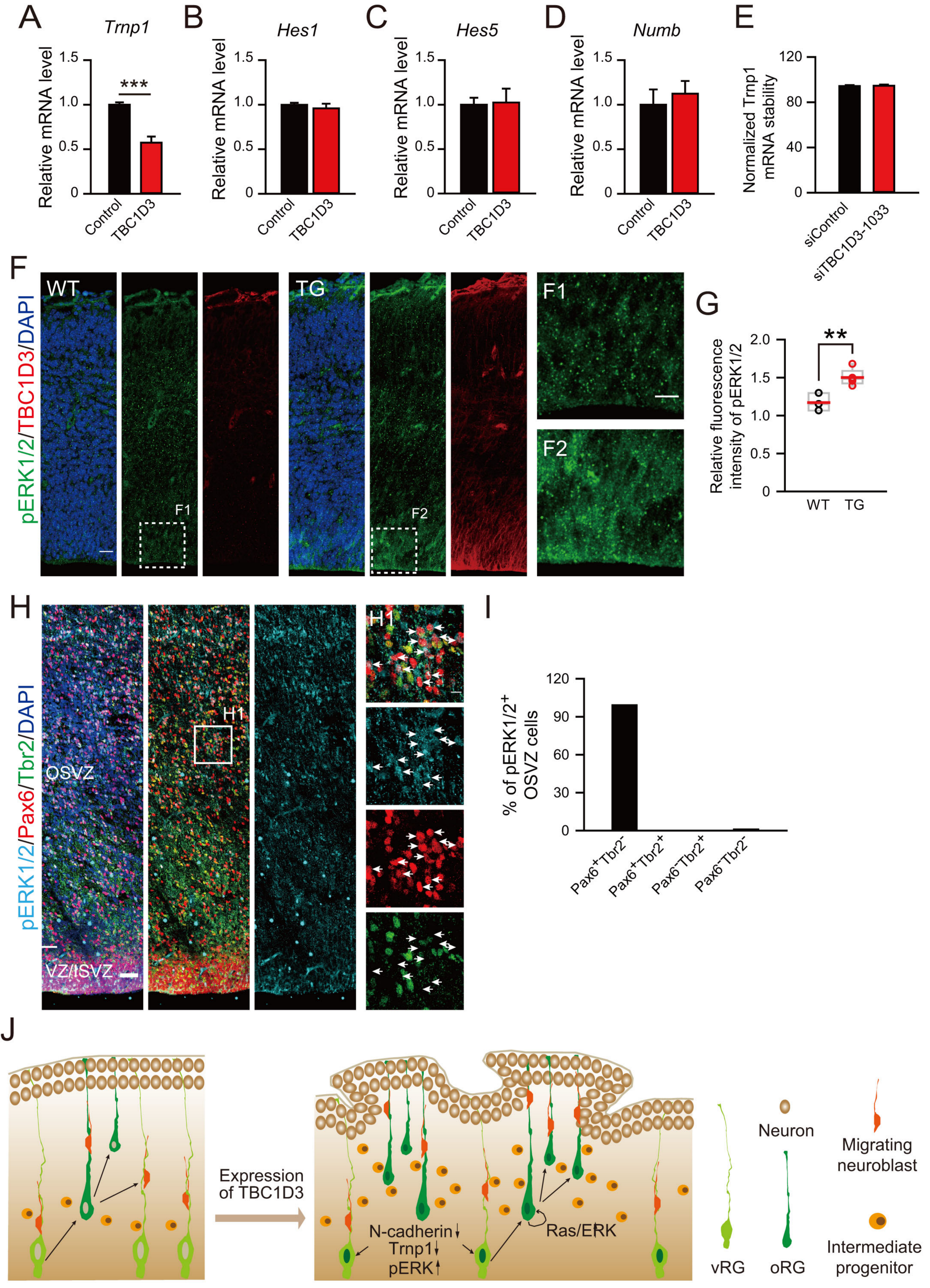




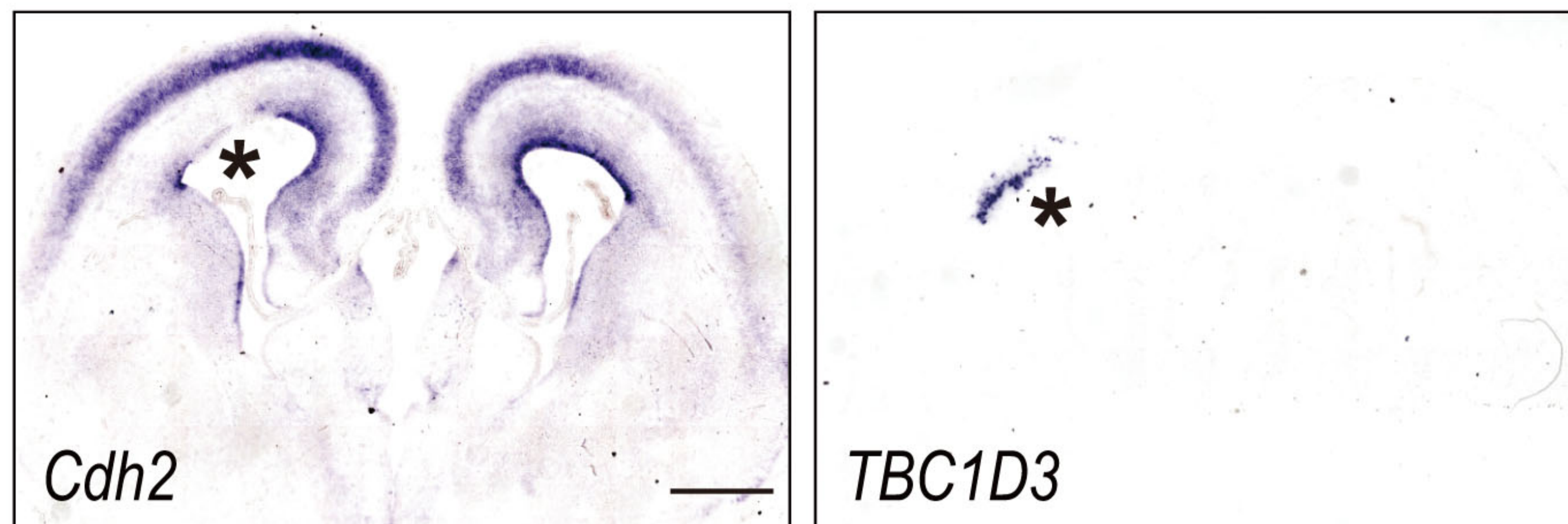




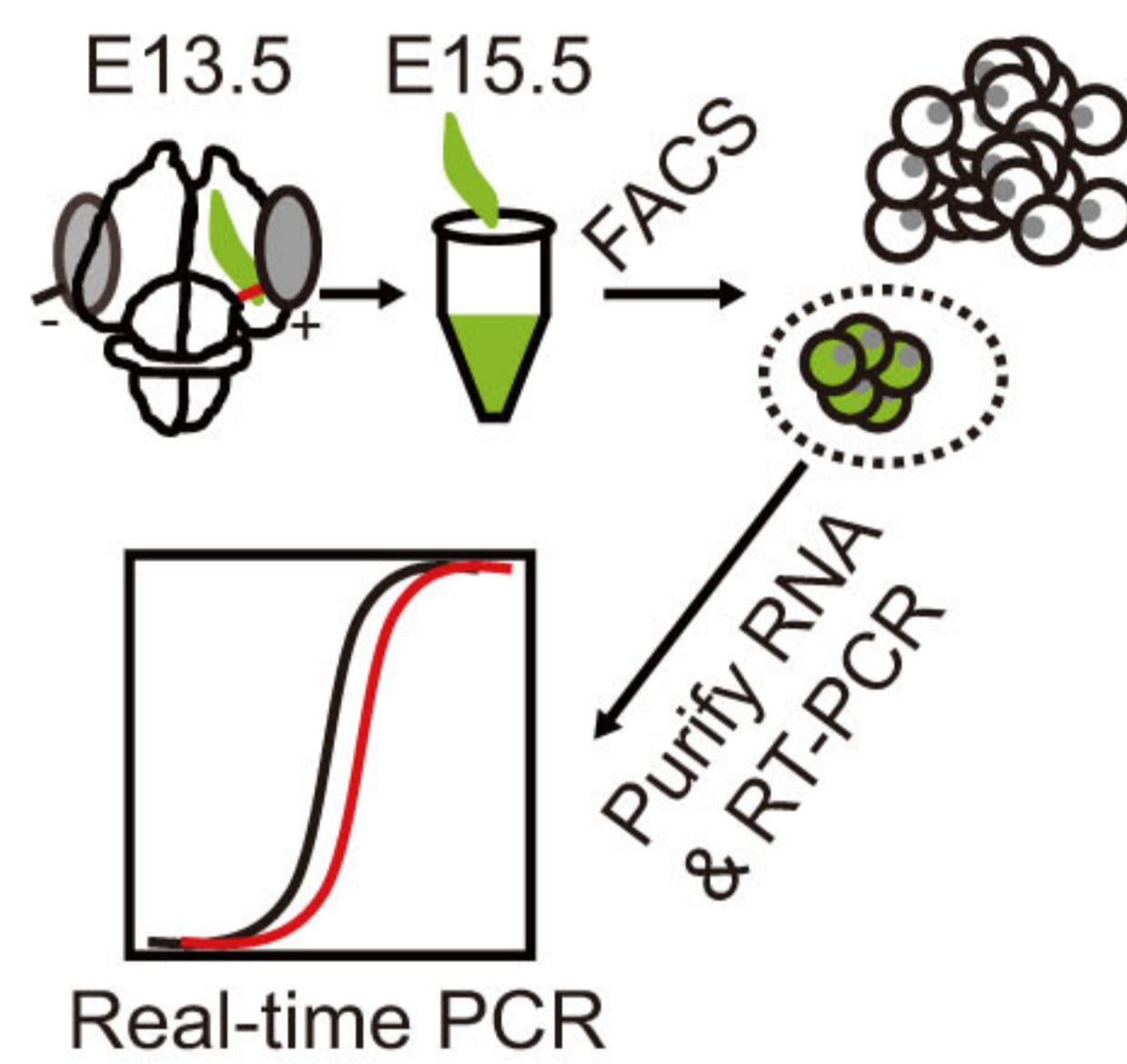




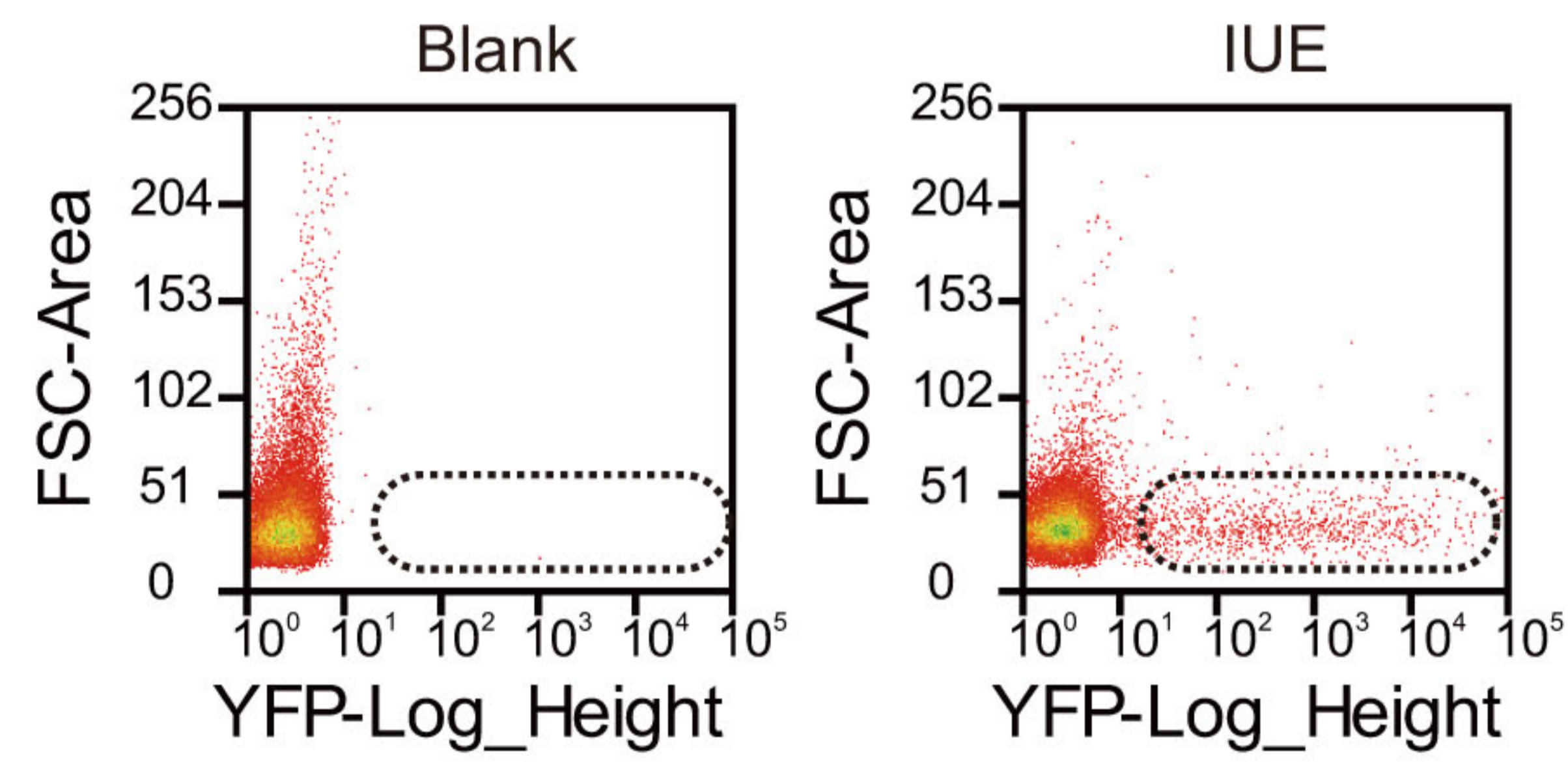
A



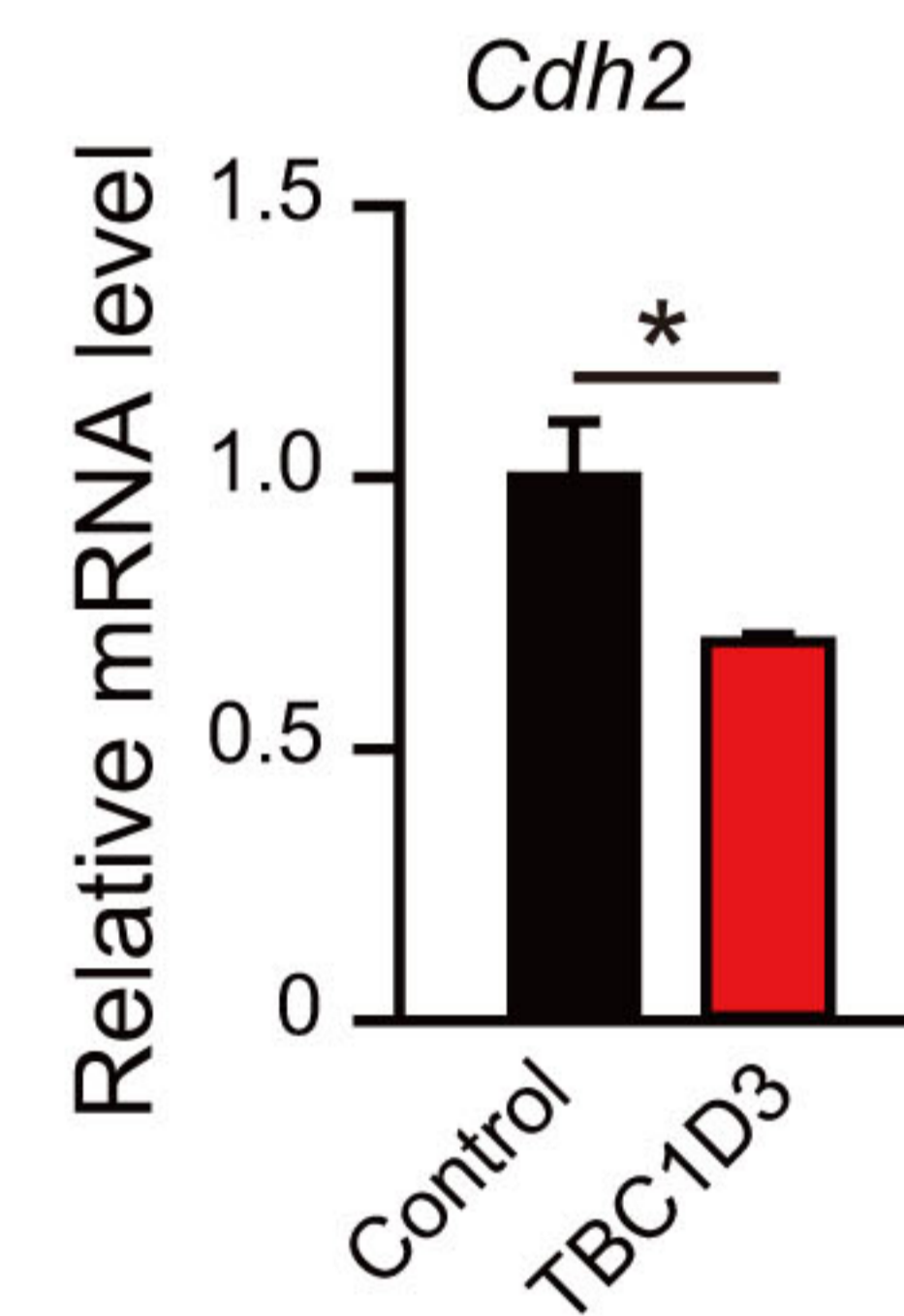
B



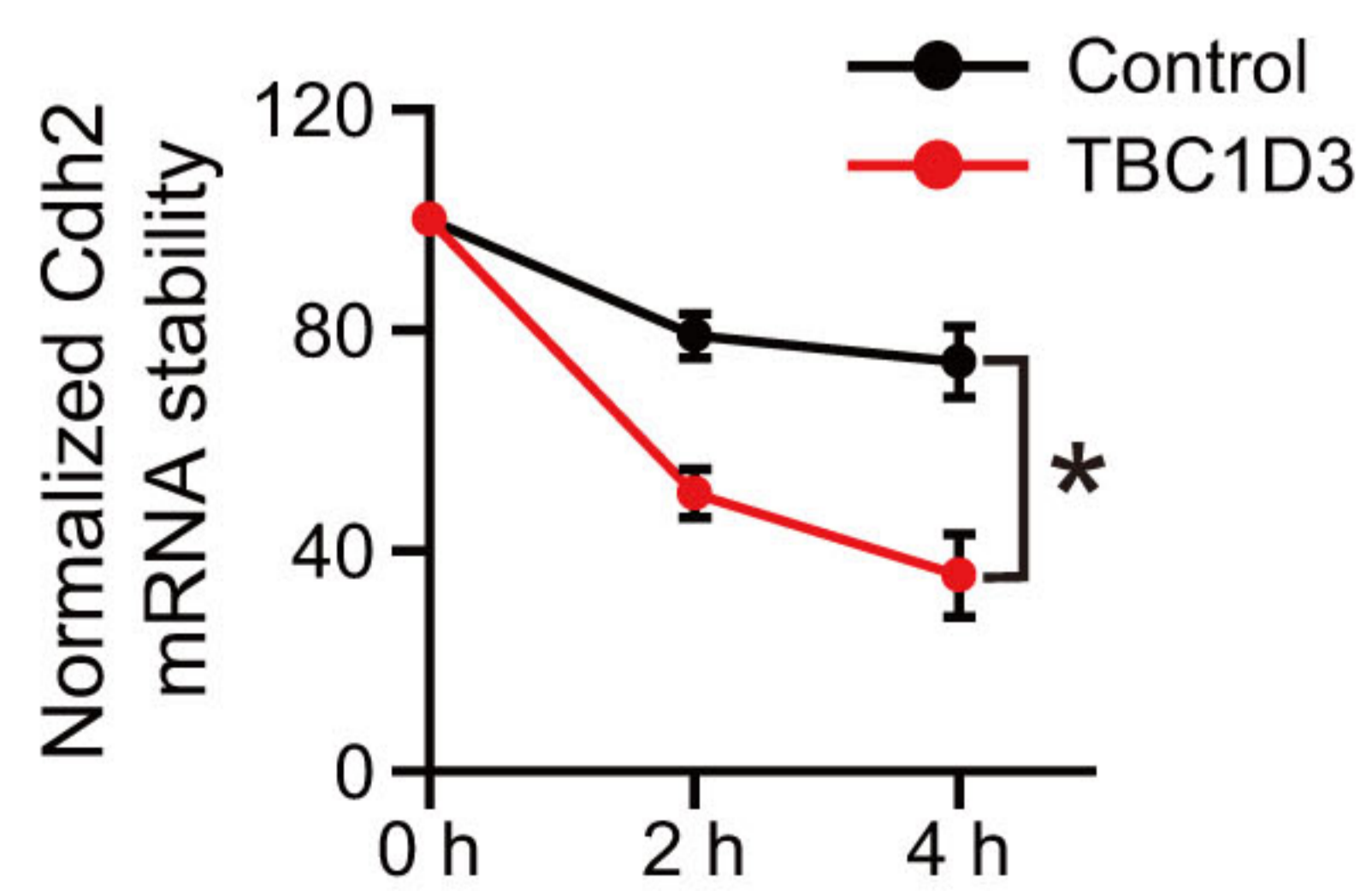
C



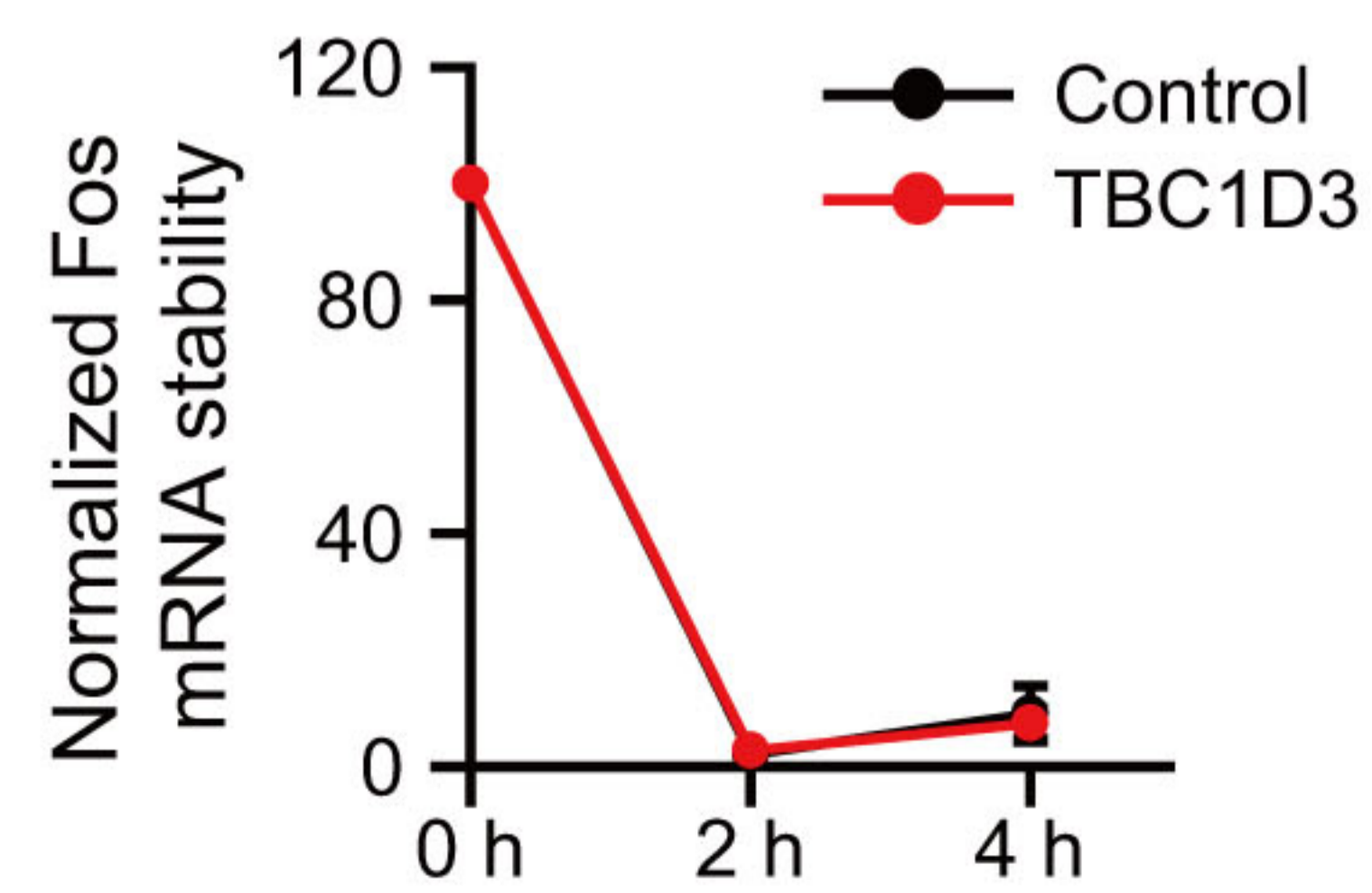
D



E

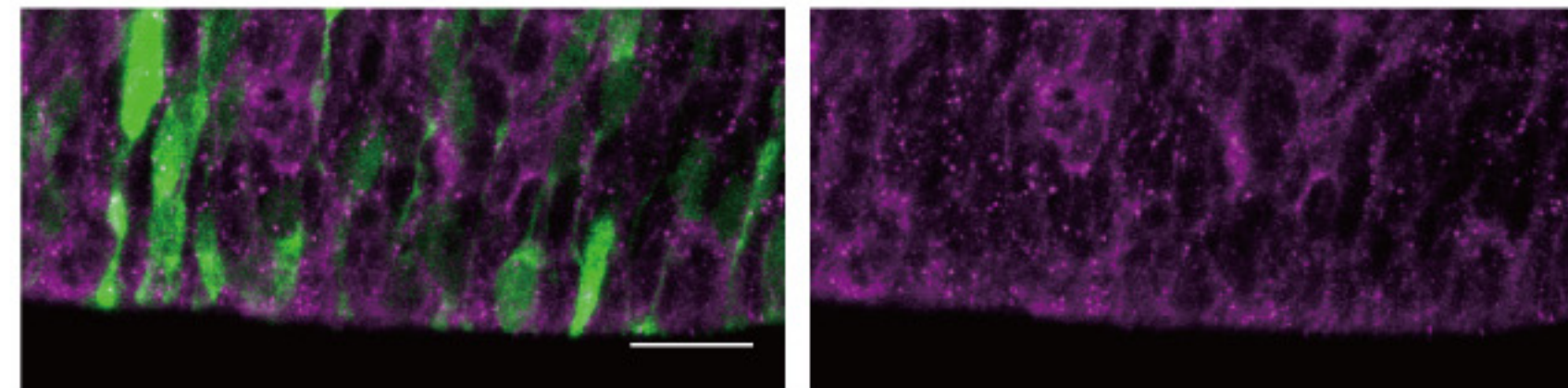


F

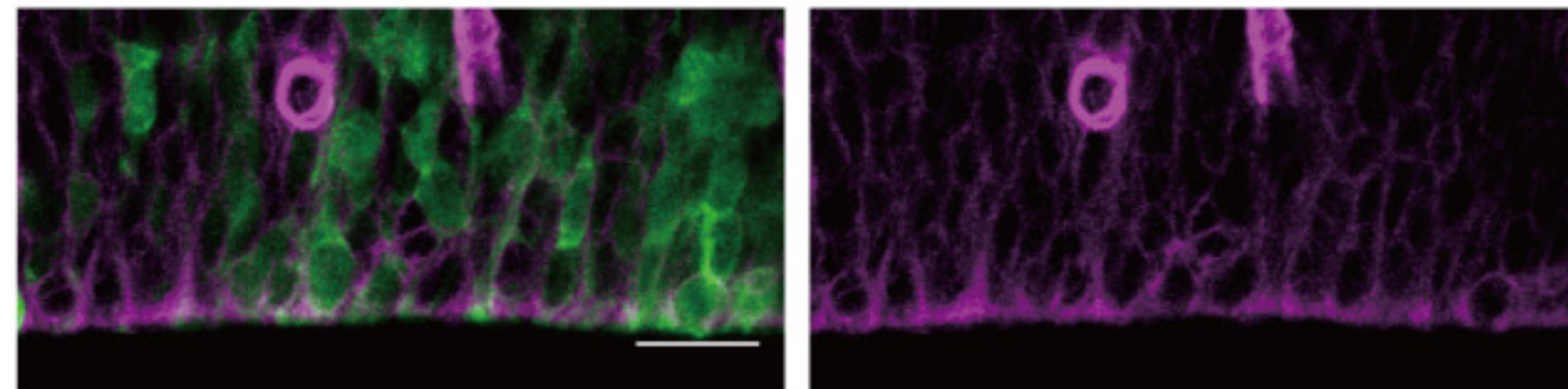


Control

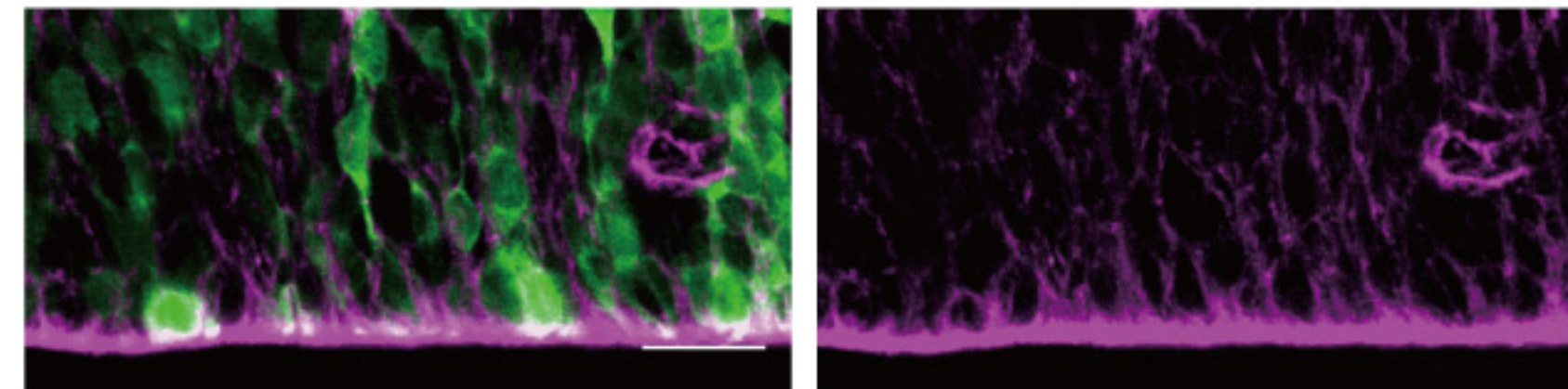
Numb/EGFP



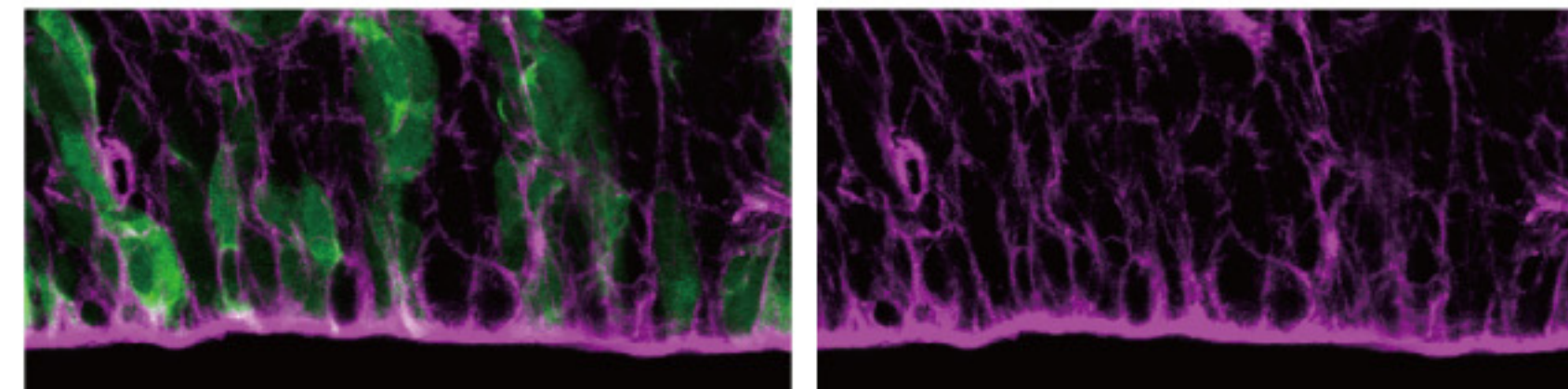
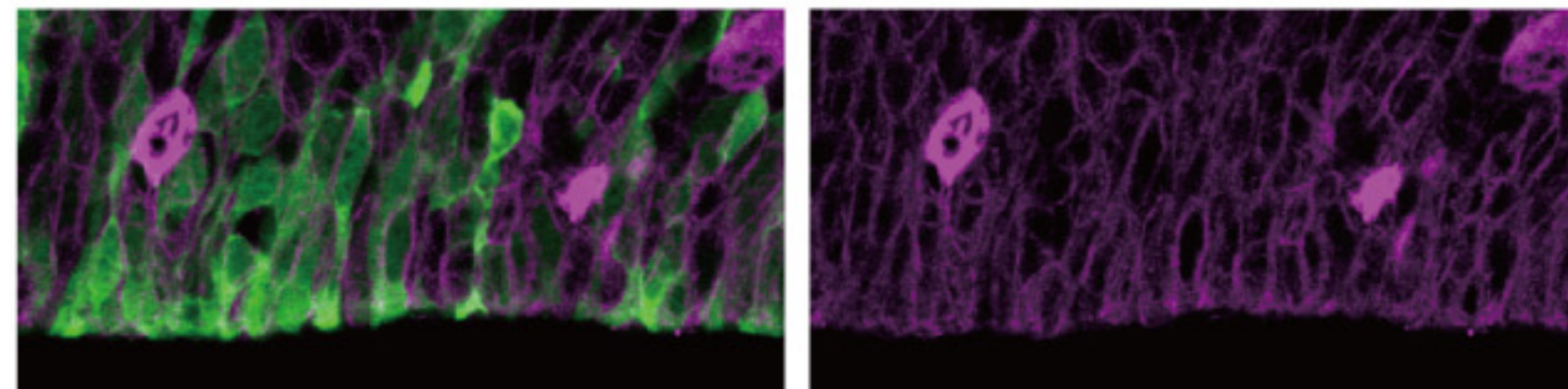
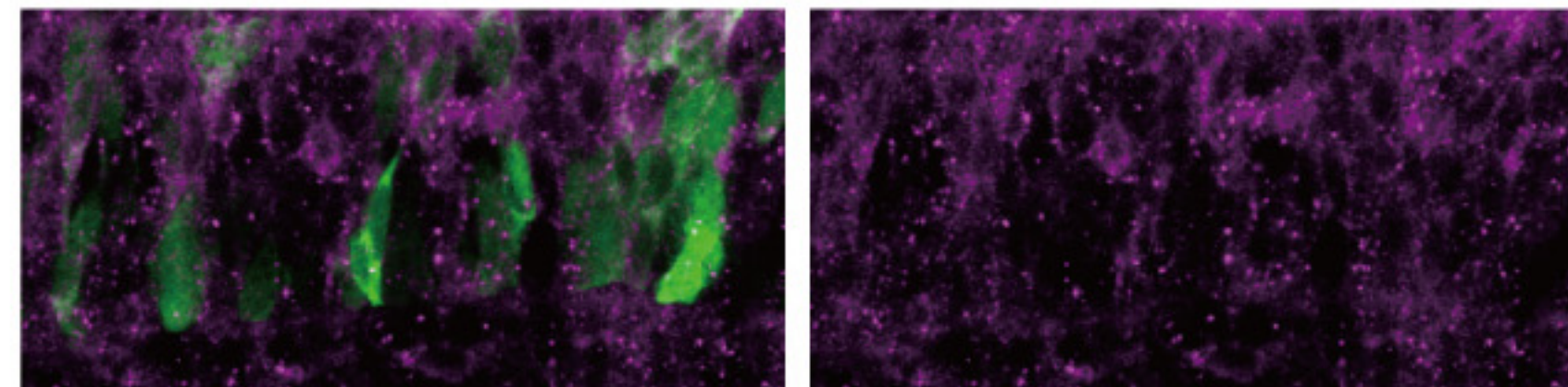
ITGB1/EGFP



F-actin/EGFP

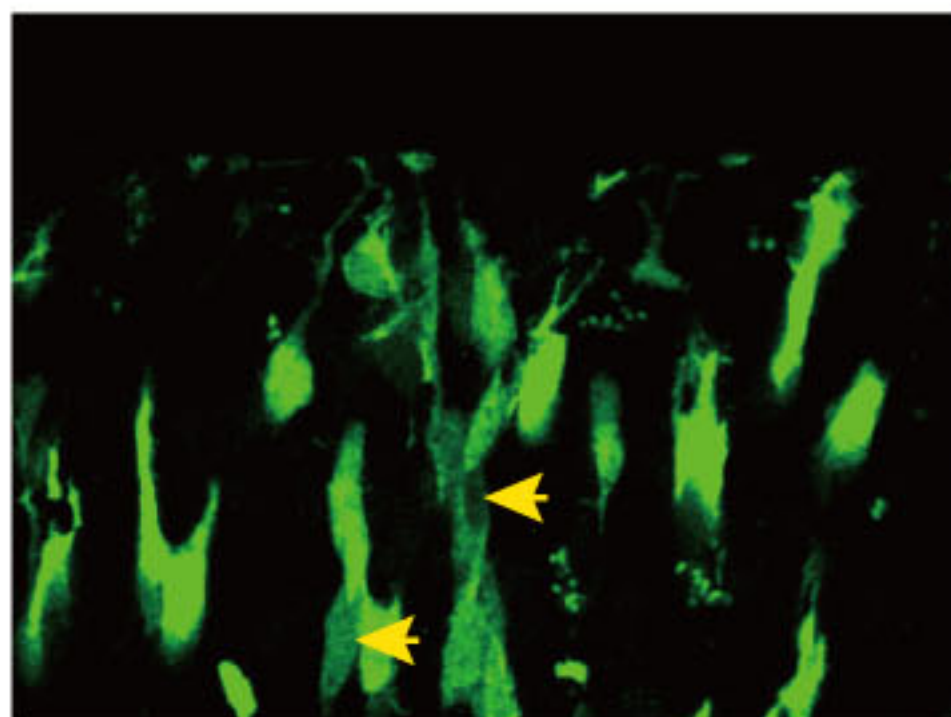


TBC1D3

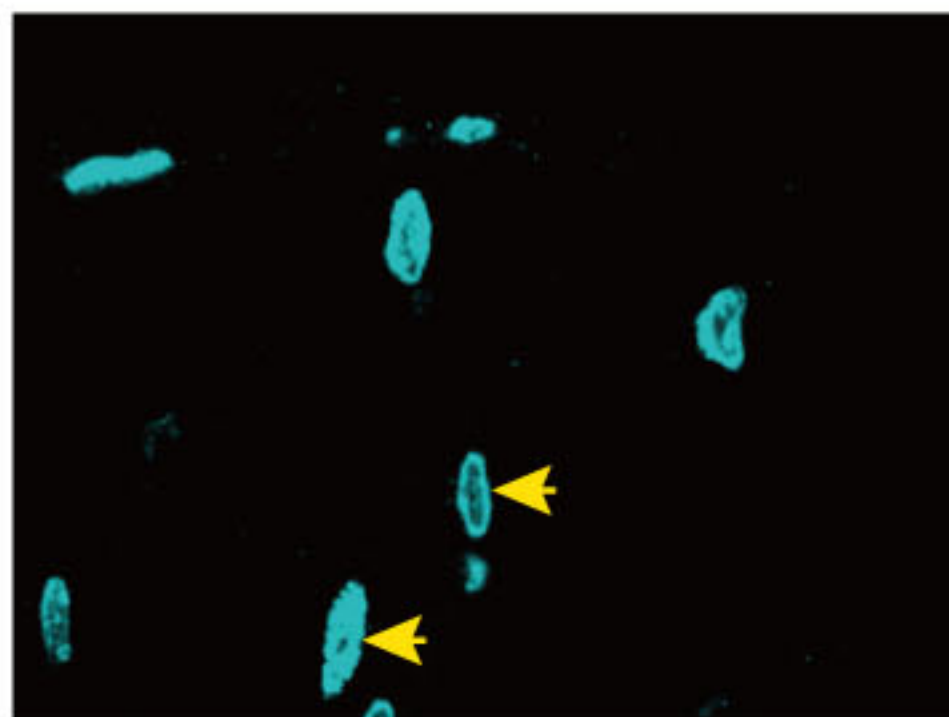


TBC1D3 + YFP

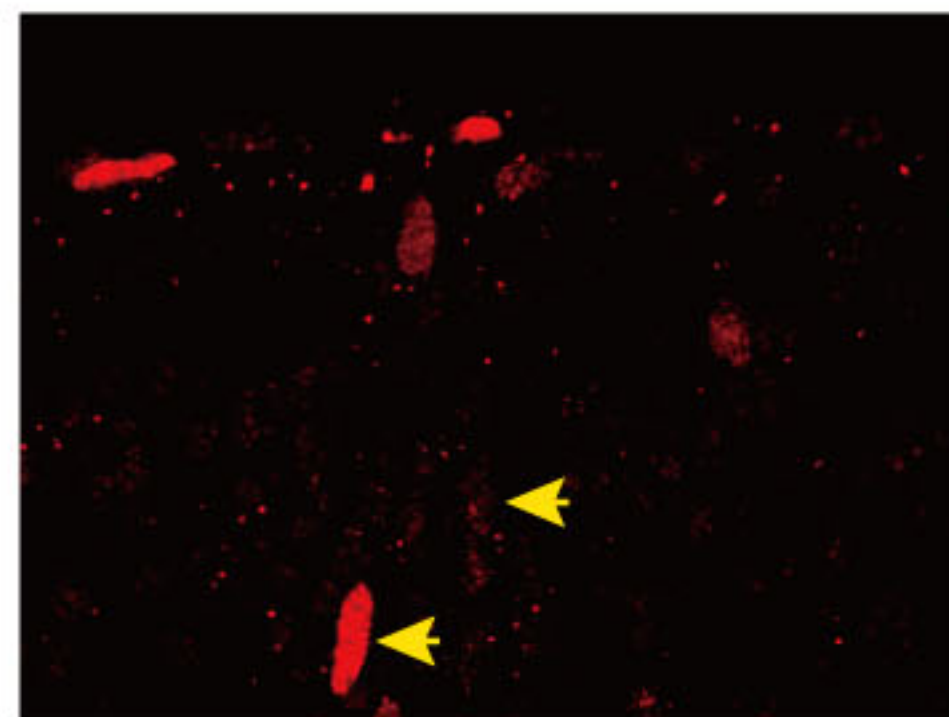
YFP



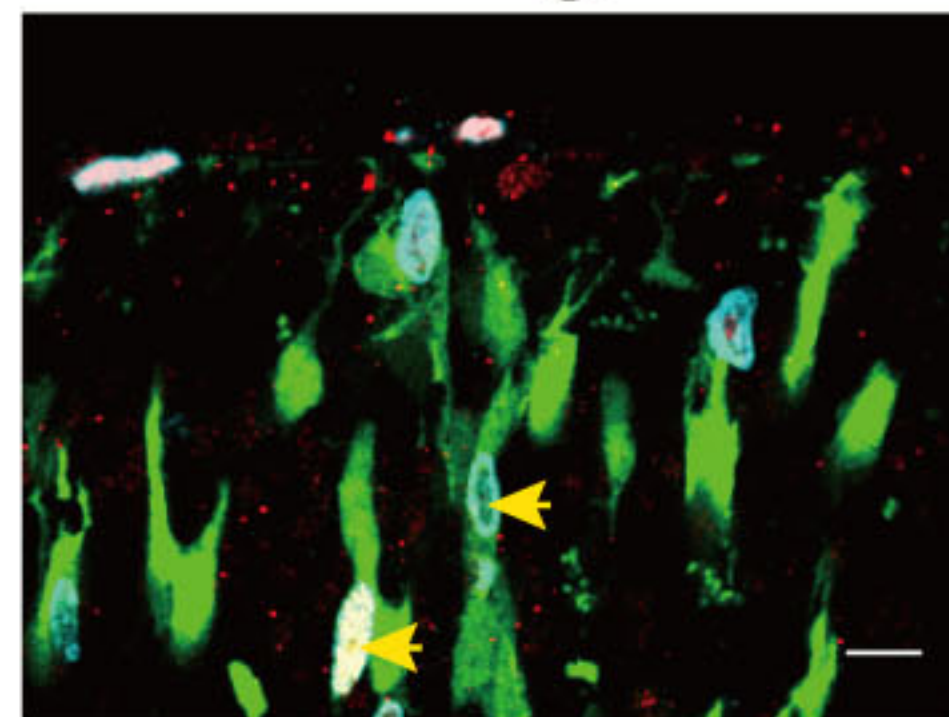
BrdU



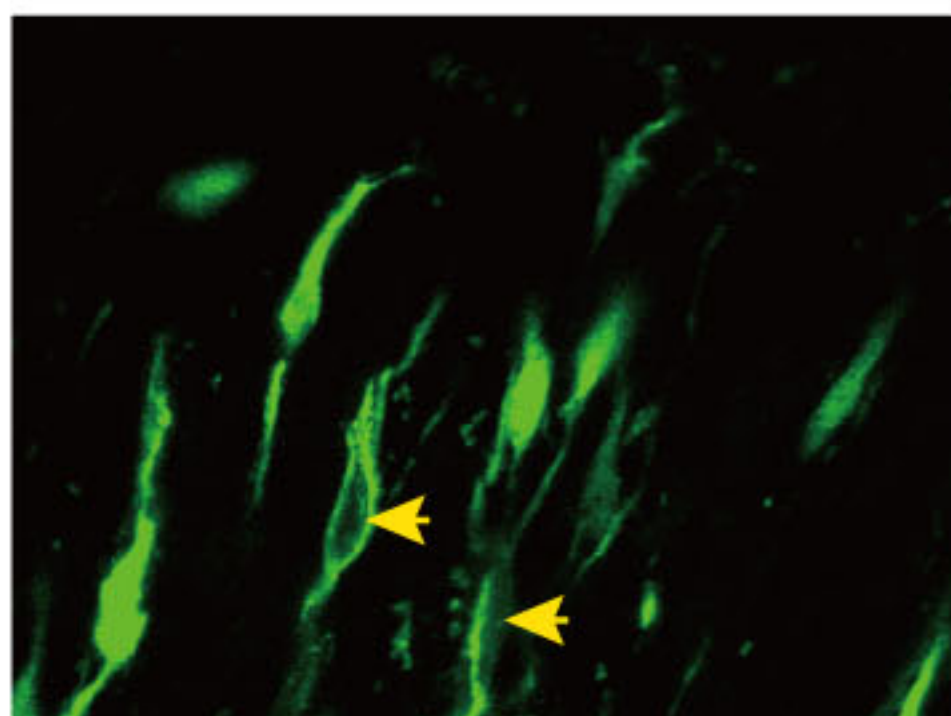
Ki67



Merge



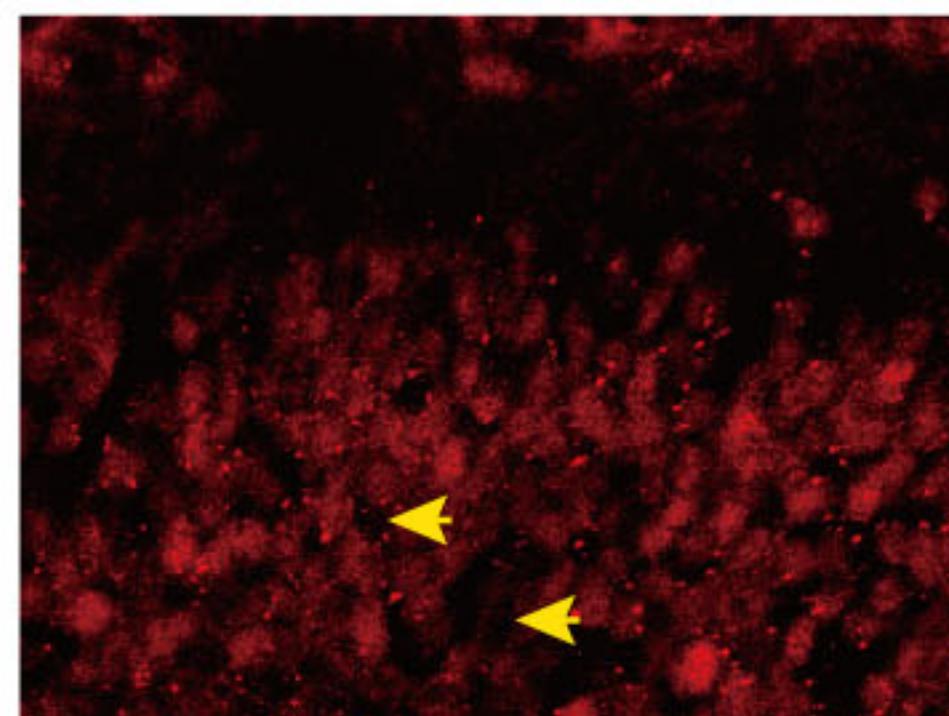
YFP



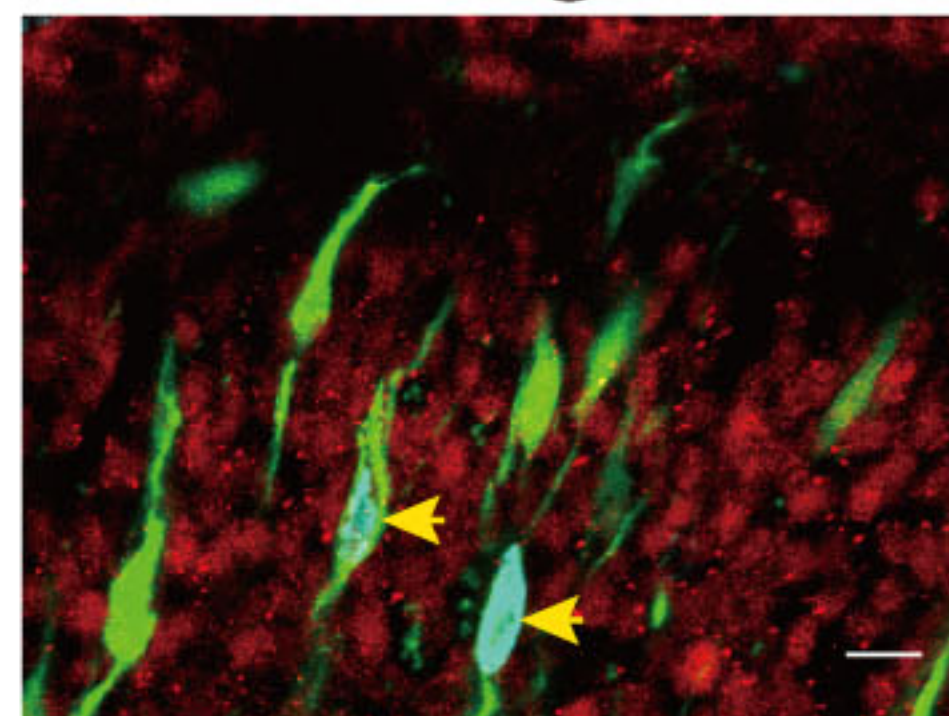
BrdU

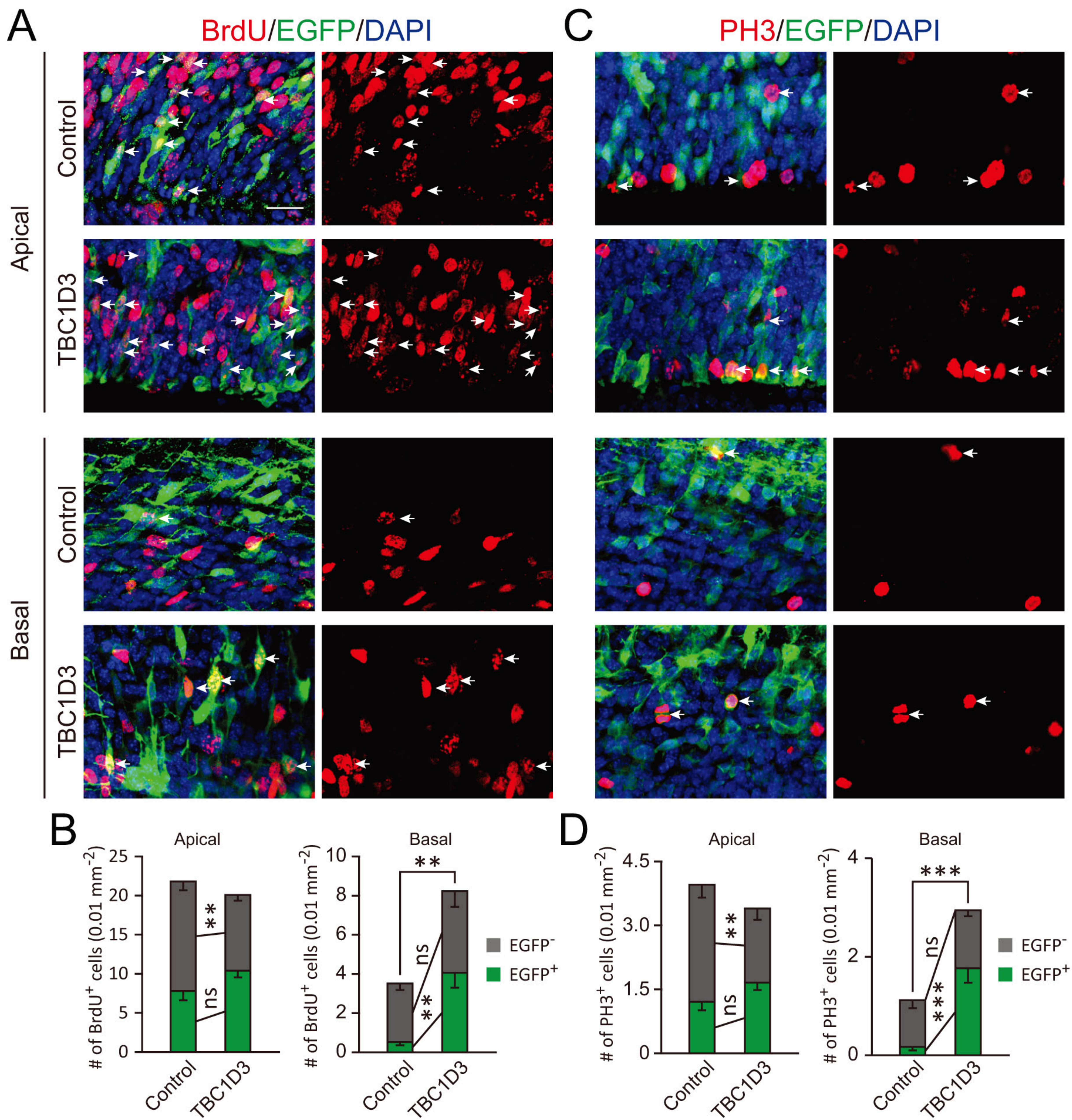


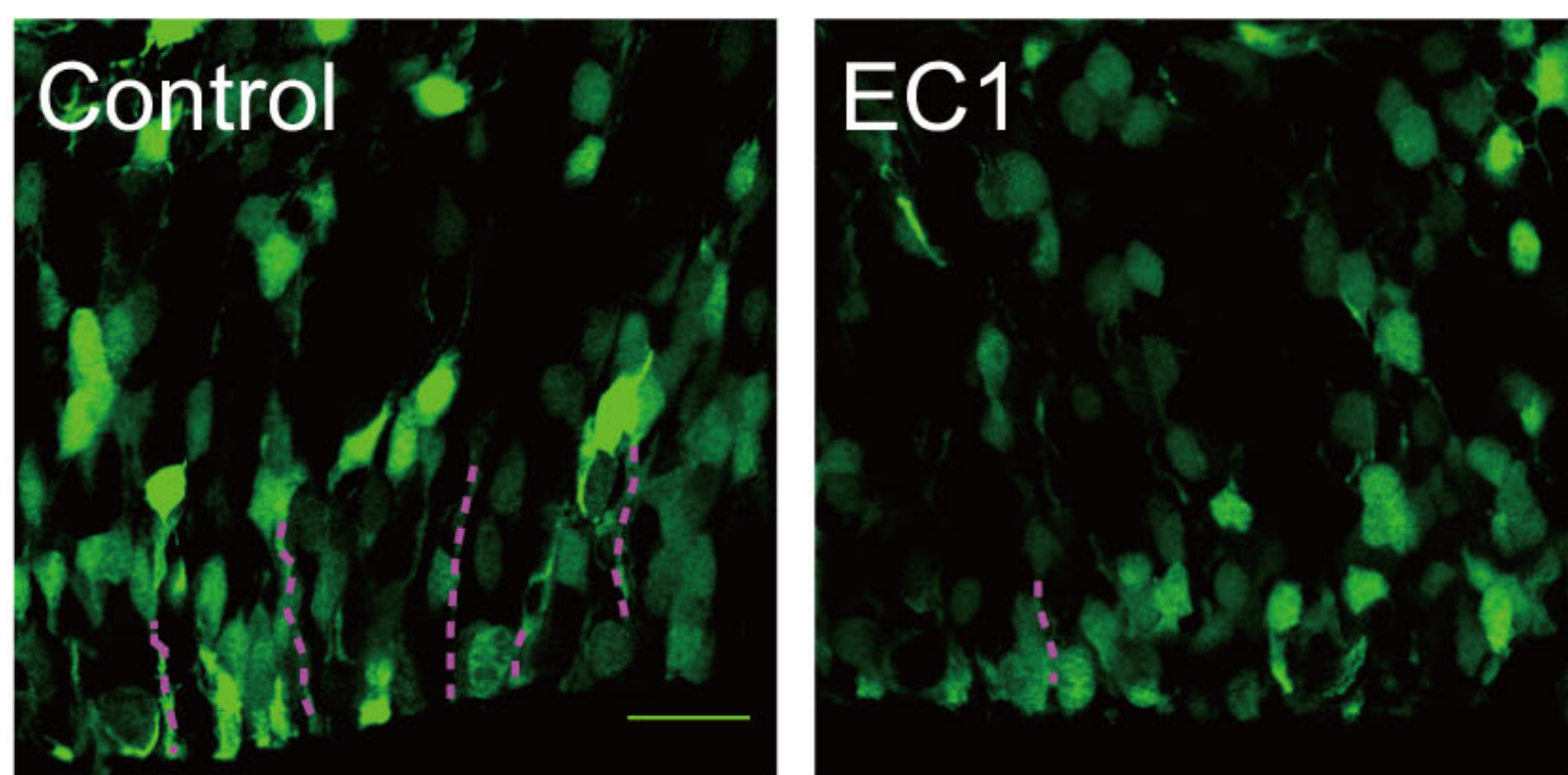
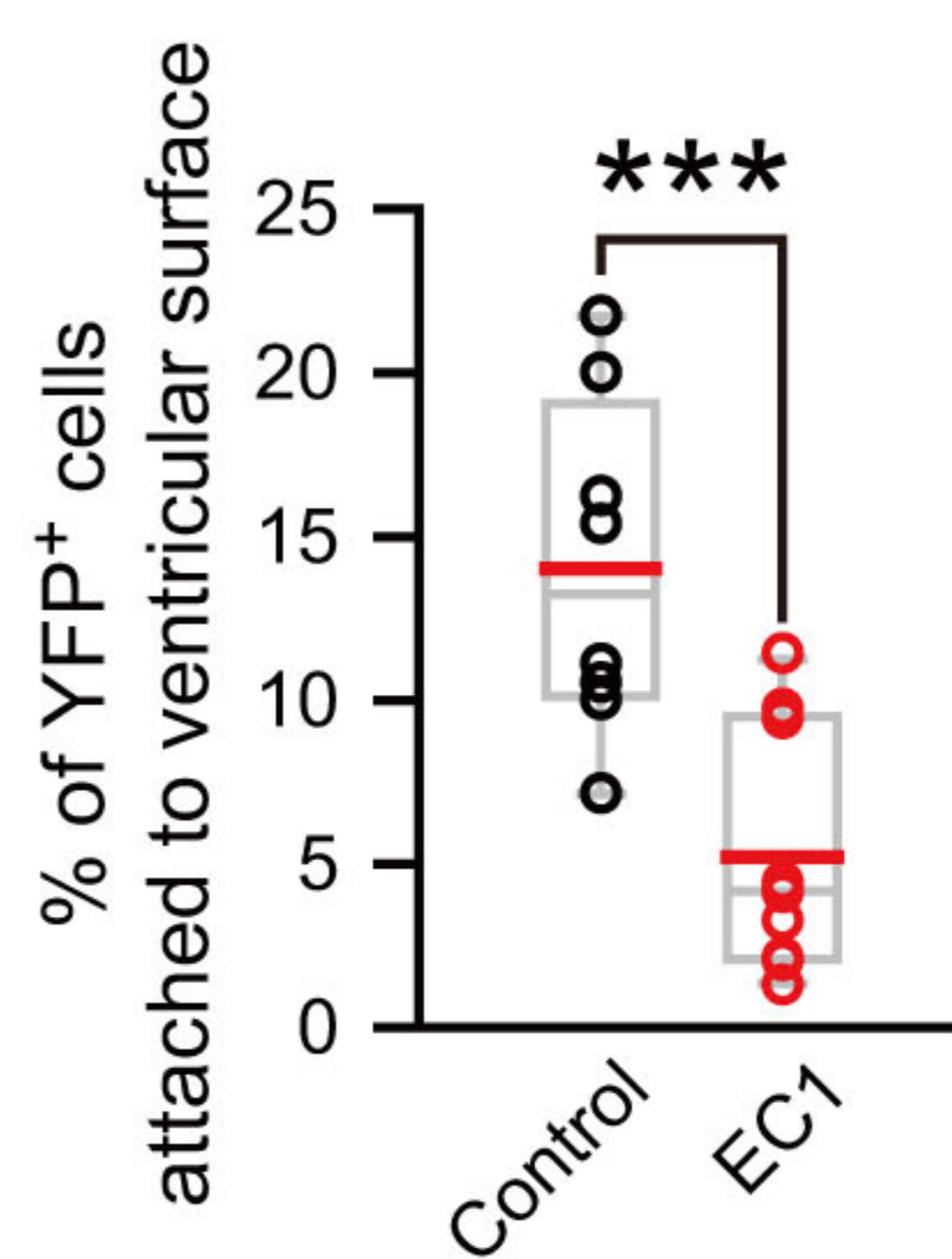
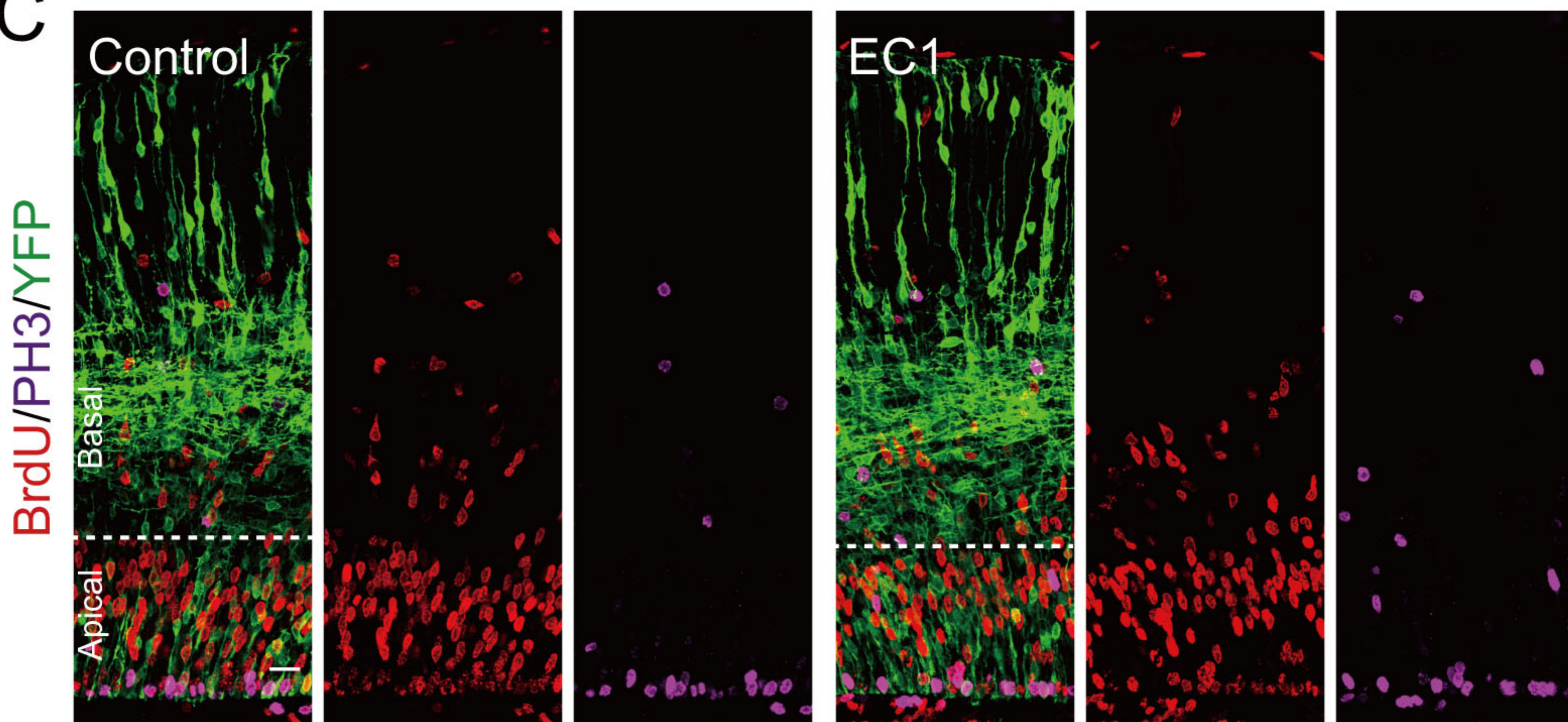
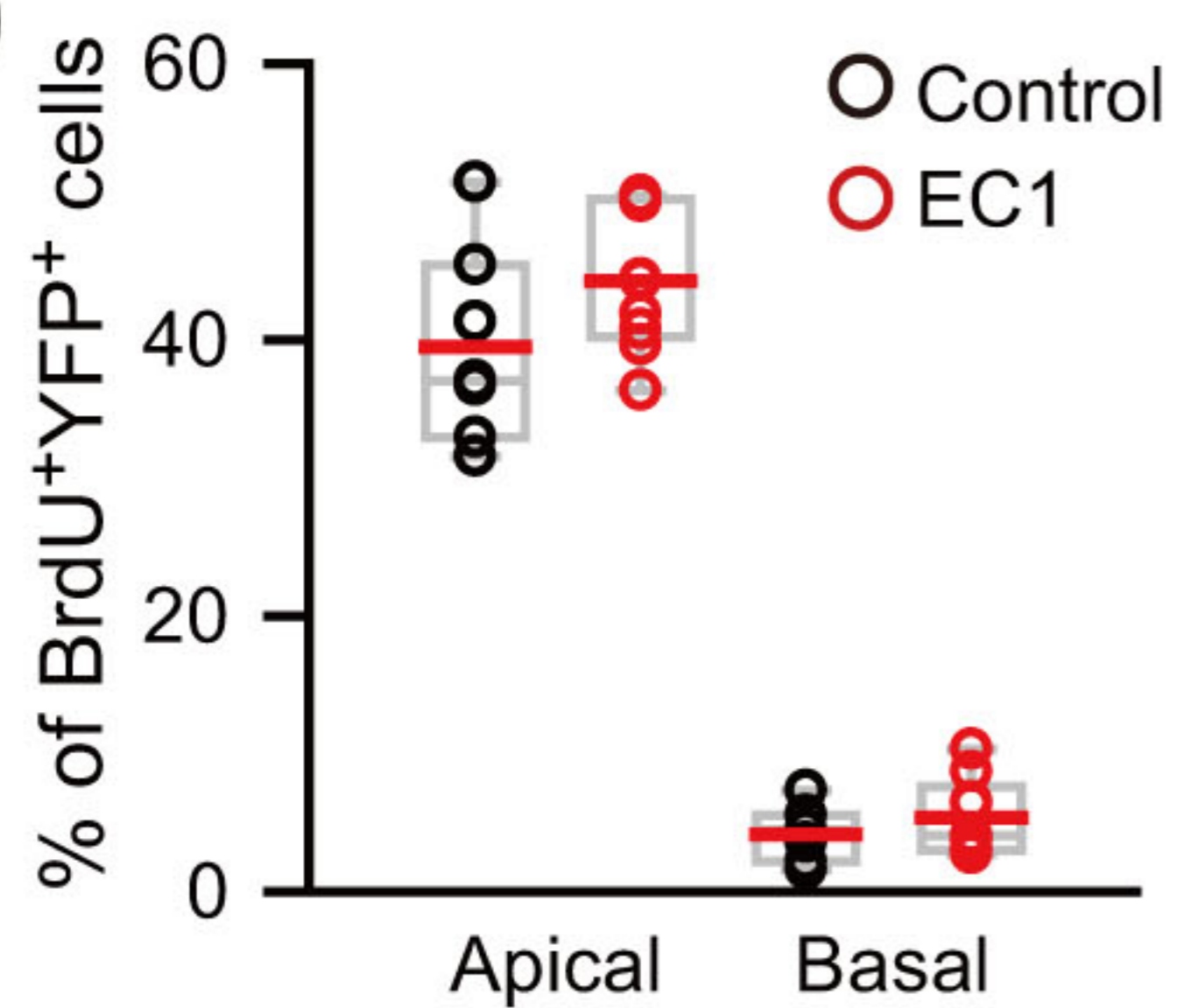
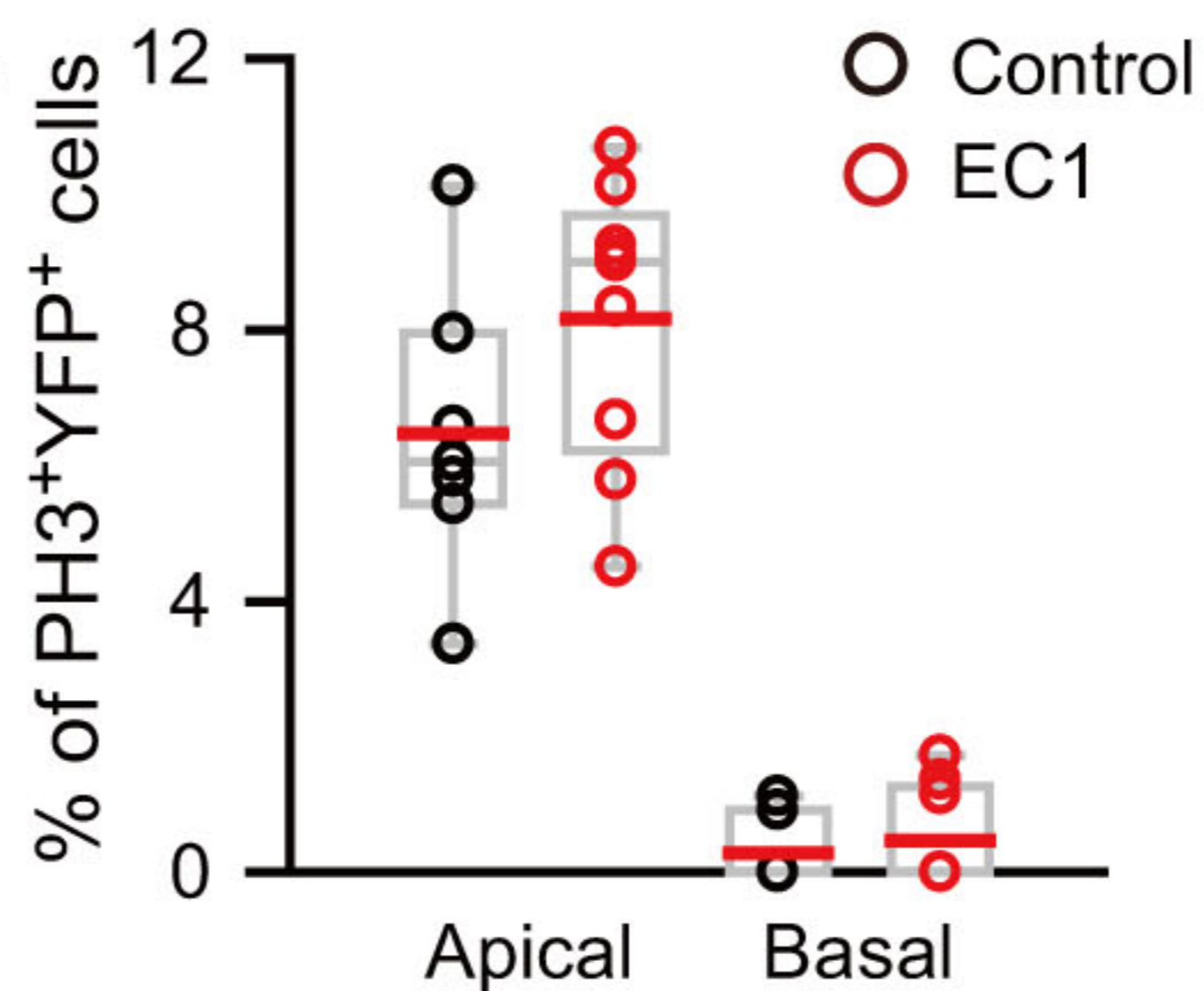
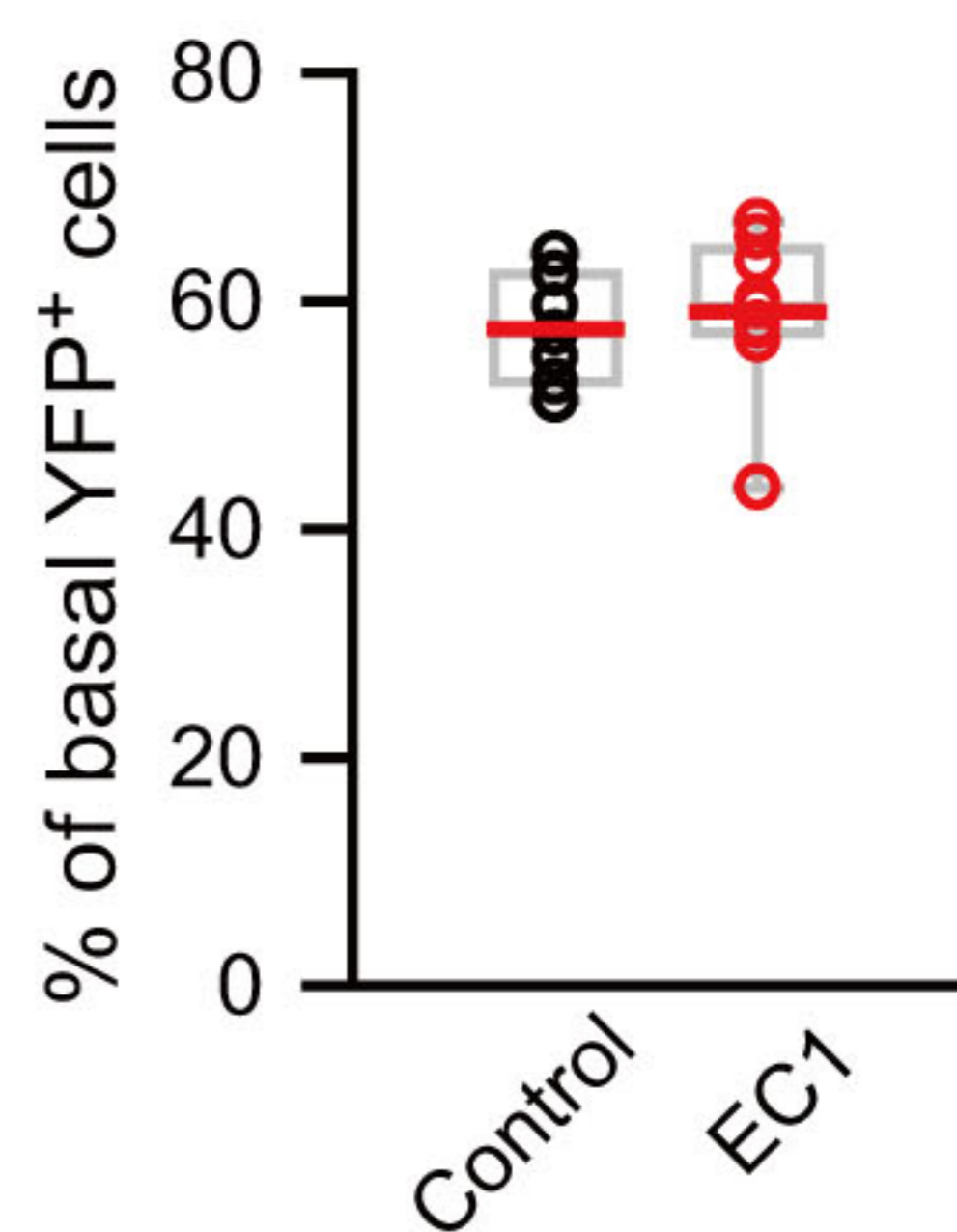
NeuN



Merge



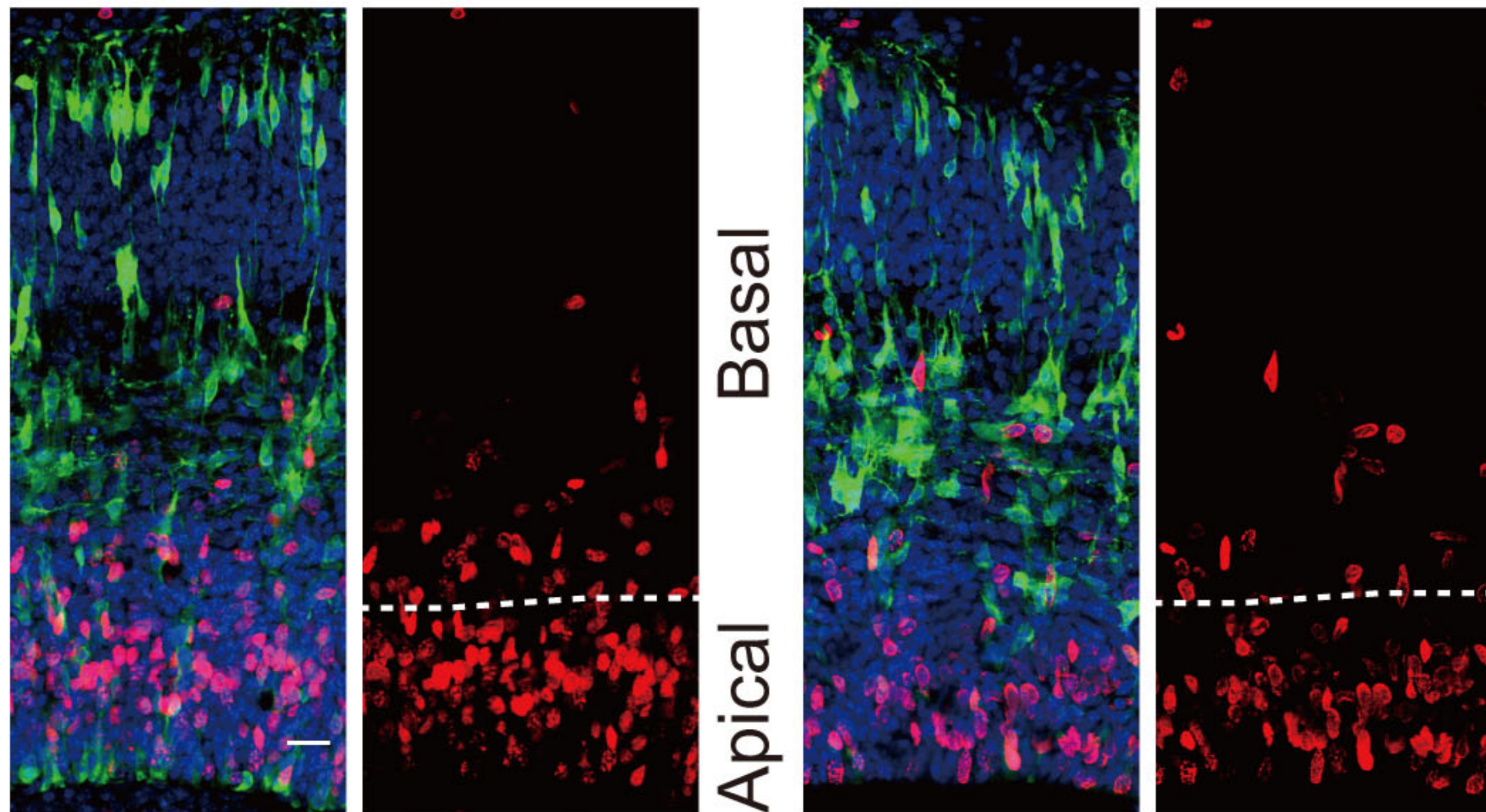
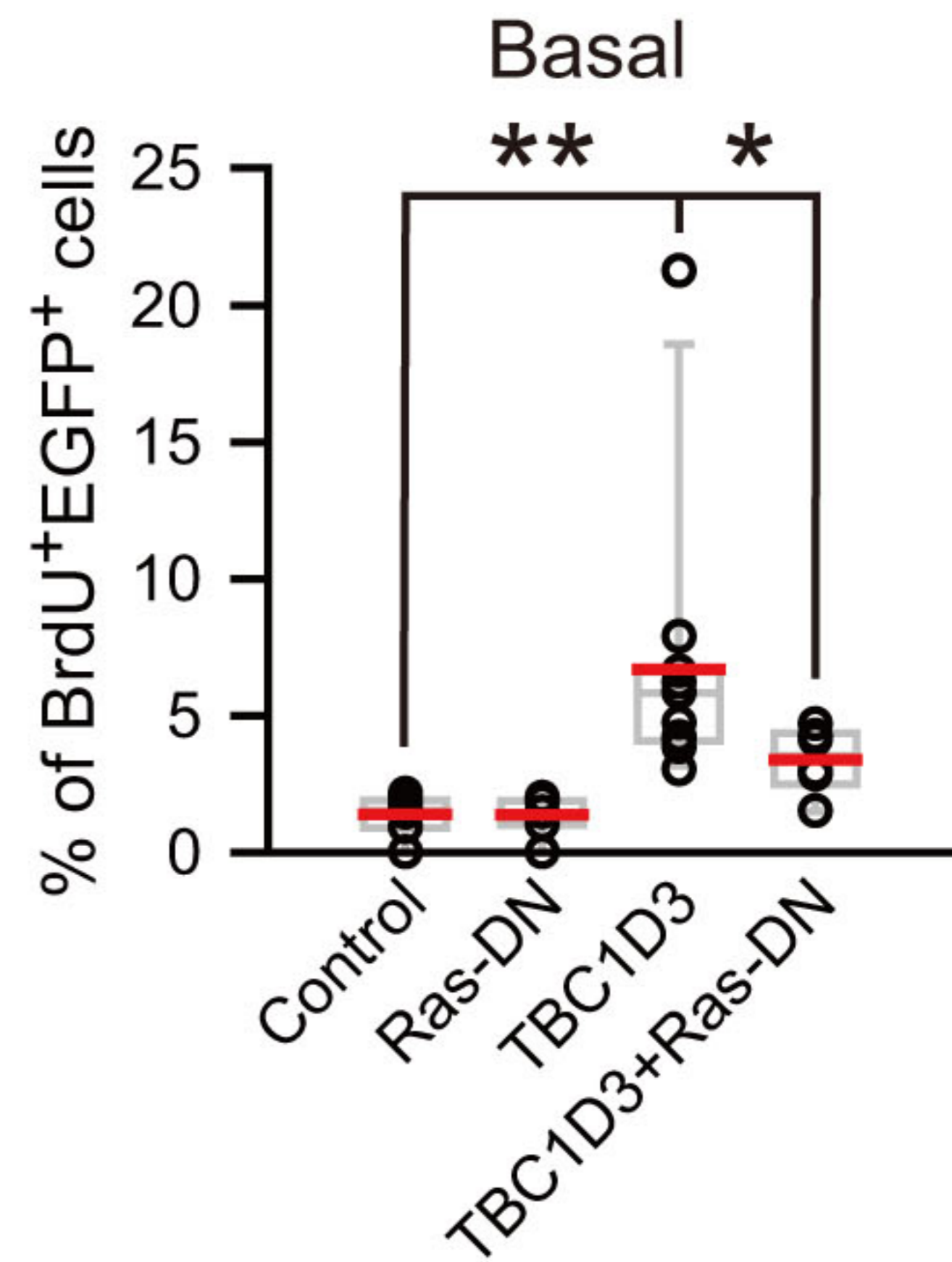
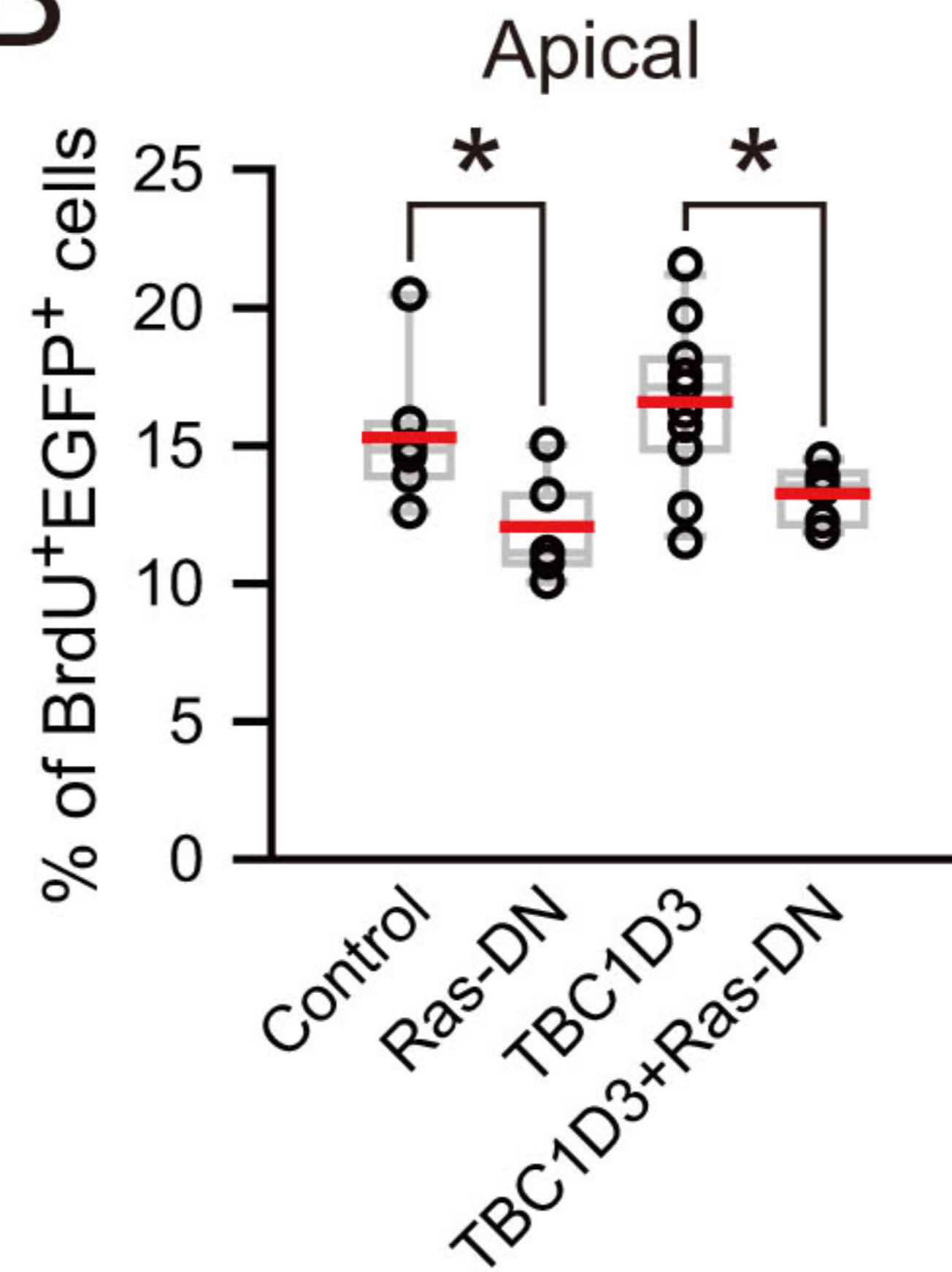


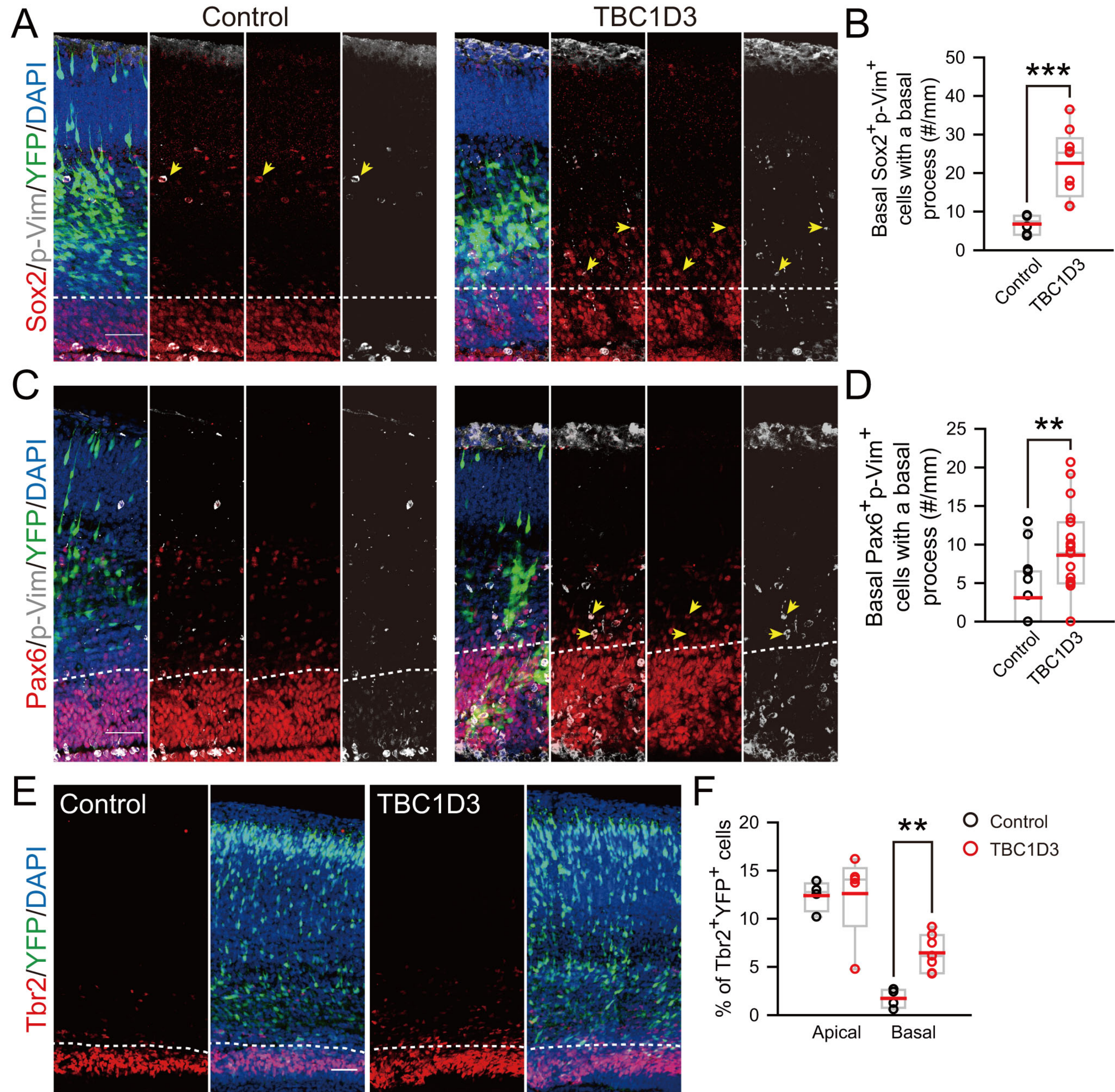
A**B****C****D****E****F**

A**BrdU/EGFP/DAPI****TBC1D3****TBC1D3 + Ras-DN**

Basal

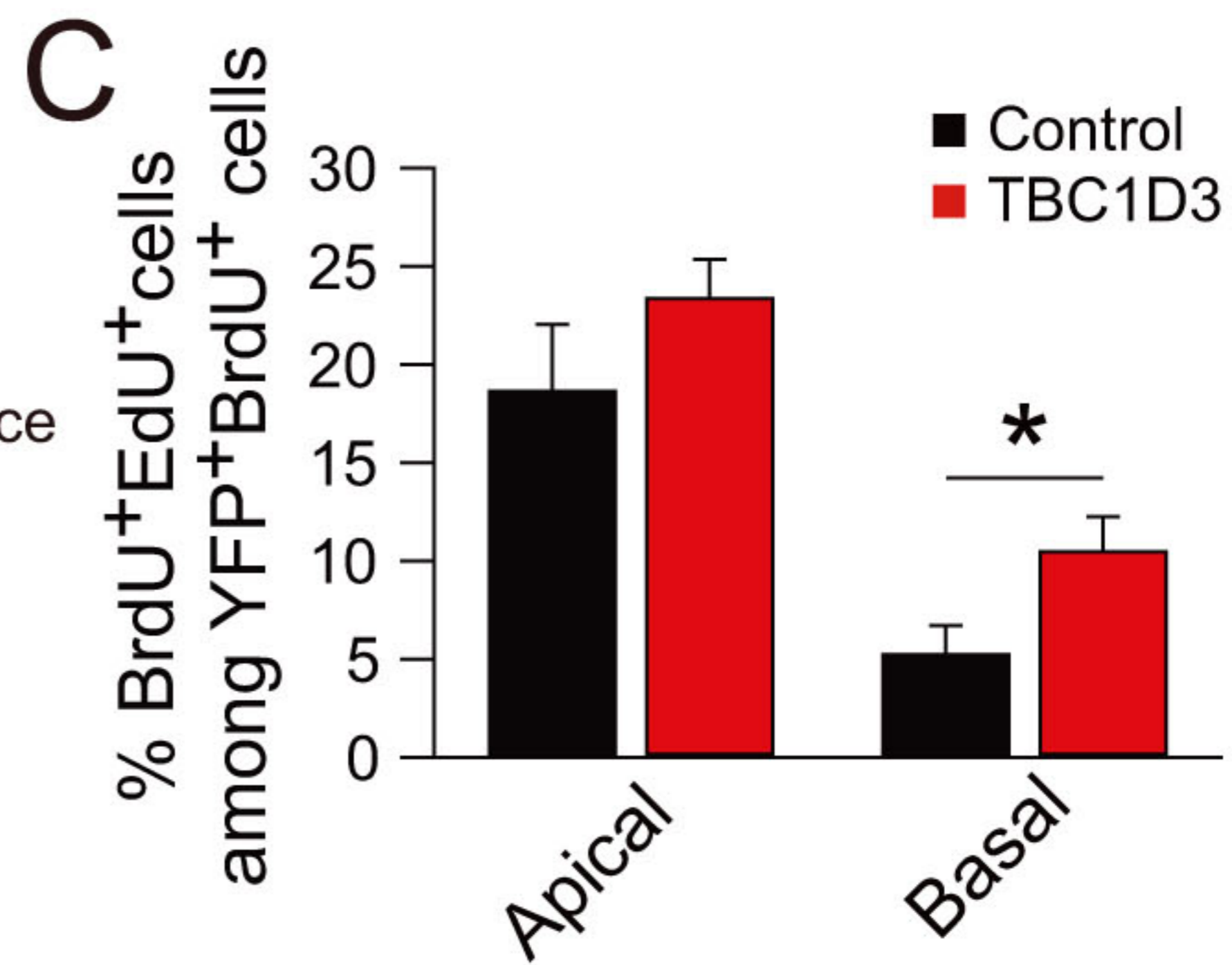
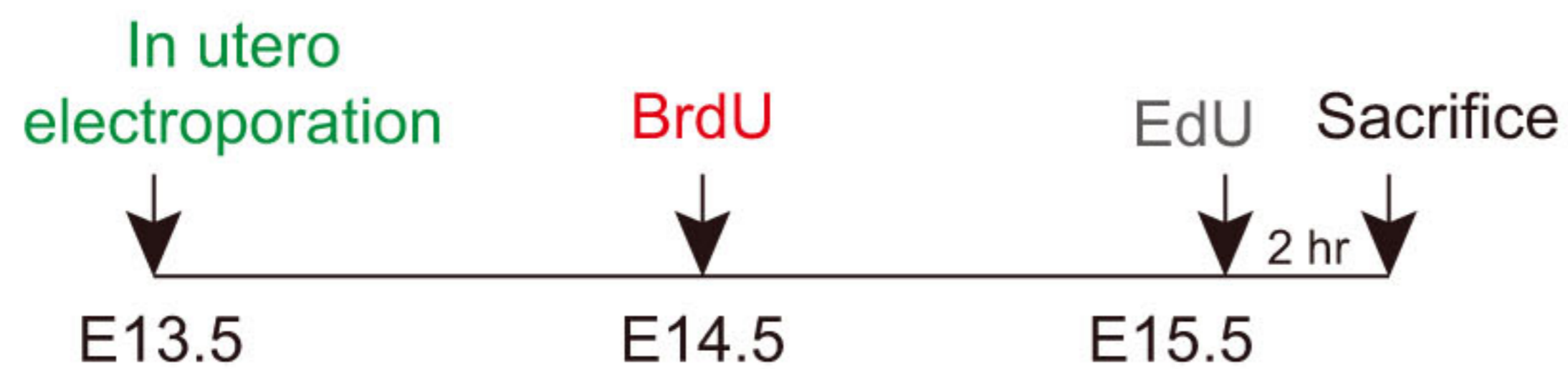
Apical

**B**



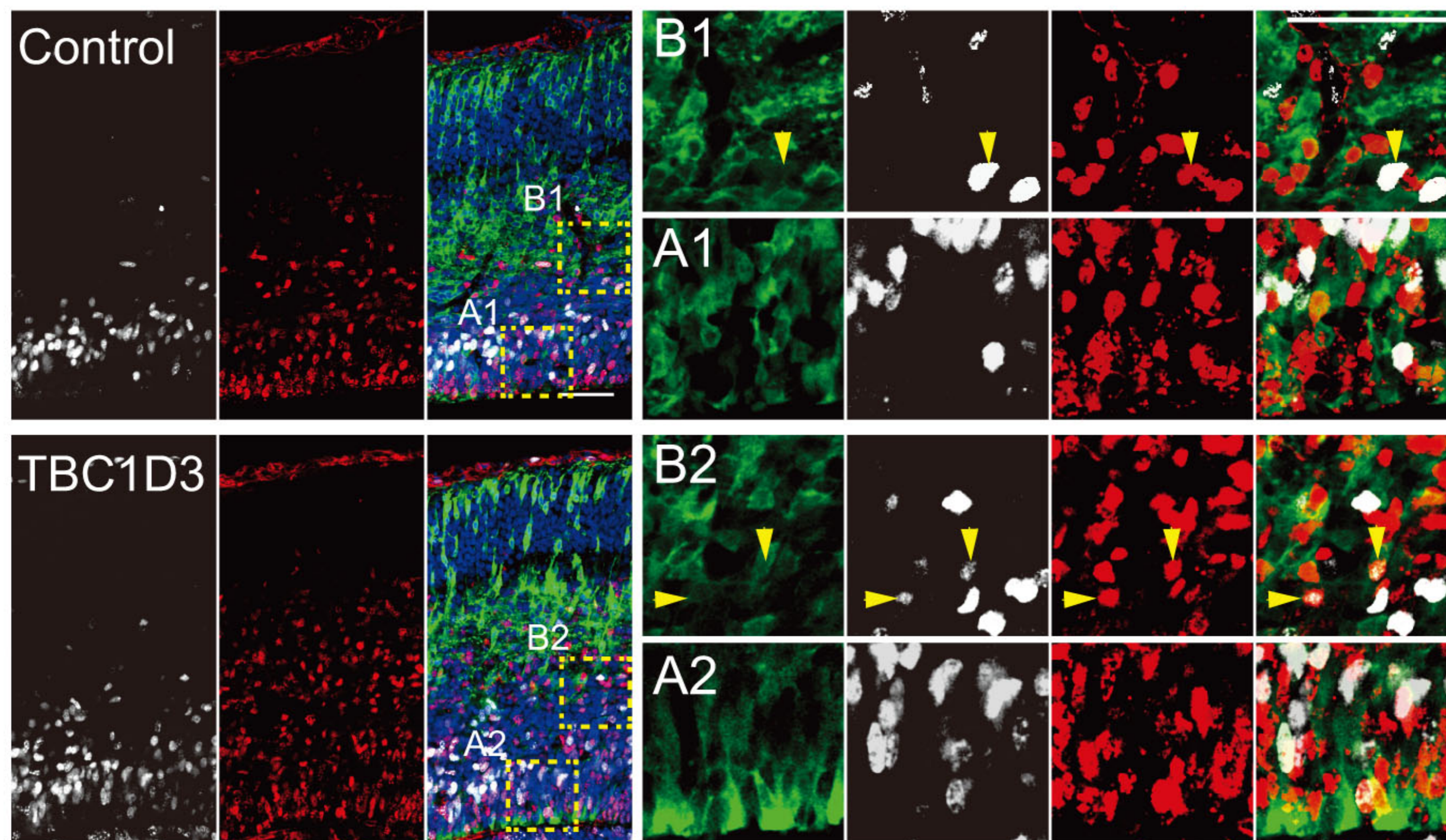
A

BrdU/EdU sequentially labeling



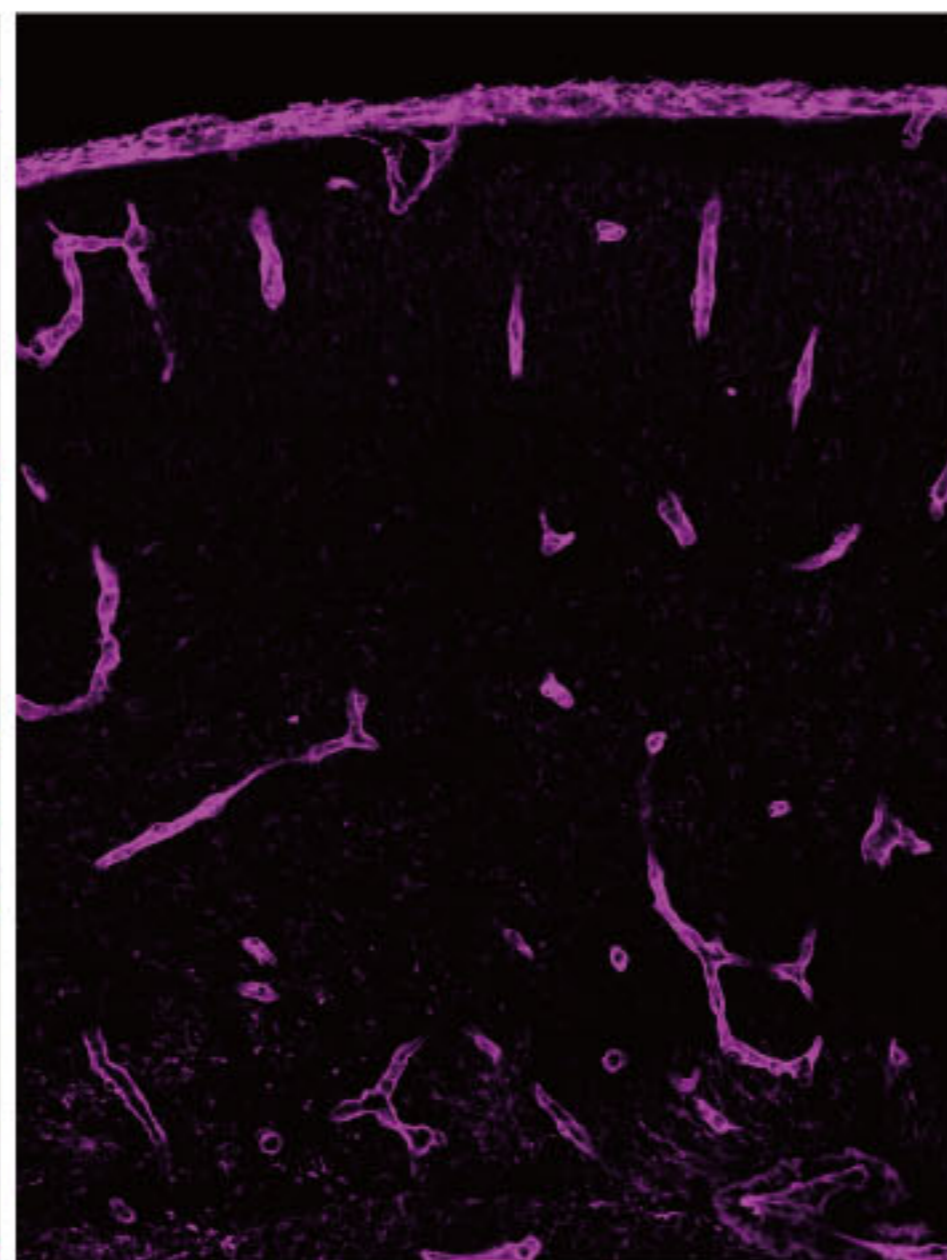
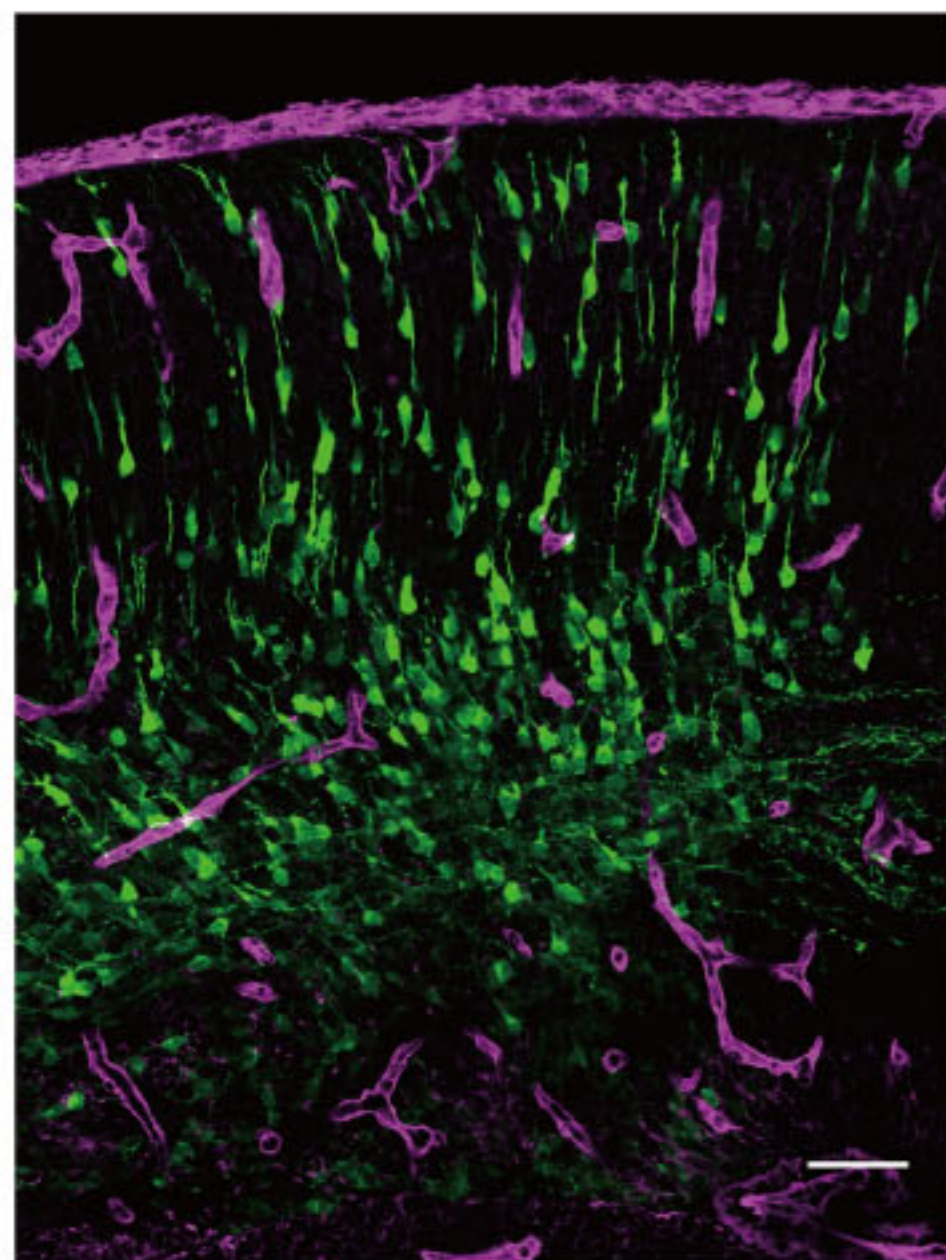
B

BrdU/EdU/YFP/DAPI

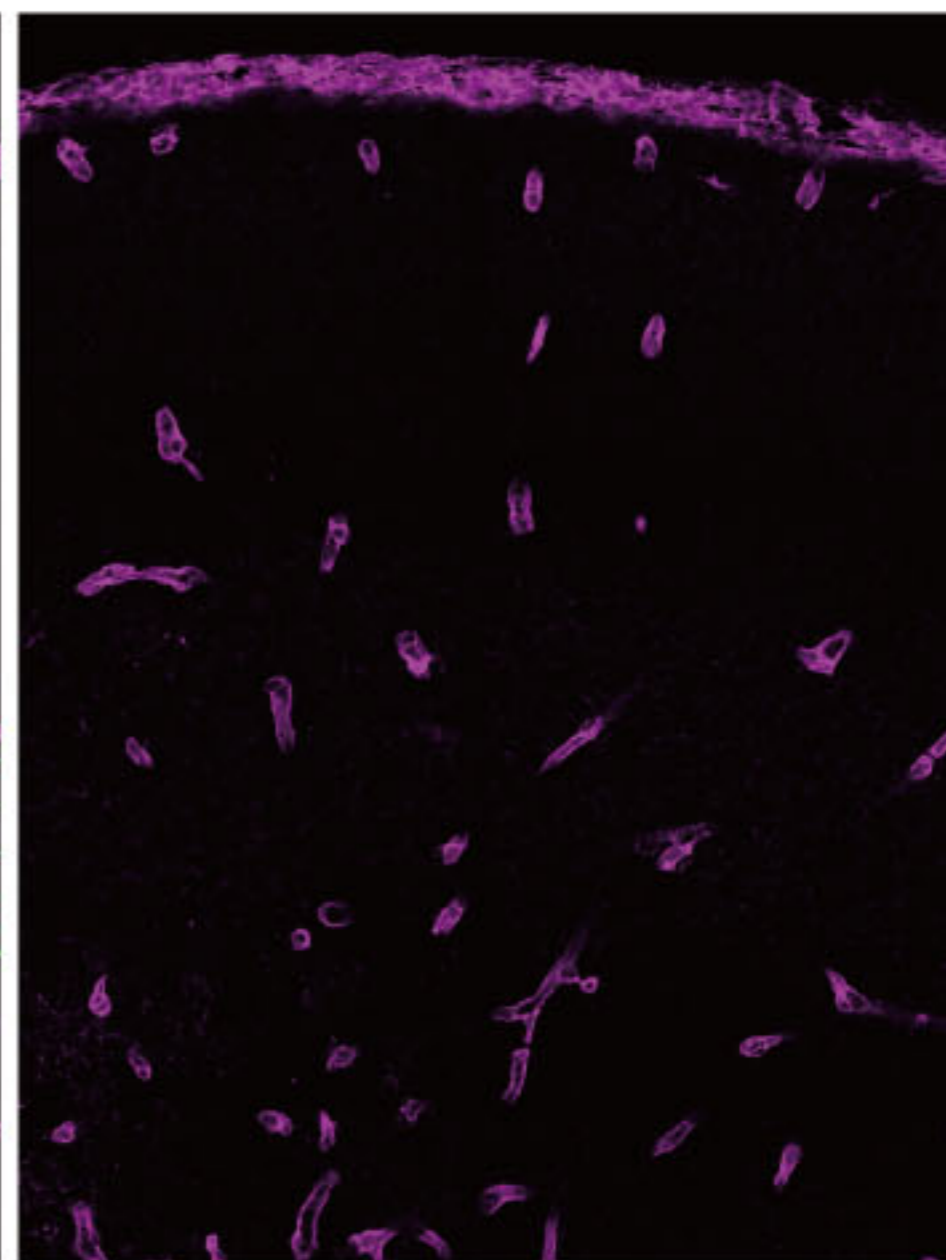
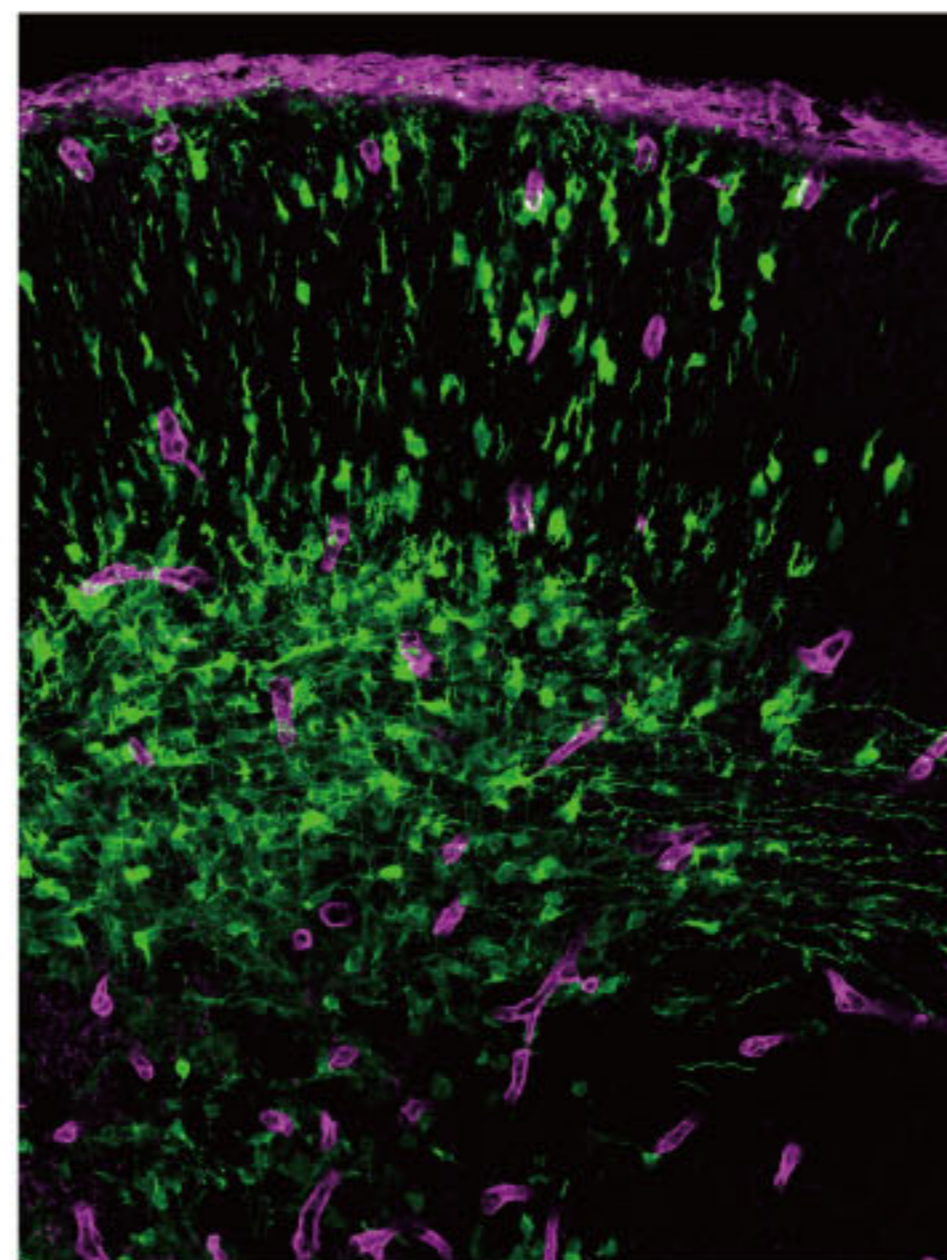


Laminin/EGFP

Control



TBC1D3

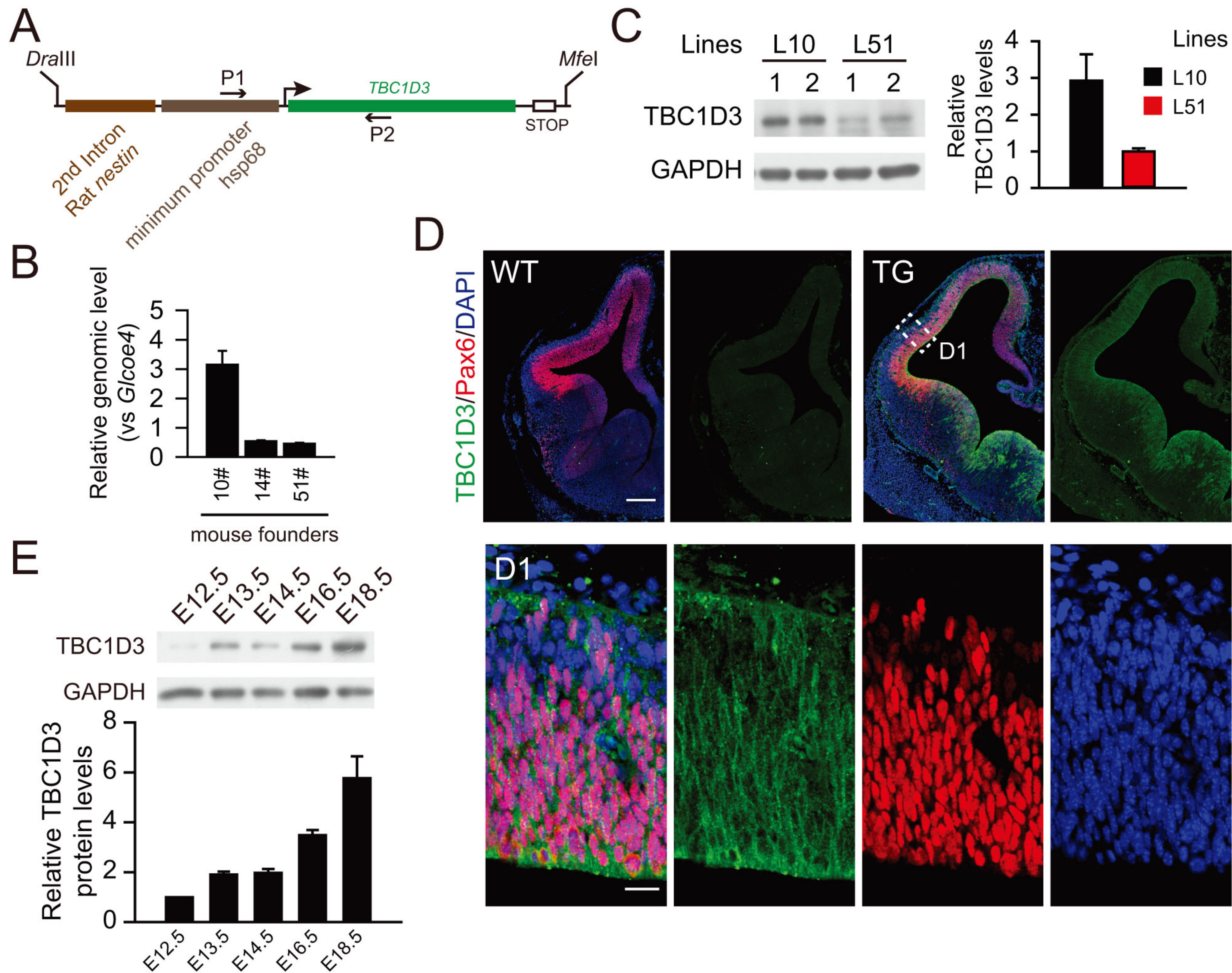


PS

CP

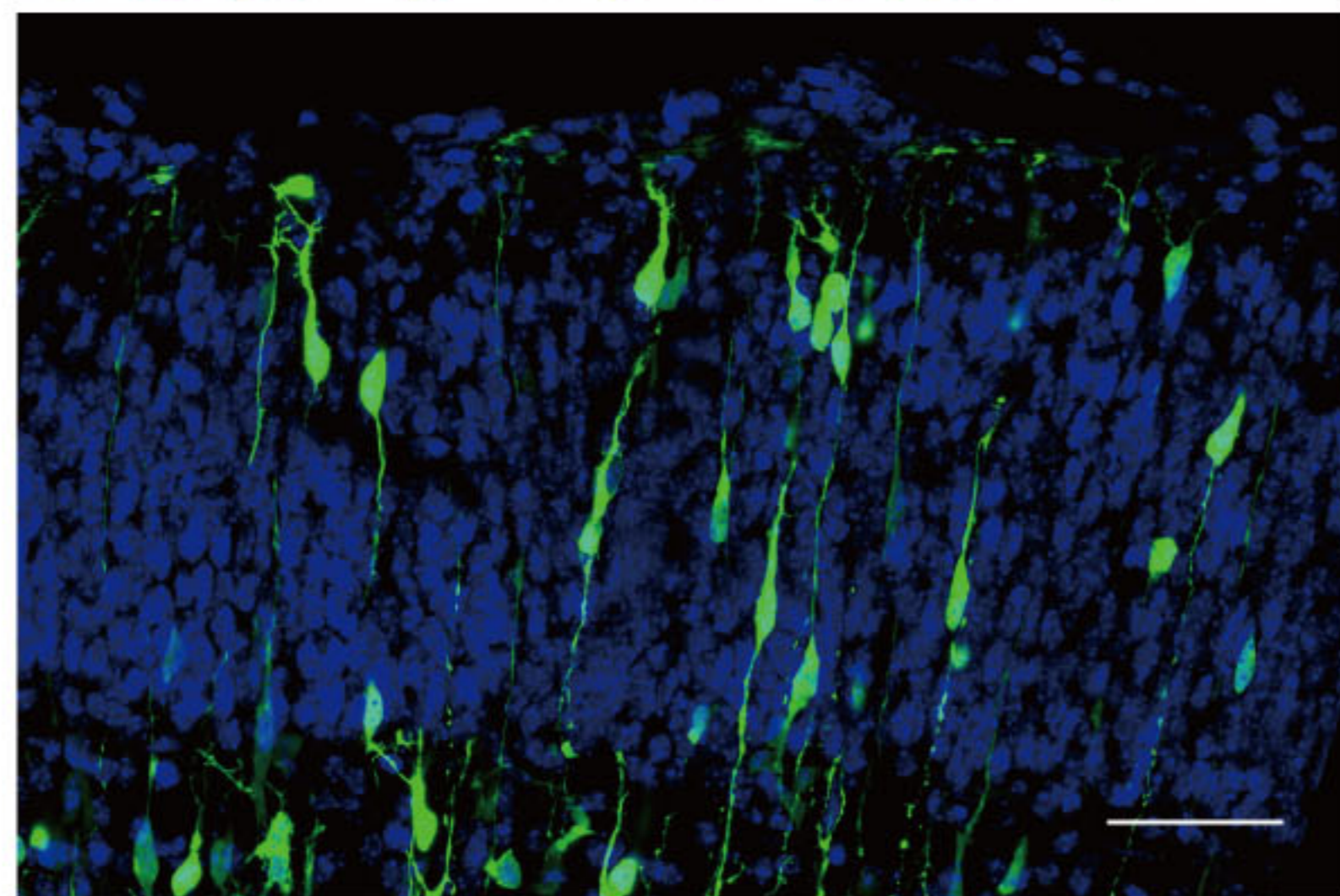
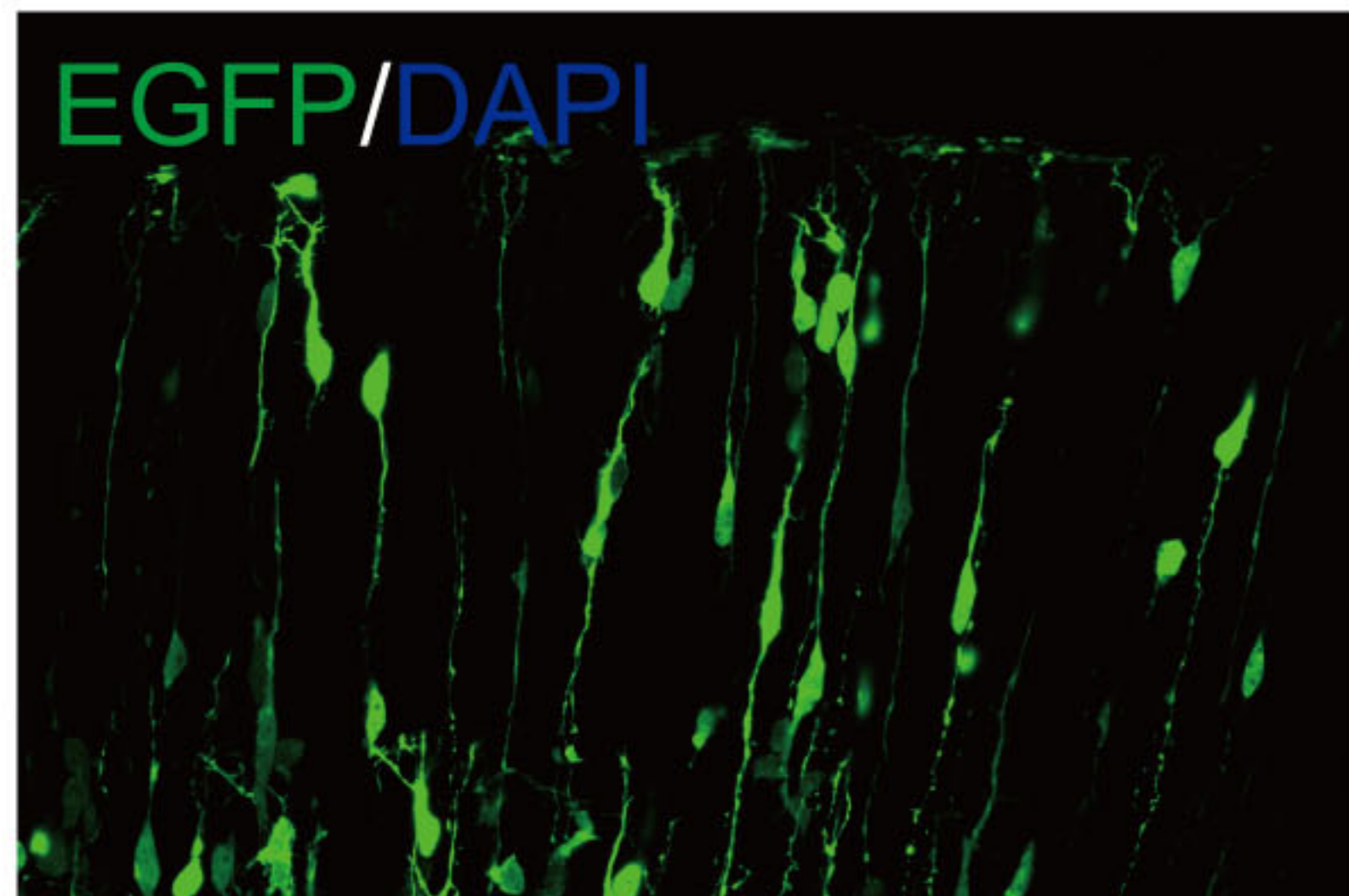
IZ

VZ/
SVZ

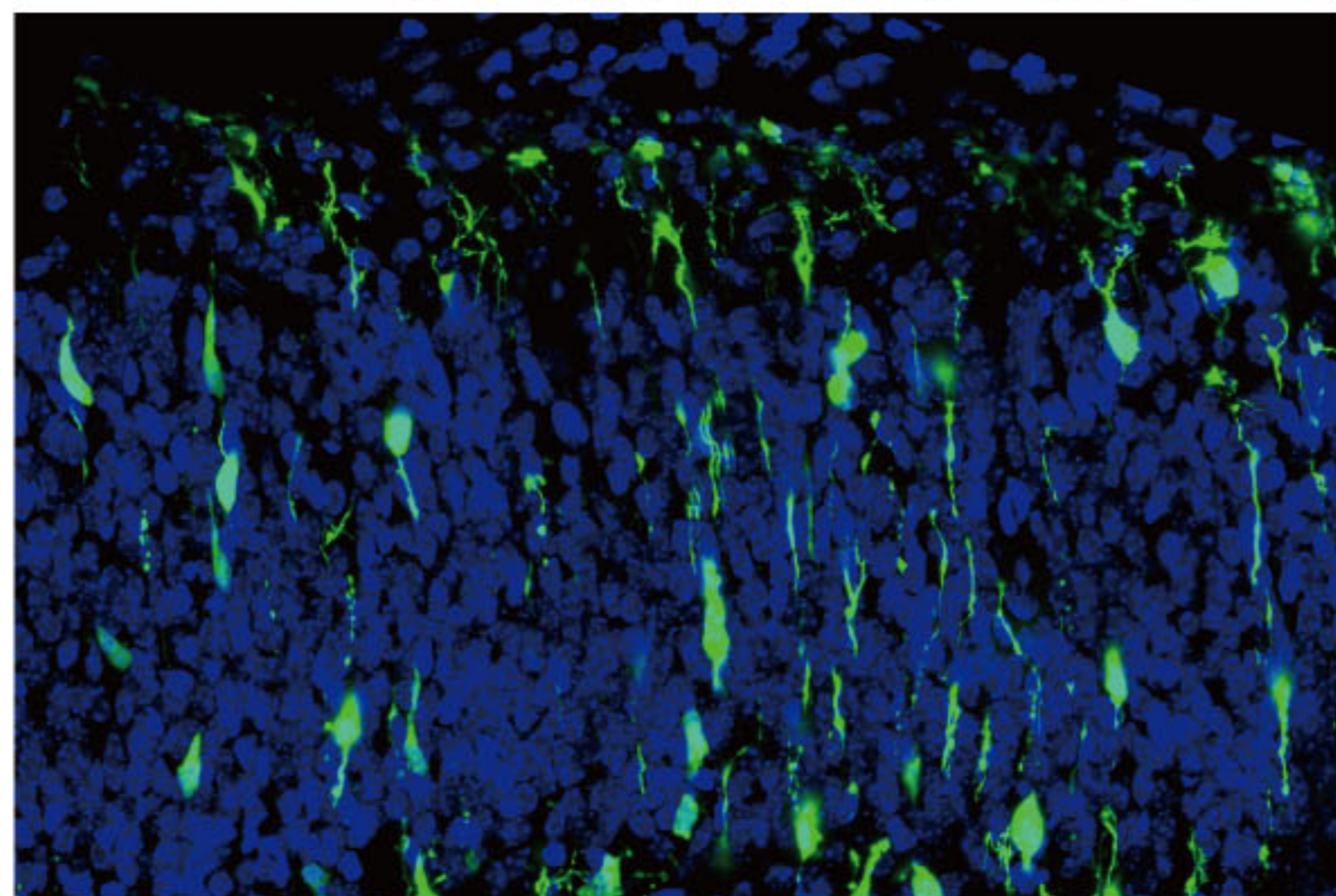
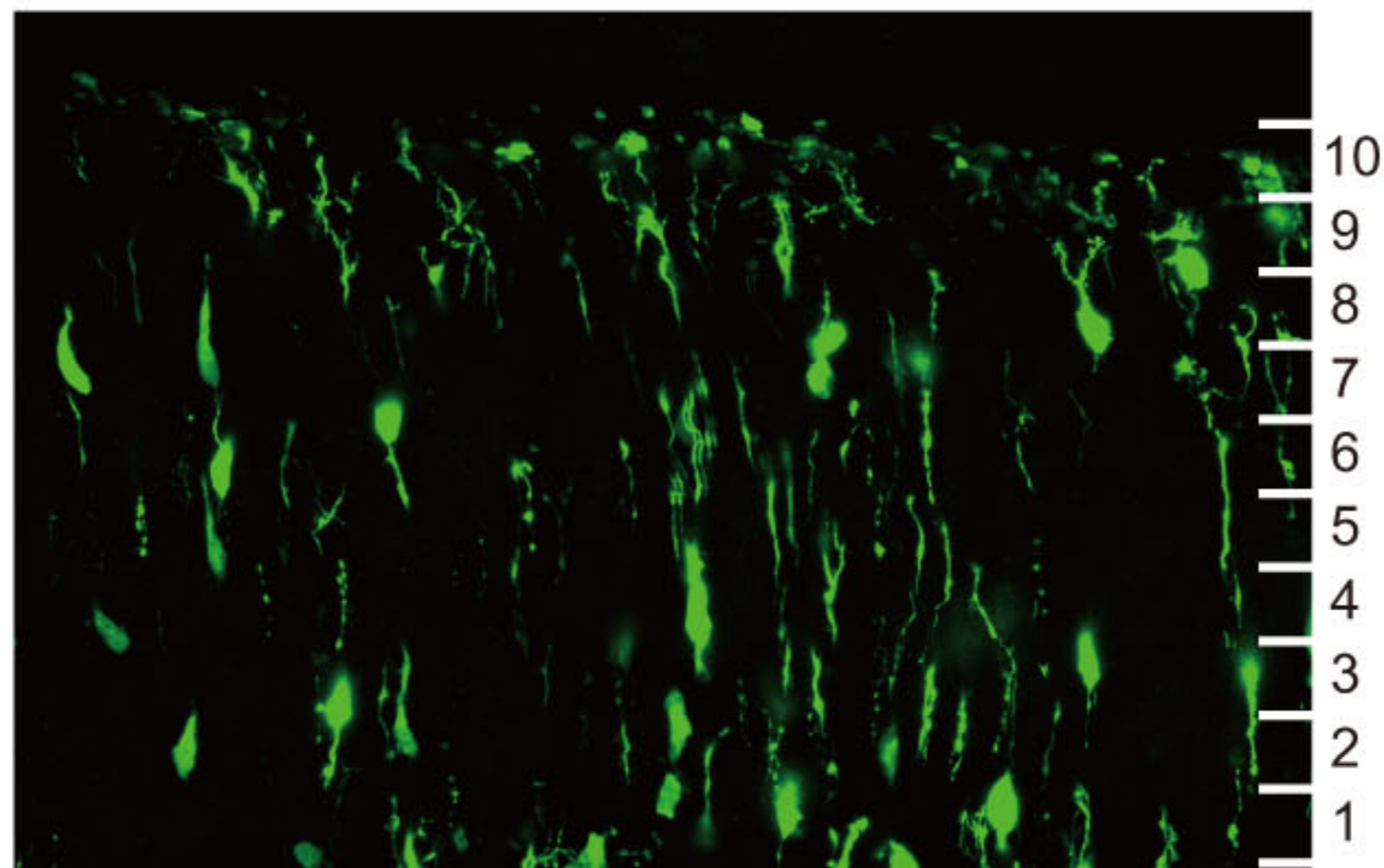


A

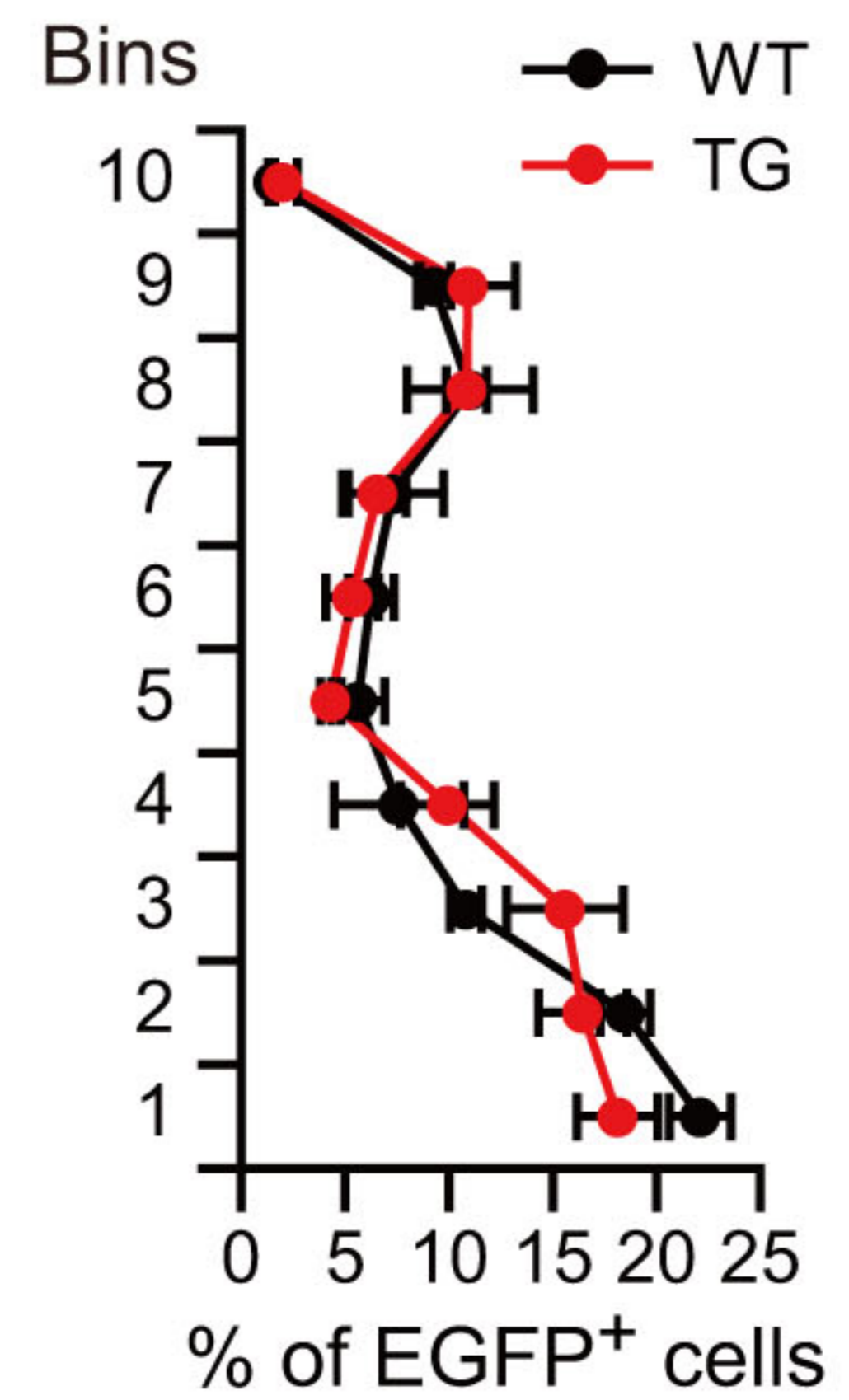
WT

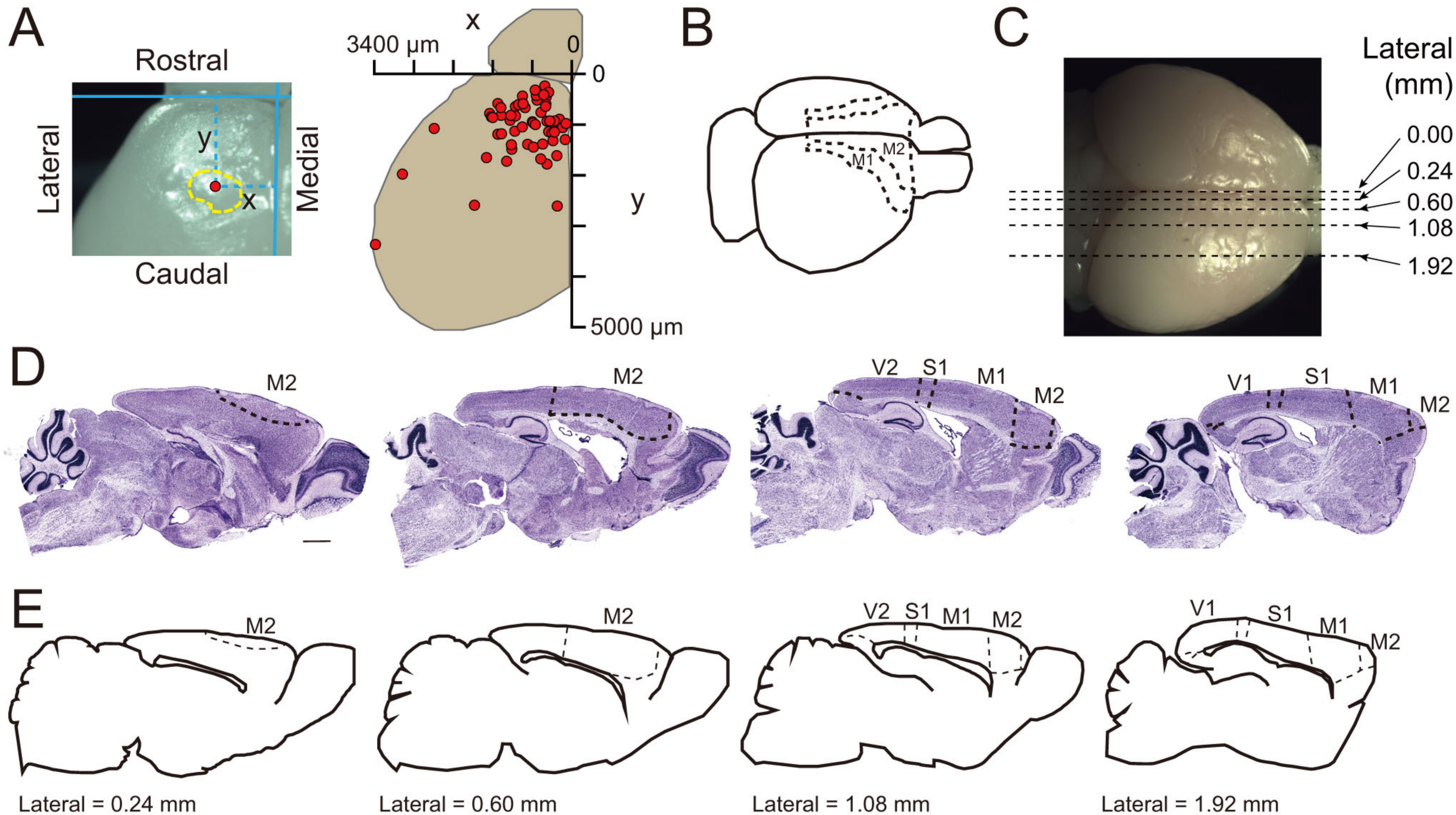


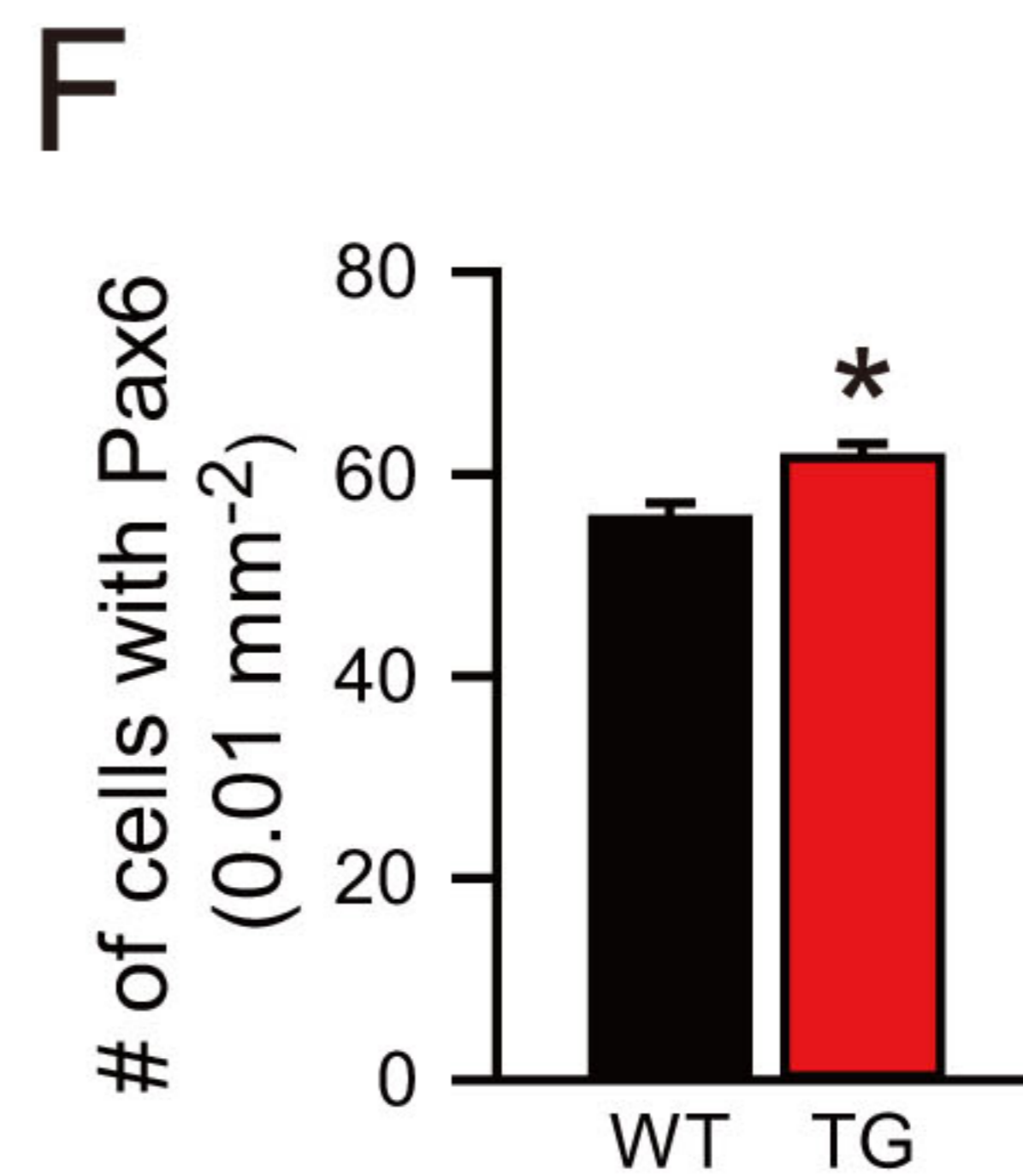
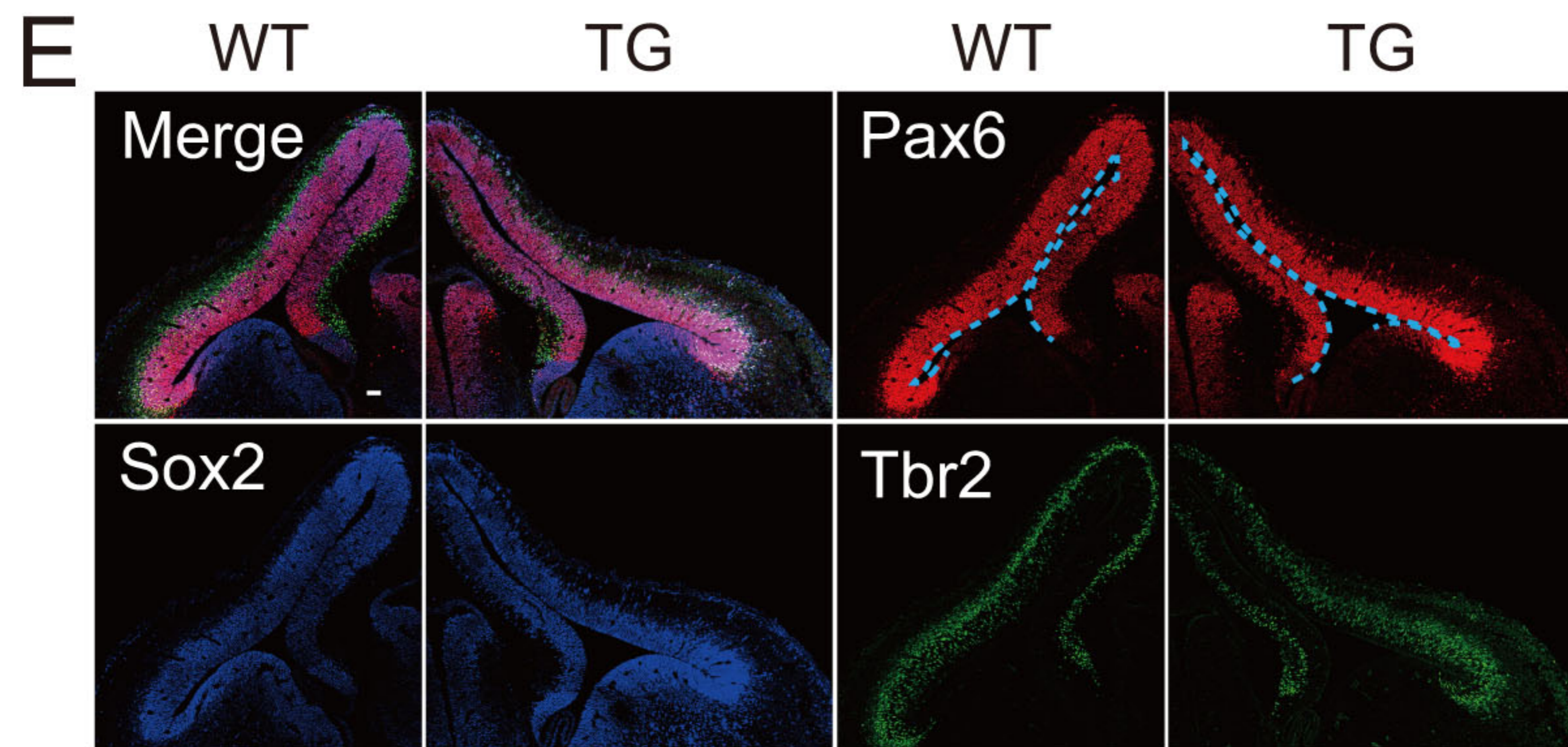
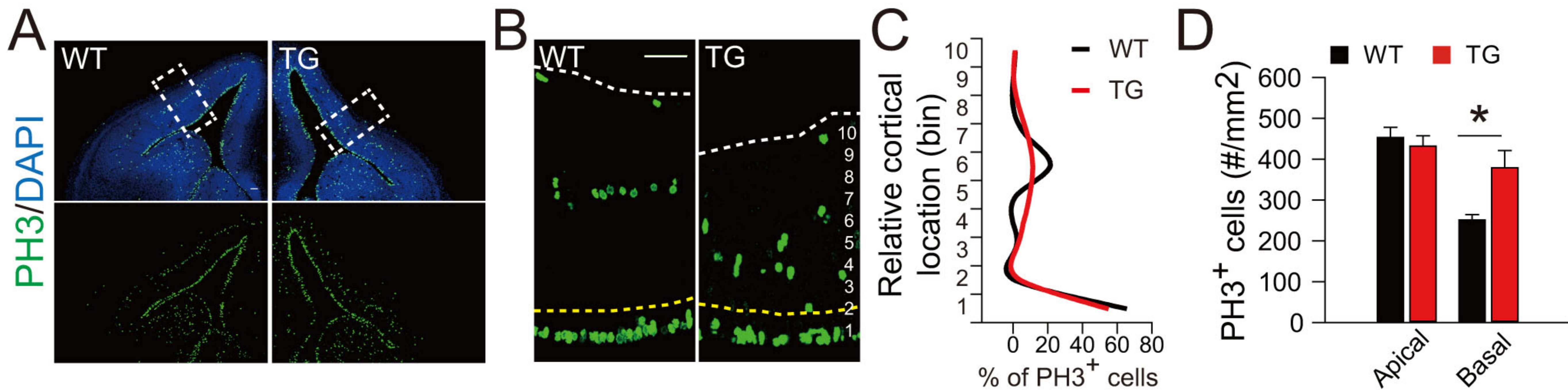
TG

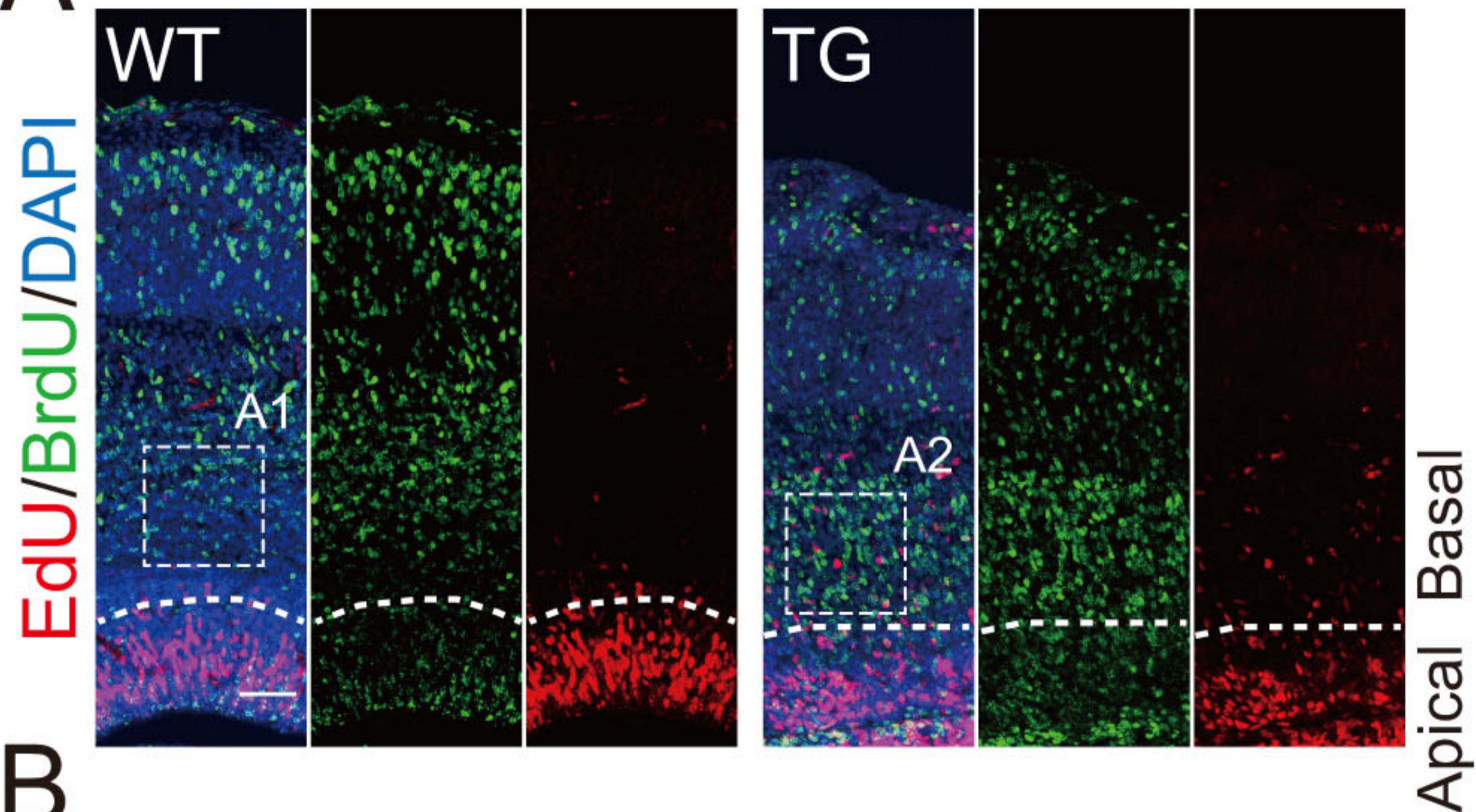
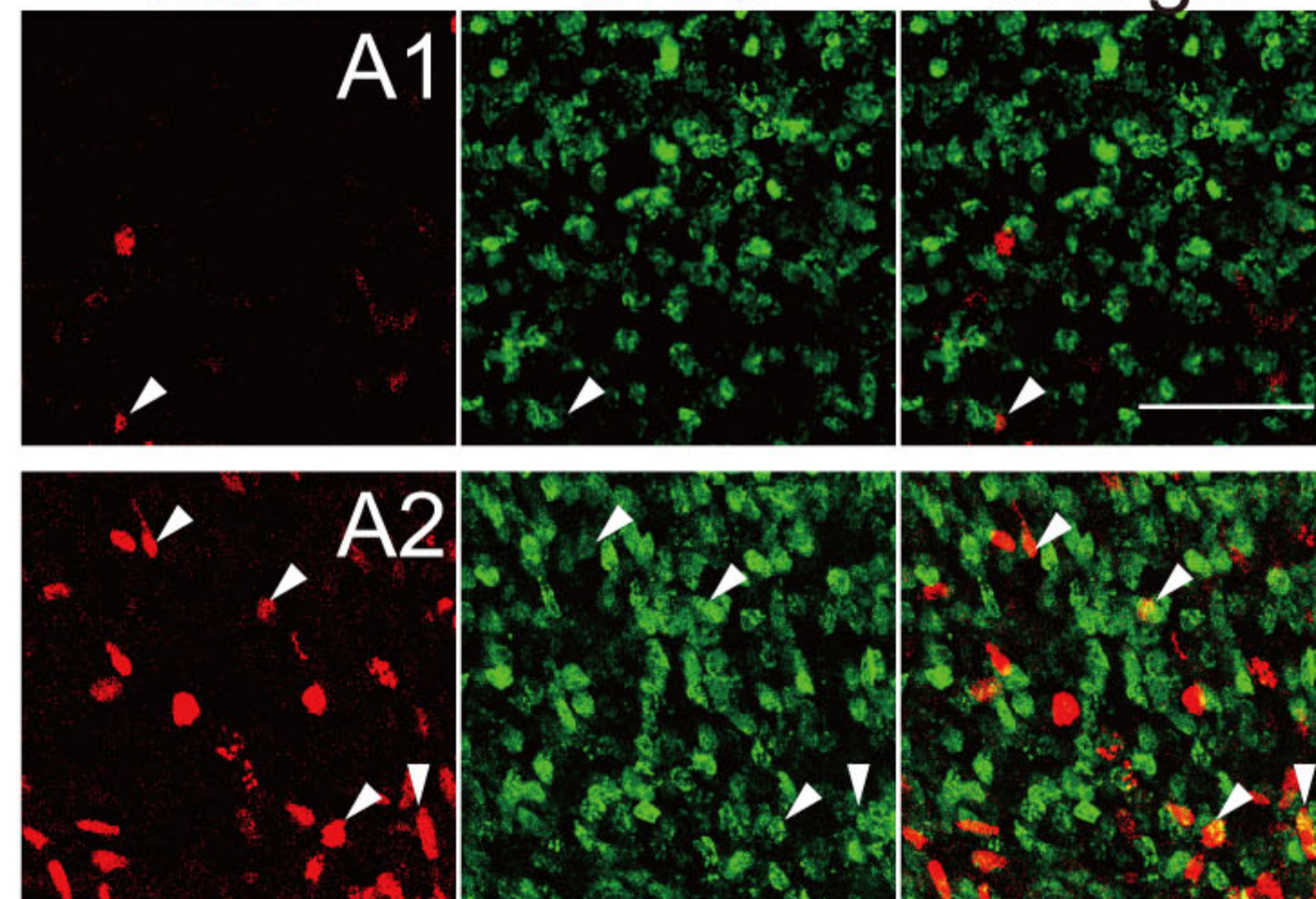


B







A**EdU****BrdU****Merge****B**